

April 2019

Piezoelectric ZnO Nanowires as a Tunable Interface Material for Opto-Electronic Applications

Anand Kumar Santhanakrishna
University of South Florida, anandkumar1@mail.usf.edu

Follow this and additional works at: <https://digitalcommons.usf.edu/etd>



Part of the [Electrical and Computer Engineering Commons](#)

Scholar Commons Citation

Santhanakrishna, Anand Kumar, "Piezoelectric ZnO Nanowires as a Tunable Interface Material for Opto-Electronic Applications" (2019). *USF Tampa Graduate Theses and Dissertations*.
<https://digitalcommons.usf.edu/etd/7926>

This Dissertation is brought to you for free and open access by the USF Graduate Theses and Dissertations at Digital Commons @ University of South Florida. It has been accepted for inclusion in USF Tampa Graduate Theses and Dissertations by an authorized administrator of Digital Commons @ University of South Florida. For more information, please contact digitalcommons@usf.edu.

Piezoelectric ZnO Nanowires as a Tunable Interface Material for Opto-Electronic Applications

by

Anand Kumar Santhankrishna

A dissertation submitted in partial fulfillment
of the requirements for the degree of
Doctor of Philosophy in Electrical Engineering
Department of Electrical Engineering
College of Engineering
University of South Florida

Co-Major Professor: Arash Takshi, Ph.D.
Co-Major Professor: Xiaomei Jiang, Ph.D.
Sylvia W. Thomas, Ph.D.
Jing Wang, Ph.D.
Rasim Guldiken, Ph.D.

Date of Approval:
February 27, 2019

Keywords: Electrochemical Characterization, Organic Photovoltaics,
Photoelectric Effect, Nanostructures, Heterojunction,

Copyright © 2019, Anand Kumar Santhankrishna

ACKNOWLEDGMENTS

First, I am forever indebted to my advisor, Dr.Arash Takshi. Since my first semester in graduate school, Dr.Takshi believed in me like nobody else and gave me endless support. He is someone that I will look up to forever. He has been highly influential in my professional and personal growth. It would not have been possible for me to complete my Ph.D without the constant motivation and support given by Dr.Takshi. I am greatly honored to be one of his graduate students.

I would like to express my special appreciation and thanks to my co-major advisor Dr.Xiaomei Jiang, for being a tremendous mentor for me. I would like to thank you for encouraging my research and accommodating me in your lab.

I would like to thank the rest of my committee: Dr.Sylvia W.Thomas, Dr.Jing Wang, and Dr.Rasim Guldiken, for their insightful comments and encouragement.

I also would like to thank Melmaruvathur amma and Sai Baba for the support that you have showed towards me.

I am forever grateful to my maternal uncle Mahendra Varman for paving a pathway to the world of higher education and helping me to stay motivated.

No amount of gratitude will be enough to express my heartfelt appreciation for the encouragement and support given by my parents, R.Santhana Krishnan and S.Santhi. They have molded me into the person that I am today.

I would like to express my deepest love and appreciation for my wife Manasa Gulur Rajanna for her continued confidence in me. My Ph.D journey would truly be incomplete without

her support. My in-laws Rajanna and Manjula have been pivotal in helping me pursue my higher education with their trust in me.

I would like to thank my sister Nithya Lakshmi for all the encouraging words during my challenging days. I would like to take this opportunity to thank my entire family for their help and support. To name a few: Mohan Chandran, Diya, Dev, Meghna, Nandan and Tanvi.

Last but not least, I would like to thank all my organic electronic laboratory colleagues and friends (Tete tevi, Houman Yaghoubi, Sara Bakhshi, Hadi Ebrahimi, David Rentz, Harrison Riddell, Christian Avila, Riaz Ahmed Liyakath, Abhay, Anusha Mohan, Pooja, Meena, Sharath, Mahesh, Hima Bindu, Aashan, Mani, Deepak, Paul, Anierutan and Praveen Durai) for their continued support..

TABLE OF CONTENTS

LIST OF TABLES	iii
LIST OF FIGURES	iv
ABSTRACT	viii
CHAPTER 1: INTRODUCTION	1
1.1 Overview	1
1.2 Background	3
1.2.1 Piezoelectricity	3
1.2.2 Piezo Energy Harvesters	6
1.2.3 Piezo Nanostructures	8
1.2.4 Piezoelectric Characterization in Nanostructures	9
CHAPTER 2: ANALYSIS OF ZnO AS FUNCTIONAL PIEZO MATERIAL	14
2.1 Introduction	14
2.2 Piezo-Phototronic Effect	17
2.3 ZnO NWs Hydrothermal Fabrication Process	19
2.4 Electrochemical Detection of Piezoelectric Response of ZnO NWs	21
CHAPTER 3: ELECTROCHEMICAL MEASUREMENT OF THE PIEZO VOLTAGE IN ZnO NANOWIRES GROWN ON CURVED AND FLAT SUBSTRATES	26
3.1 Abstract	26
3.2 Introduction	26
3.3 Experimentation	28
3.3.1 ZnO NWs Fabrication Using Hydrothermal Technique	28
3.3.2 Sample Curvature Measurement	28
3.3 Results and Discussion	31
3.4 Conclusion	37
CHAPTER 4: PIEZO CHARACTERIZATION OF ZnO NANOSTRUCTURES USING ELECTROCHEMICAL APPROACH	38
4.1 Abstract	38
4.2 Introduction	38
4.3 Experimentation	40
4.3.1 1D ZnO Nanostructure Fabrication	40
4.3.2 Piezo Characterization of ZnO Morphologies	41
4.4 Results and Discussion	41
4.5 Conclusion	48

CHAPTER 5: PHOTO-ELECTRIC MEMORY EFFECT IN AN ORGANIC BULK HETEROJUNCTION DEVICE.....	49
5.1 Abstract.....	49
5.2 Introduction	50
5.3 Experimental Section.....	51
5.3.1 Materials and Equipment	51
5.4 Results and Discussion	54
5.5 Conclusion.....	67
 CHAPTER 6: OPTICAL MEMORY EFFECT IN ZnO NANOWIRE-BASED ORGANIC BULK HETEROJUNCTION DEVICES	 69
6.1 Abstract.....	69
6.2 Introduction	70
6.3 Methodology.....	72
6.3.1 Materials and Equipment	72
6.3.2 Device Fabrication	72
6.3.3 Glove Box Setup.....	74
6.4 Results and Discussion	74
6.5 Conclusion.....	79
 CHAPTER 7: CONCLUSION AND SUGGESTED FUTURE WORK.....	 81
7.1 Conclusion.....	81
7.2 Suggestions for Future Work.....	83
 REFERENCES	 85
 APPENDIX A: COPYRIGHT PERMISSIONS.....	 94

LIST OF TABLES

Table 1	Correlation between the number of turns applied in the sample holder to the curvature of the samples with an initial length of $A = 1.94$ cm 31
Table 2	Open circuit voltage study of the cells under various conditions 79

LIST OF FIGURES

Figure 1	Possible combinations of piezoelectricity, semiconductor and photoexcitation including optoelectronics, organic electronics, biotechnology and others	3
Figure 2	Pictorial illustration of piezoelectric effect upon (a) stress along the material and (b) shear stress	4
Figure 3	(a) Monocrystal and (b) polycrystal classification of materials for piezoelectric property demonstration	5
Figure 4	Schematic representation of the piezo charge generation as a result of tension and compression to the piezoelectric material	6
Figure 5	Illustration of a piezoelectric cantilever with a tip mass energy harvester	7
Figure 6	The atomic structure of ZnO crystal (Wurtzite structure).....	8
Figure 7	SEM image of the hydrothermally grown ZnO nanowires on an indium tin oxide (ITO) substrate	9
Figure 8	Schematic drawing of the experimental setup for the measurement of the converse piezoelectric effect by nanoindentation	10
Figure 9	Schematic drawing of the experimental setup for the measurement of the direct piezoelectric effect by nanoindentation.....	11
Figure 10	Different forms of ZnO crystals	16
Figure 11	Energy band diagrams for a p-n junction (a) with the absence of piezo-charges, and (b, c) with the presence of positive and negative piezo-charges at the junction, respectively	18
Figure 12	Visual representation of the ZnO NWs fabrication process.....	21
Figure 13	A picture of the sample holder designed for bending the samples (left) and diagram of the electrochemical cell when the sample was tested in the flat and bended mode (right)	24

Figure 14	(a) Displays CV scans for both ITO in Tris and ITO in ferrocene which demonstrates that the redox reaction with ferrocene will show a peak in the CV scan	25
Figure 15	(a) Flat position sample growth holder (b) bent position sample holder	28
Figure 16	Custom setup used for bending samples during the electrochemical measurements	30
Figure 17	SEM images of 4 hrs grown ZnO NWs on (a) the flat substrate and (b) the curved substrate (Inset: indicative of the ZnO NW clusters)	32
Figure 18	CV results from the 4 hrs grown ZnO NW sample on a flat substrate at (a) different outward and (c) inward curvatures	34
Figure 19	CV results from the 4 hrs grown ZnO NW sample on a curved substrate at (a) different outward and (c) inward curvatures.....	35
Figure 20	Ferrocene peak potential versus curvature in flat grown and curved grown ZnO NWs samples	36
Figure 21	SEM image of the hydrothermally grown ZnO nanowires on an ITO substrate.....	42
Figure 22	SEM image of the hydrothermally grown ZnO nanoforest on an ITO substrate.....	43
Figure 23	CV results from the 4 hrs grown ZnO NW sample on a flat substrate at different (a) outward and (c) inward curvatures.....	44
Figure 24	CV results from the two-step hydrothermally grown ZnO nanoforest sample on a flat substrate at different (a) outward and (c) inward curvatures	45
Figure 25	CV results from the 100 nm planar ZnO nano film on a flat substrate at different (a) outward and (c) inward curvatures.....	46
Figure 26	Microscopic image of ZnO nanofilm in different stages of mechanical straining (a) Flat ZnO nano film with no strain (b) small crack formation due to outward bending and (c) slightly bigger cracks due to inward bending	47
Figure 27	Ferrocene peak potential versus curvature for ZnO nanowires, nanoforest and nanofilm.....	47
Figure 28	(a) Device structure of an inverted bulk heterojunction ITO/ZnO NWs/P3HT:PCBM/PEDOT/ Ag paste device	53

Figure 29	(a) SEM image of hydrothermally growth ZnO nanowires on ITO substrate.....	55
Figure 30	I-V characteristics of the bulk heterojunction device (ITO/ZnO NWs/P3HT: PCBM/PEDOT/Ag paste) in the dark and under illumination (80 mW.cm ⁻²)	56
Figure 31	Device recovery process through I-V characterization of an inverted bulk heterojunction photoelectric memory device from illuminated behavior to dark response.....	58
Figure 32	Light intensity study on the bulk heterojunction photoelectric memory device under 80%, 60%, and 40% light intensity	59
Figure 33	Light exposure study on ITO/ZnO NWs/P3HT:PCBM/PEDOT:PSS/ Ag paste photoelectric memory device under 1000 seconds illumination and four different light intensities ranging from 100% to 40% in 20% decrements.....	60
Figure 34	(a) Linear and (b) semi-log scale I-V curves for the device tested under the dark and light conditions	62
Figure 35	(a) Magnitude and (b) phase impedance of the ITO/ZnO NWs/P3HT:PCBM/PEDOT/ Ag paste photoelectric memory device at 0 V bias	63
Figure 36	Energy diagram of the device at 0 V bias in (a) the dark and (b) under illumination (or in the transition mode after cessation of the light).....	65
Figure 37	SEM image of the hydrothermally grown ZnO nanowires on an ITO substrate.....	73
Figure 38	(a) Pictorial illustration showing the structure of the bulk heterojunction organic memory device and (b) the transfer box used to isolate the sample to maintain conditions similar to glove box for IV characterization and memory effect study.....	74
Figure 39	I-V characterization of the device in the dark and under illumination performed in ambient conditions.....	75
Figure 40	Memory effect experimentation of the sample tested under ambient conditions through I-V characterization showing gradual return to the dark response.....	76
Figure 41	I-V characterization of the bulk heterojunction device in the dark and under illumination performed using a sealed transfer glove box with conditions similar to glove box	77

Figure 42 Device recovery process of the sample in a sealed transfer box through I-V characterization of an inverted bulk heterojunction photoelectric memory device from illuminated behavior to dark response 78

ABSTRACT

Organic electronic devices are sustainable alternatives to the conventional electronics, due to their advantages of low cost, mechanical flexibility and wide range of applications. With the myriad list of organic materials available today, the opportunities to imagine new innovative devices are immense. Organic electronic devices such as OLEDs (organic light emitting diode), OPVs (Organic photovoltaics) and OFETs (organic field effect transistors) are among the leading device categories. Although OLED's have been a huge commercial success, other categories are not lagging.

Radical thinking is necessary to improve on the current performances of these devices. One such thinking is to combine the versatile ZnO (Zinc Oxide) material to organic semiconductors. This can be achieved by exploiting the dual nature of ZnO's semiconducting and piezoelectric property. Many devices have used ZnO in combination with organic semiconductors for applications ranging from sensors, photovoltaics, OFET's, memory and many others. The goal of the work is to incorporate the piezoelectric nature of hydrothermally grown ZnO nanowires for Opto-electronic applications.

Although the initial research work was done on incorporating the piezo effect of bulk grown ZnO nanowires in improving the efficiency of an OPV, we discovered a unique memory effect in this device by incorporating ZnO nanowires in an inverted organic photovoltaic architecture. The device switched between a rectifying response in dark to resistive behavior under illumination with a finite transition time and was reversible. Since then we decided to explore few of the opto-electronic applications of this technology.

The synthesis and characterization of crystalline ZnO nanowires, nanoforest and planar ZnO nanofilm are reported along with the application of these ZnO nanostructures in optoelectronic devices. Noncentro symmetry of crystalline ZnO nanostructures makes it an excellent candidate to be used as piezo functional material and these nanostructures are characterized using electrochemical cell containing ZnO electrode as the working electrode.

ZnO nanostructures like nanowires, nanoforest and planar nanofilm are similarly characterized for piezo property using electrochemical technique. Different devices require distinguishing physical and electrical properties of ZnO nanostructures, hence morphology, effect of pre-strain, surface area, surface coverage and thickness of these nanostructures were evaluated for its piezoresponse. It is shown that it was possible to obtain similar piezoresponse among different ZnO nanostructures in addition to taking advantage of the structural benefits among various categories of nanostructures as per requirement.

The presented research can be used as the proof-of-the-concept that ZnO nanostructures can be designed and fabricated with a prestrain to adjust the piezo response of the material under external forces. Therefore, the structure with the prestrain can be employed in various electronic and optical devices where the piezo voltage can be used for adjusting the energy band bending at an interface.

CHAPTER 1: INTRODUCTION

1.1 Overview

Nanotechnology has been the epicenter of innovation with focus on research and development in the recent years. In this modern era of miniaturization, there has been an influx of nanotechnology devices and materials for targeted solutions in applicable fields such as medicine, biotechnology, engineering, electronics, clean energy, and many more. As devices are continuously shrinking ever so rapidly, energy requirement for these power hungry devices has become a critical roadblock for progress to occur [1]. Energy harvesters refer to the breed of devices that can harvest energy through ambient sources such as wind, heat, vibration and so on. Many energy-harvesting devices have been developed previously, such as solar cells, piezoelectric energy generators, rectennas, thermoelectric generators, and many more. Also, hybrid devices have been developed for more efficient energy harvesting and better use of available energy sources [2]. An emerging technology for self-powered wireless electronics is the new generation of piezoelectric-based nanogenerators for harvesting mechanical vibrations and converting the power to the electric form[3].

Piezo technology has applications in fields such as medical technology, automotive engineering, and semiconductor technology. Consumer and industrial electronics alike uses piezoelectric materials and devices for applications such as diesel fuel injectors, ultrasonic transducers, vibration sensors, engine knock sensors, pressure sensors, and sonar equipment. In these lines, looking deep into the market of piezoelectric technologies gives a better understanding on the economics of this particular technology and its importance. According to the new market

research report on piezoelectric devices, the market is expected to reach USD 31.33 billion by 2022, growing at a Compound Annual Growth Rate (CAGR) of 4.88% between 2016 and 2022 [4]. The prime factors driving this growth are the increased demand for piezoelectric devices and technologies. A greater interest from government and corporate investors towards piezoelectric technologies has helped in the increased research and development. Although there is an increase in the demand for piezoelectric technologies, some piezo technologies enjoy greater interest than others. For example, piezoceramics have a greater share in market owing to better piezoelectric sensitivities and ability to manufacture piezoceramics of the desirable shapes and sizes [5]. Currently the most widely used piezoelectric ceramic is Lead Zirconate Titanate (PZT) [5]. Piezoelectric actuators and sensor use in automotive industry are in line to witness a huge growth due to its improved reliability and low cost [5]. Industrial and manufacturing is the main application region for piezoelectric devices. Piezoelectric motors, sensors, actuators, and transducers have various critical uses in industrial procedures [6]. A main reason behind the difficulties faced in the development of the business sector for piezoelectric devices includes the high cost of materials utilized as a part of assembling piezoelectric items, high R&D cost identified with the advancement of piezo items, and legitimate prohibitive measures that confine the utilization of lead in these items [5].

In addition to the traditional applications of piezo devices, the piezo effect has been employed in other fields such as photonic and semiconductor technologies, generating new fields called piezophotonics and piezotronics (Figure 1). Professor Zhong Lin Wang and his group from Georgia Tech have worked on the founding principles of piezotronics and helped in better understanding the physical phenomenon of piezoelectric application in conventional semiconductor electronics [7]. Optoelectronics, Piezophotonics, Piezotronics and Piezo-

phototronics all require the thorough understanding of piezoelectricity exhibited among many materials. With the ever increasing piezoelectronic applications, it only necessitates more focused research and development on the different materials and their properties to further improve on the current status quo.

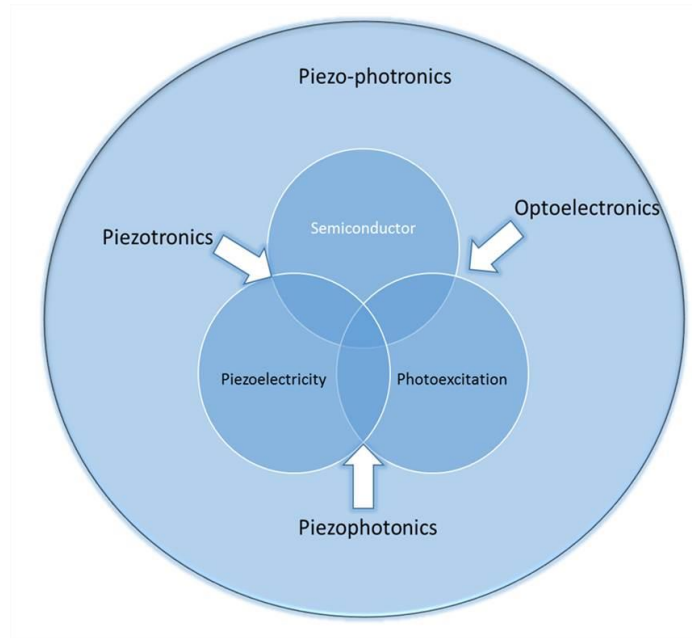


Figure 1. Possible combinations of piezoelectricity, semiconductor and photoexcitation including optoelectronics, organic electronics, biotechnology and others.

1.2 Background

1.2.1 Piezoelectricity

The phenomenon of electric charge accumulation by certain solid materials in response to the applied mechanical stress, or mechanical dimensional change upon electrical stimulus is called as piezoelectricity or piezoelectric effect. Piezoelectric effect is a reversible process where the materials are able to amass electric charge upon mechanical stimulation and are also able to induce mechanical strain resulting from applied electric field. Piezoelectric effect is a product of electrostatics and mechanics.

The piezoelectric effect was discovered in 1880 by the Jacques and Pierre Curie brothers. It was discovered that when a mechanical stress was applied on crystals including tourmaline, topaz, quartz and others, electrical charges were generated and were found to be proportional to the stress applied [8]. Curie brothers were unable to demonstrate the reversible nature of piezoelectric effect (i.e. Mechanical deformation under applied electric field) [9]. Latter Lippmann (1881) mathematically deduced the reversible property from fundamental thermodynamic principles [9]. Curie brothers immediately acknowledged the converse effect in their next publication [9].

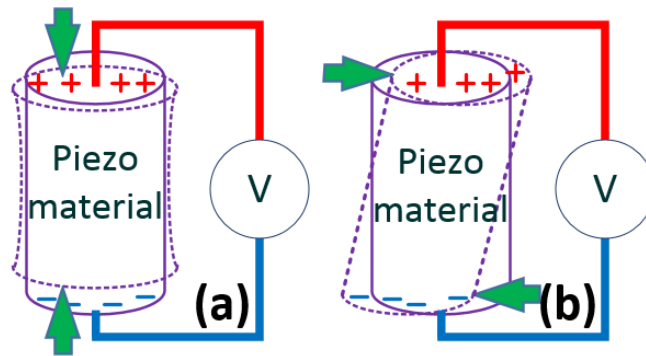


Figure 2. Pictorial illustration of piezoelectric effect upon (a) stress along the material and (b) shear stress.

The materials that present piezoelectric effect are called piezo materials. Piezo materials can be found in different forms including but not limited to single crystals, ceramics and thin films. Figure 2 pictorially depicts the piezoelectric effect. In general, piezo materials have a non centro symmetry, meaning the materials without center of symmetry in the molecular structure. Upon mechanical deformation, the nonsymmetrical structure generates a charge dipole.

In a monocrystal, all the dipoles are aligned as shown in figure 3(a). Hence, the monocrystal exhibits the effect of summation of all dipoles by introducing a net positive charge at one side of the material and a net negative charge at the opposite side of the material. Comparing this to a

polycrystal with random orientation of the dipoles in the volume of the material (figure 3(b)), the net charge is almost zero at the surfaces of the material (no net piezo effect).

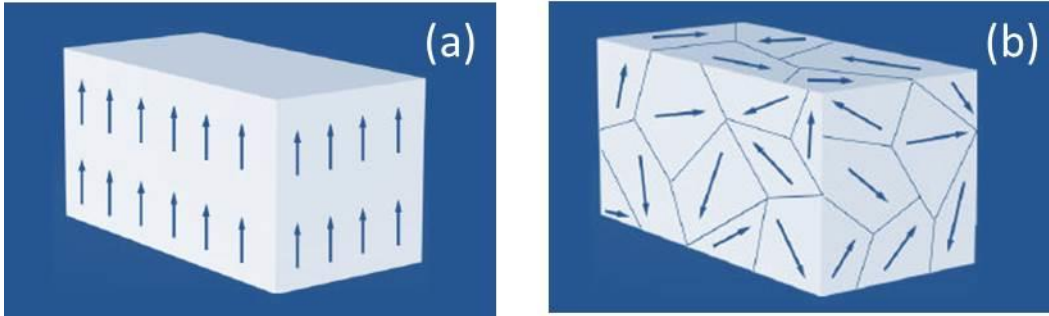


Figure 3. (a) Monocrystal and (b) polycrystal classification of materials for piezoelectric property demonstration.

The amount of the charge generated from the dipoles (piezo charge) is characterized by the charge density at the surface (unit C/cm^2) which is same as the electric displacement (\mathbf{D}). The amount of the electric displacement is a function of the applied mechanical stress (\mathbf{T}). The mechanical stress can be either in a tensile or compressive form and that affects the polarity of the piezo charges. At the same time, because of the dielectric nature of the piezo-materials, the piezo charges introduce a potential difference across the material (ΔV) and an electric field (\mathbf{E}) through the material. The situation when a piezo-material generates electric displacement in response to a mechanical stress is called sensing mode and can be calculated by:

$$D = d.T + \varepsilon.E, \quad (1)$$

where d is the piezoelectric charge coefficient and ε is the dielectric constant. Since the piezoelectric effect is a mutual effect between mechanical deformation and polarization of the material, a piezo-material can be used in the actuation mode when an electric field is applied to produce strain (S) (elongation or contraction). In this mode, the strain can be calculated by:

$$S = s.T + d.E, \quad (2)$$

where s is the elasticity coefficient [8].

Considering that S , T , D , and E are vectors, generally s , d , and ϵ are in form of matrices [8]. Therefore, Equation 1 suggests that any stress to a piezo material may generate electric displacement (D), which is linearly related to the electric dipole moment in the material [8]. According to equation (1), the magnitude of the generated dipole depends on the magnitude and direction of the stress and the value of d in the material. The piezo electric coefficient is different in different materials, and its value depends on the molecular structure and the orientation of the crystal. Likewise, the different mechanical stresses applied on the piezoelectric material also play a critical role in the piezoelectric effect and its piezoelectric potential as depicted in Figure 4.

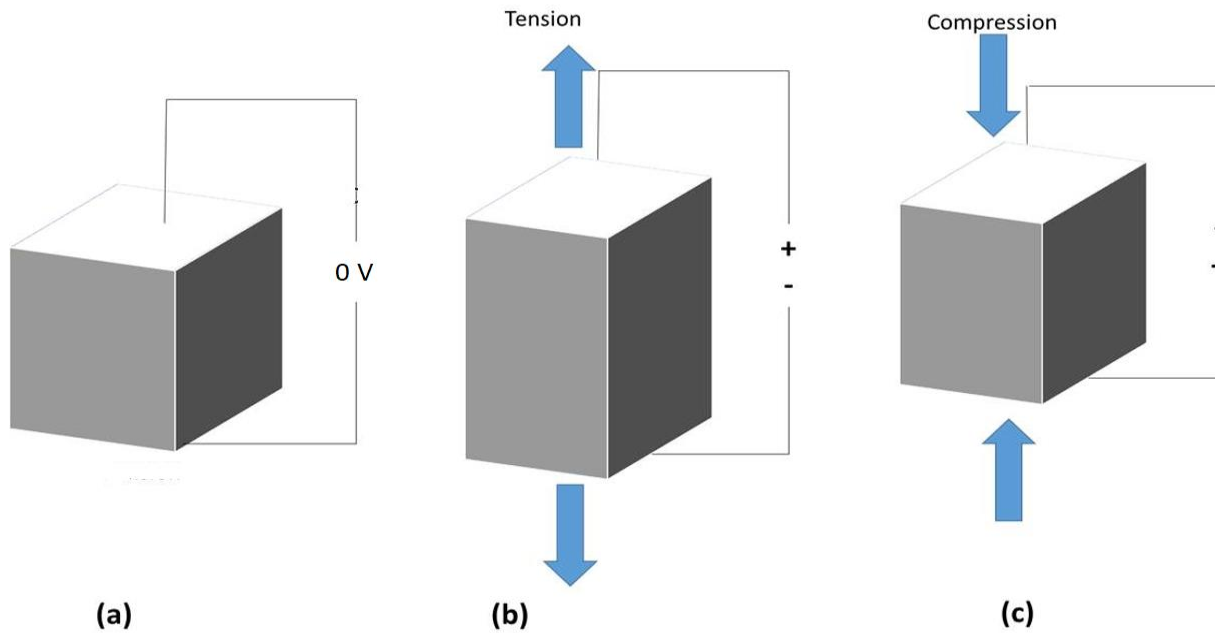


Figure 4. Schematic representation of the piezo charge generation as a result of tension and compression to the piezoelectric material. (a) Piezoelectric material under no strain (b) energy generation under tension and (c) energy generation under compression.

1.2.2 Piezo Energy Harvesters

Although the presented work is not much about usage of piezo-materials for energy harvesting, due to a significant amount of studies on nanoscale piezo-generators, this application of the piezo-materials is reviewed in this section.

Vibrational energy harvesting covers a wide variety of materials from large micro sized devices to nanoscales systems. The most commonly investigated device type is that of resonant mass spring system, piezoelectric cantilever with a tip mass (Figure 5). A major pitfall for such devices is that they are tuned to a specific frequency and the output power declines significantly due to the departure from the resonant frequency. Several types of vibrational energy harvesters such as non-linear oscillators, non-linear bi-stable laminates, tuneable resonators and others have been studied. Also, potential applications of piezo-generators were demonstrated in shoe implants, pressure mats, flexible sails and flag shaped scavengers [10].

Although PZT is the most used piezoceramic, it is not suitable for most of the previously mentioned harvesting methods due to its inherent mechanical ruggedness. Hence, the use of novel nanostructured piezoelectric materials is very much necessary. A few important criterion for these large-area, compliant piezoelectric nanostructures are manufacturability with large degrees of bending to withstand stress.

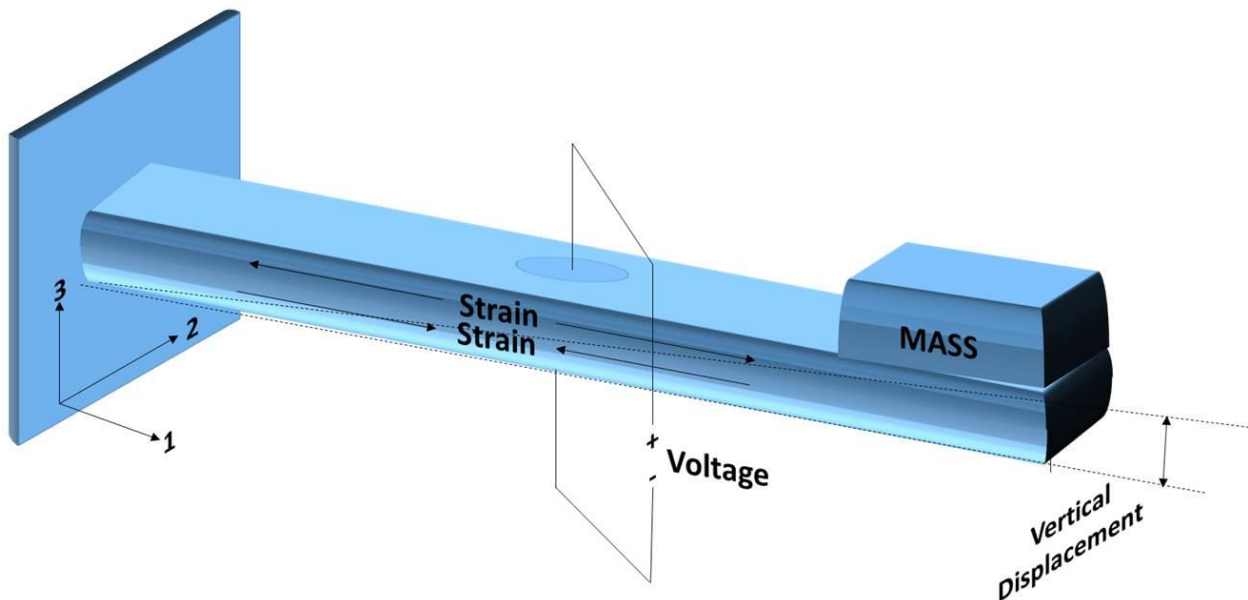


Figure 5. Illustration of a piezoelectric cantilever with a tip mass energy harvester.

1.2.3 Piezo Nanostructures

A wide range of piezoelectric nanostructures have been studied for its electromechanical properties such as (Zinc Oxide) ZnO, Sodium Niobate (NaNbO_3), Barium Titanate(BaTiO_3), Gallium Nitride (GaN), polyvinylidene difluoride (PVDF), PZT, Zinc Sulfide (ZnS) etc. [5]. Among all, ZnO has been vastly studied for nano-generators and nano-sensors, due to feasibility of fabricating/growing various forms of ZnO nanostructures [11]. The atomic structure of ZnO crystal is shown in Figure 6.

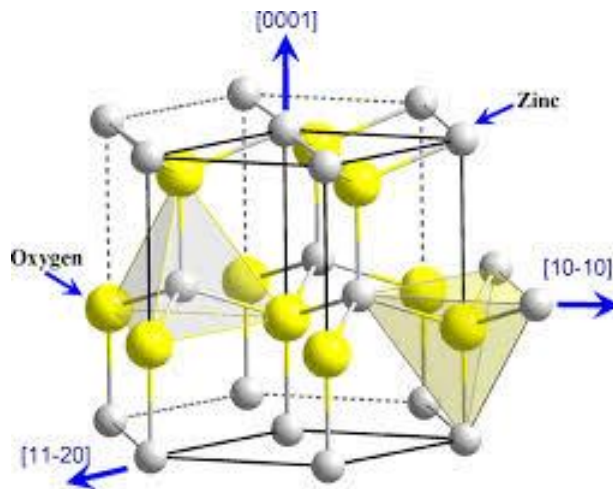


Figure 6. The atomic structure of ZnO crystal (Wurtzite structure). Adapted from [12].

For example, Figure 7 shows a scanning electron microscopy (SEM) image of ZnO nanowires grown using the hydrothermal process. There are distinct advantages of nanostructured piezomaterials in comparison to the bulk piezo counterparts, for example their nano-micro dimensions permits their use in integrated micro-electro mechanical systems (MEMS) and miniaturized optoelectronic devices [13]. Also, the flexibility of nanostructures is useful in fabricating flexible and stretchable electronics. This is mainly due to the small scale of nanostructures. A common method of fabricating piezo-nanostructures is through bottoms-up techniques. Various forms of nanostructures, including nanowires, nanorods, nanoribbons, and nanoflowers can be fabricated by controlling the growth process [14].

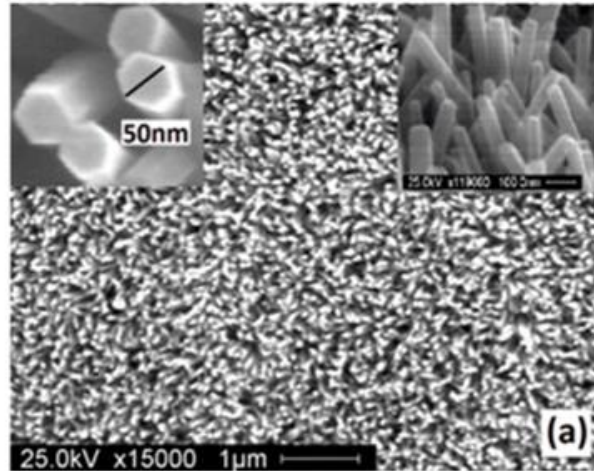


Figure 7. SEM image of the hydrothermally grown ZnO nanowires on an indium tin oxide (ITO) substrate. Adapted from [15].

1.2.4 Piezoelectric Characterization in Nanostructures

Designers of piezo actuators, sensors, or generators often use Equations 1 and 2 to estimate the output of their system based on material characteristics. Employing the equations requires knowing d (piezoelectric charge coefficient), ϵ (dielectric constant), and s (elasticity coefficient). The parameters, especially d , can be measured in a relatively large piece of crystalline material by applying a stress to the material and measuring the piezo response of that. However, piezo characterization of the materials in a nanostructure form is more complicated. Electromechanical characterization of piezoelectric nanostructures either fall under converse piezoelectric or direct piezoelectric measurement [16]. In converse piezoelectric characterization, a piezo response force microscopy is most commonly employed to detect any surface displacement as a result of applied electric field [16]. The displacement usually ranges a few pico meters for materials in nano-dimensions [16]. A conducting tip of atomic force microscope (AFM) can be used to apply the local electric field to the 1D piezo nanostructures such as nanowires or nanorods [16].

Direct piezoelectric measurement involves tensile loading of the piezoelectric nanostructure and simultaneous measurement of the induced piezo charge. Piezoelectric

nanogenerators comprising 1D nanostructures are typically characterized using the direct piezoelectric characterization. Although there are several ways to electromechanically characterize piezomaterials, both the characterization techniques cannot be satisfactorily used for large area 1D piezo nanostructures, due to the countless number of individual structures to be analyzed and characterized. The correlation between the individual characterizations may be a problem to get a complete idea of the piezo layer. A newer technique for piezo electromechanical characterization is called nano-indentation method[17]. Converse piezoelectric effect can be measured by applying a DC voltage to the sample and measuring the displacement with a fixed load nano indentator as shown in Figure 8.

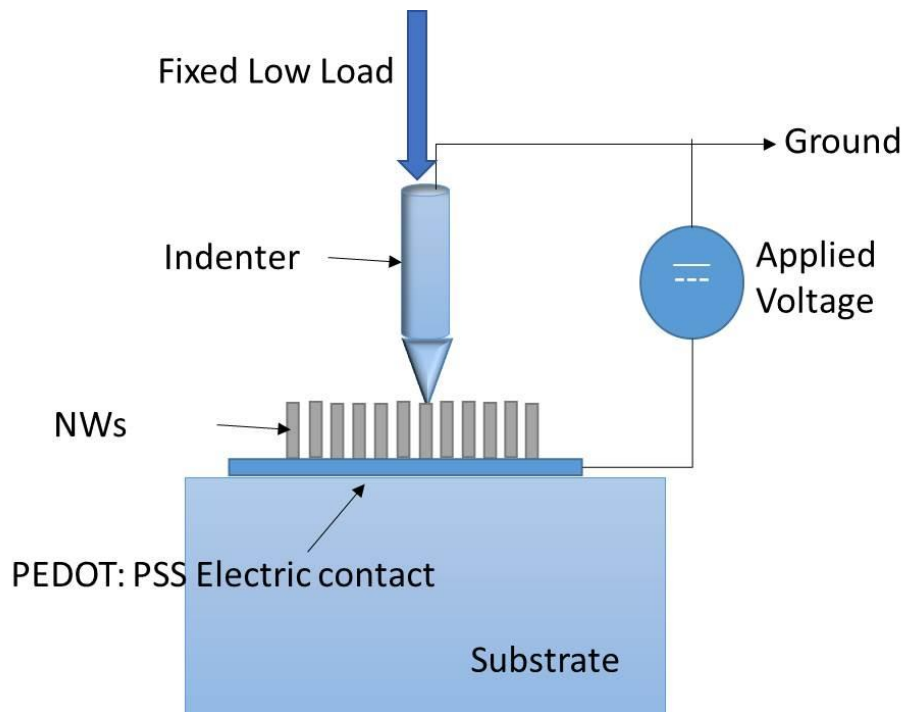


Figure 8. Schematic drawing of the experimental setup for the measurement of the converse piezoelectric effect by nanoindentation. Adapted from [17].

Direct piezoelectric effect can be measured by using nanoindentator under load control and the generated piezoelectric voltage can be measured as a function of the applied load. A pictorial depiction of the direct piezoelectric effect measurement is shown in figure 9.

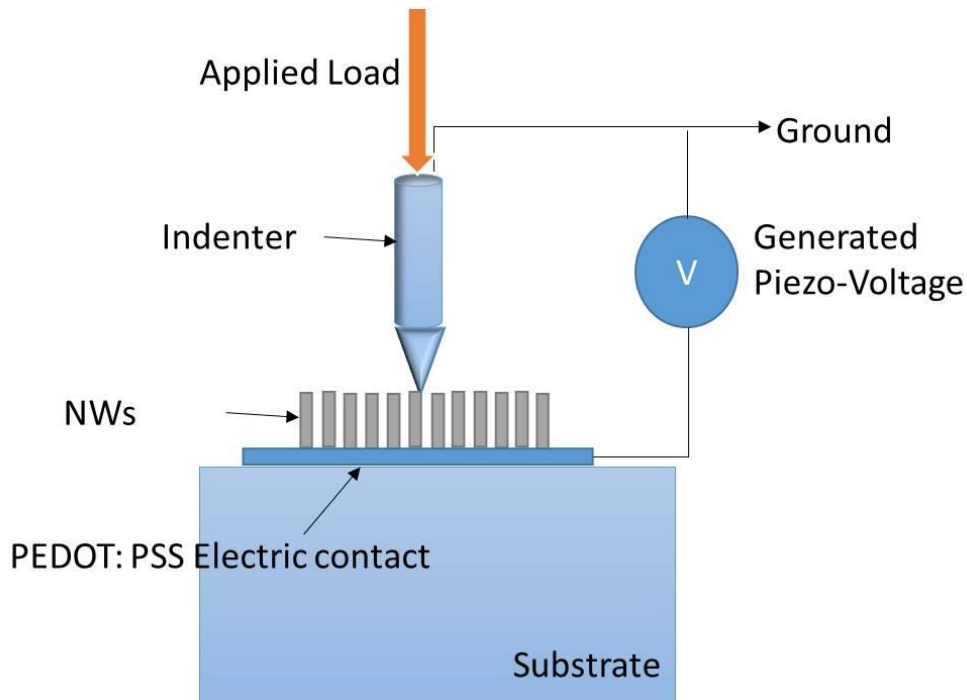


Figure 9. Schematic drawing of the experimental setup for the measurement of the direct piezoelectric effect by nanoindentation.

Nanoindentation technique provides an efficient way to obtain the electromechanical coefficients, converse and direct piezoelectric effect measurement, however it is relatively a slow process and requires high precision electronics to perform accurate measurements. In addition, the nanoindentation technique cannot be scaled up for large area piezo application and characterization. As it has been established that it is critical to characterize the electromechanical property of piezo materials precisely to fully utilize their piezo property in various applications, it creates a unique opportunity to explore piezo potential measurement techniques to suit large area piezo applications.

In exploring the best possible measurement technique to characterize piezo materials, it is important to be mindful of the research problems that need to be solved. Few of the research questions are, firstly if a fast and facile measurement technique available to perform electromechanical characterization on large area piezo surfaces. Secondly, if the measurement

strategy is suitable for different morphologies of ZnO nanostructures. Finally, what can the measured characteristics be used for? It should be noted that ZnO is not only a piezo-material but also a semiconductor that is used in various optical devices. While the semiconducting and optical properties of ZnO have been employed to make efficient optoelectronic devices, exploiting the piezo characteristics of the material in those devices is the subject of new studies.

A part of this work focuses on analyzing the piezoelectric effect from a packed layer of ZnO nanowires (NWs) through a devised electrochemical study method. Compare to the slow method of characterizing all NWs individually with the nano-indenter, the new method is able to give a relatively fast response to a stress applied to a flexible substrate where NWs were grown. This method was employed to study the effect of various shapes of ZnO nanostructures. Other part of this dissertation is focused on employing ZnO nanowires for fabricating and studying a new electro-optical sensor with a dynamic optical memory.

To summarize the chapters in the dissertation, Chapter 1 introduces the market need for piezoelectric technology, piezoelectricity concepts and the background of the problem being studied, in this case being the piezoelectricity in ZnO nanostructures through electrochemical characterization rather than other established techniques. Purpose of the study is investigated through the need for a solution to characterize large area piezo surfaces. Key research questions are highlighted along with the significance of this study.

Chapter 2 describes the material properties of the piezoelectric material of interest, in this case ZnO. Arguments are presented to justify the selection of ZnO for piezo applications as well as its usage in optoelectronics. ZnO NWs low temperature hydrothermal fabrication is detailed. The electrochemical detection method of piezoelectric effect from ZnO NWs is explained. Chapter 3 presents the finding from the flexible substrate orientation for growth to optimize piezo charge

generation. Chapter 4 details the morphology study performed to understand the best morphology to use for various applications and feasibility. Sputtered Planar, hydrothermally grown ZnO NWs and ZnO nanoforest are investigated. Chapter 5 is about the integration of hydrothermally grown ZnO NWs into a photovoltaic device to study the energy band engineering capability of ZnO through piezoelectric effect. An Optical memory made by ZnO NWs integration into an organic bulk heterojunction device is discussed in detail. Oxygen absorption and desorption effect on the optical memory is analyzed. Chapter 6 captures the idea of oxygen deprivation organic bulk heterojunction device in order to understand the effect on the optical memory. Chapter 6 discusses the application of the developed piezo characterization technique and future enhancements to the work.

CHAPTER 2: ANALYSIS OF ZnO AS FUNCTIONAL PIEZO MATERIAL

This chapter dwells deep into the selection of ZnO as the material of interest for both piezoelectric and optoelectronic applications looking into the key properties of ZnO and its nanostructures. Piezo-phototronic effect is analyzed for its application in many optoelectronic devices utilizing the dual property of ZnO as a piezoelectric and semiconducting material. Also, the fabrication of ZnO NWs is elaborated. Electrochemical detection of piezoelectric effect from misaligned ZnO NWs grown on a flexible electrode has been explained.

2.1 Introduction

ZnO has attracted significant attention due to its excellent physical, chemical, electrical and optical properties and is being increasingly used in electronics, optics, acoustics and sensing applications. ZnO is a wide direct band gap (3.37 eV) compound semiconductor with a high exciton binding energy (60 meV) suitable for short wavelength optoelectronics and room temperature efficient exciton emission [18]. ZnO is transparent to visible light and its conductivity can be increased by doping. High thermal and mechanical stability at room temperature makes ZnO an excellent multifunctional material for some sensing and nanogenerator applications.

Other key factors that make ZnO a versatile technology material are its biocompatibility, biodegradability and piezoelectric effect [18, 19]. Synthesis of ZnO nanostructures can be broadly classified into two groups: metallurgical and chemical methods [20]. Metallurgical method focuses on oxidizing Zinc ore to obtain ZnO. Among the chemical methods sol-gel method, solvothermal and hydrothermal method are a few techniques [20]. Hydrothermal method is one of the low temperature technique to synthesize ZnO NWs; and it is the method used for this work. The

hydrothermal method produces vertically aligned ZnO NWs on the substrate. Generally, this structure is suitable where high surface area is needed.

The crystalline structure of hydrothermally grown ZnO NWs is in form of Wurtzite structure. A specific feature in Wurtzite structure - which can be found in many materials such as gallium nitride (GaN), indium nitride (InN), and zinc sulfide (ZnS) – is its non-central symmetric crystal structure, resulting in an inherently piezoelectric behavior [11, 21, 22].

As briefly explained in Chapter 1, piezoelectric effect is due to surface polarization as a result of the mechanical strain exerted to the material. The piezo charge coefficient, d , (also known as piezoelectric constant) varies with different morphologies of ZnO, particularly, the aspect ratio of the ZnO structure is critical in its piezo response [23]. The piezoelectric effect of ZnO has been used in microelectromechanical (MEMS) devices, sensors, actuators and in surface wave acoustic filters and bulk wave acoustic filters [2,3,4,7]. Generally, the effective piezoelectric constant in ZnO NWs is larger than that in the bulk ZnO, due to the free boundary of nanowires assisting in polarization [24]. One-dimensional (1D) nano-structures have the unique advantage over thin films with respect to their aspect ratio, with higher aspect ratio in 1D structures such as rods, ribbons, wires and belts presents a high surface area.

ZnO crystallizes in three forms as hexagonal Wurtzite, cubic zincblende and the rarely observed cubic rocksalt (Figure 10). The ZnO structure has a polar surface (0001), which is either Zn or O terminated and non-polar surfaces (1120) and (1010) possessing an equal number of both atoms [25]. This polar nature is responsible for its high electromechanical coefficient.

One-dimensional ZnO nanostructures are of special importance because they can be used to create piezoelectric diodes and piezoelectric field effect transistors [26, 27]. Electronic components fabricated using nanobelts and nanowires have potential advantage due to the

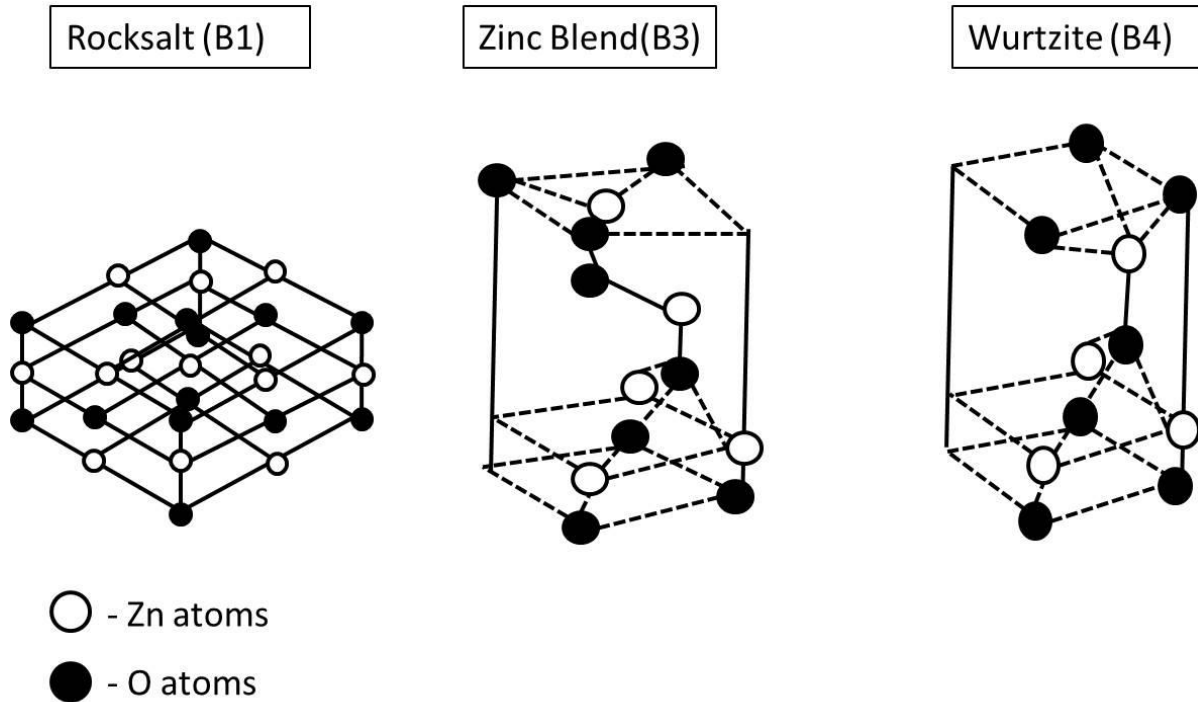


Figure 10. Different forms of ZnO crystals. Adapted from [25].

confined charge motion to one dimension and therefore allow for better charge carrier mobility [23, 26]. The ability to fabricate an electronic component of such a small scale could advance applications where size and space are of extreme importance. The ZnO diode takes advantage of the fact that ZnO exhibits both semiconductor and piezoelectric properties. Normal semiconductor diodes operate using a potential barrier that is set up when an n-type doped and p-type semiconductor come in contact. While ZnO has displayed great potential for n-type doping, methods of p-type doping of ZnO is relatively new and not as reliable at this point [24]. In order to surpass the limitation of the lack of p-type ZnO, the ZnO diode uses the piezoelectric properties of ZnO to create a potential barrier similar to the one that would be present in a normal semiconductor p-n junction [24].

ZnO nanowires can also be used to fabricate field effect transistors. Regular field effect transistors use a potential applied to a gate electrode to create a conductive channel between the

drain and source of the transistor. Due to the piezoelectric and semiconductor properties of ZnO nanowires, a field effect transistor can be fabricated in which the potential from the piezoelectric effect creates the conductive channel between gate and source when the device is under stress. This type of transistor can be used as a force sensor for detection of forces in the nanonewton range or lower [26]. The ability to measure such small forces could prove very useful in the development of nanoscale devices. While the discussions here only highlight a few examples of the several applications of ZnO nanowire based devices, overall ZnO displays remarkable potential for advancing nanoscale devices.

2.2 Piezo-Phototronic Effect

Piezo-phototronic effect is to utilize the piezoelectric potential (piezo potential) that is produced by applying a strain to a semiconductor with piezoelectricity to control the charge generation, transport, separation and/or recombination at metal-semiconductor intersection or p-n intersection for enhancing the performance of optoelectronic devices, for example, photodetector, solar cell and light-emitting diode. Professor Zhong Lin Wang at Georgia Institute of Technology proposed the essential guideline of this effect in 2010 [28].

When a p-type semiconductor and a n-type semiconductor form a junction, the holes in the p-type side and the electrons in the n-type side have a tendency to redistribute around the interface zone to adjust the nearby electric field, which results in a charge depletion layer. The dissemination and recombination of the electrons and holes in the intersection region is closely linked with the optoelectronic properties of the device, which is enormously influenced by the nearby electric field distribution. The presence of the piezo-charges at the interface presents three impacts: (1) a shift in local electronic band structure due to the introduced local potential, (2) a tilt of the electronic band structure over the junction region for the polarization existing in the piezoelectric semiconductor, and (3) a change in the charge depletion layer due to the redistribution of the local

charge carriers to balance the local piezo-charges. The positive piezoelectric charges at the intersection lowers the energy band and the negative piezoelectric charges bring the energy band up in n-type semiconductor area close to the intersection region. A change in the local band by piezo potential might be compelling for trapping charges so that the electron-hole recombination rate can be generally upgraded, which is extremely advantageous for enhancing the performance of a light emitting diode [28, 29]. Besides, the inclined band tends to change the mobility of the transporters moving toward the intersection. The materials for piezo-phototronics ought to have three essential properties: piezoelectricity, semiconductor property, and photon excitation property.

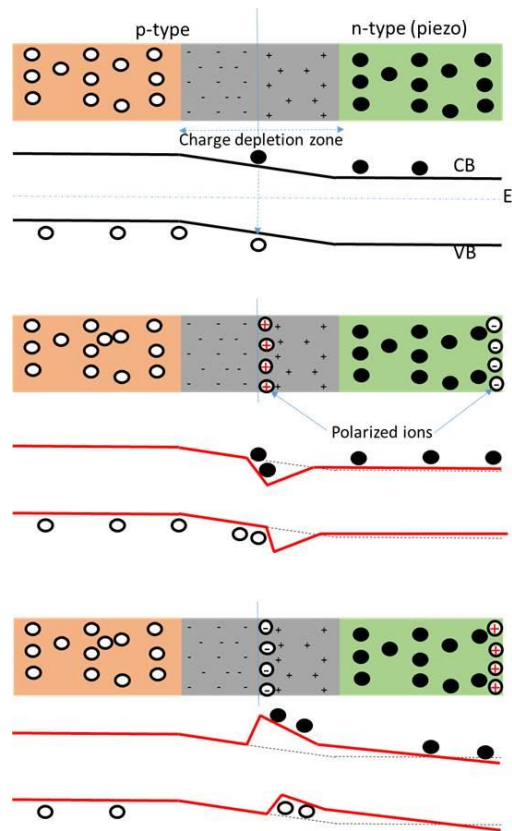


Figure 11. Energy band diagrams for a p-n junction (a) with the absence of piezo-charges, and (b, c) with the presence of positive and negative piezo-charges at the junction, respectively. The red solid lines are the band diagrams with considering the piezopotential. Holes are trapped at the interface due to the piezopotential modified energy band, which will enhance the electron-hole recombination efficiency. Adapted from [30].

ZnO is one of the emerging piezo materials with possible applications in various electro-mechanical devices [31]. ZnO can be deposited as a film with conventional methods such as sputtering [32]. Also, ZnO NWs can be grown vertically on a substrate using a simple hydrothermal growth process [33]. Zhu et al., have shown that vertically grown ZnO NWs can be shaved and laid on a flexible substrate for making piezo sensors [34]. The experiments demonstrated that a voltage difference appears along the NWs when they are bent [34]. Also, Wang et al., have probed the piezo voltage along vertically grown ZnO NWs upon shear stresses applied through an AFM tip [11]. Recently, our lab has found an easy method to induce piezo charges along vertically grown ZnO NWs without any need for shaving them or bend them individually [15].

In this method, ZnO NWs were grown on a flexible substrate, where the growth solution was agitated and hence producing misaligned NWs instead of being in parallel. Due to the physical contact between NWs, stress was applied to the NWs when the substrate was bent. The produced voltage was in the range of 350 mV and was measured using a devised method in an electrochemical cell [15]. The hydrothermal process for producing misaligned NWs and the devised electrochemical measurement are explained in the following sections in this chapter. The details of the process are explained in a published work by a former lab member in the journal of *Electrochimica Acta* [15].

2.3 ZnO NWs Hydrothermal Fabrication Process

This section contains the detail recipe of growing ZnO NW used in various devices presented in this dissertation. The fabrication of ZnO NWs requires the following materials: Indium Tin Oxide (ITO) coated polyethylene terephthalate (PET) to be used as a substrate, 10 mM solution of zinc acetate dehydrate prepared in ethanol to be used as the seeding layer, and equimolar 25 mM zinc nitrate hexahydrate and hexamethylenetetramine (HMTA) in deionized

(DI) water for the growth solution. All chemicals can be purchased from Sigma-Aldrich. A sample of ITO substrate is cut (19.5 mm x 18.53 mm) and secured to a glass slide using double-sided tape. It is important to note at this point to ensure that the double-sided tape is secured to the slide as evenly as possible with no air bubbles; any air bubble or obstructions in the double sided tape could lead to an uneven coating of the seeding layer in later stages of the growth process.

100 μ L of the seeding layer is then deposited onto the substrate using a pipette. The substrate is then spin coated for 45 seconds at 1500 rpm. After spin coating, the sample is dried on a hotplate for two minutes at 150°C. The process of spin coating and drying is repeated 10 times to ensure sufficient coverage of the seeding layer. After the seeding layer has been deposited, the substrate should be secured to the growth mount with the seeding layer facing the bottom of the growth apparatus. The growth apparatus consists of two beakers: one larger beaker to act as a water bath for regulating temperature, and a smaller beaker filled with growth solution for which to submerge the sample. A temperature probe is connected to the hot plate and submerged in the outer beaker to ensure the temperature remains constant. It is important to secure the thermometer since any event of the thermometer leaving the beaker would drastically increase the temperature causing the growth solution to evaporate rapidly. The temperature of the growth solution is kept at 90 °C during growth and stirred using a magnetic stirrer at 425 rpm. The growth time can vary from an hour (minimum time to have partial growth of NWs) to several hours. The level of both the water in the outer beaker and the growth solution in the inner beaker are important during this stage. The inner beaker is filled to maximum capacity while avoiding overflowing so that the sample remains submerged even in the event of some evaporation of the growth solution as any period of time with the sample not completely submerged would lead to critical failure of the sample. Additionally, the water level in the outer beaker should match the level of the growth

solution in the inner beaker as closely as possible to avoid a temperature gradient. When repeating the growth process, both the growth solution and seeding layer are sonicated for 5 minutes prior to being used to ensure consistency of the solution. The beaker containing the growth solution is thoroughly cleaned between fabrication of samples using the following method: scrub and rinse with tap water and wire brush, rinse, in the following order, with DI water, isopropanol, acetone, and DI water, and the thoroughly dry using a standard hair blow dryer. Figure 12 shows a pictorial representation of the fabrication process for ZnO NWs growth.

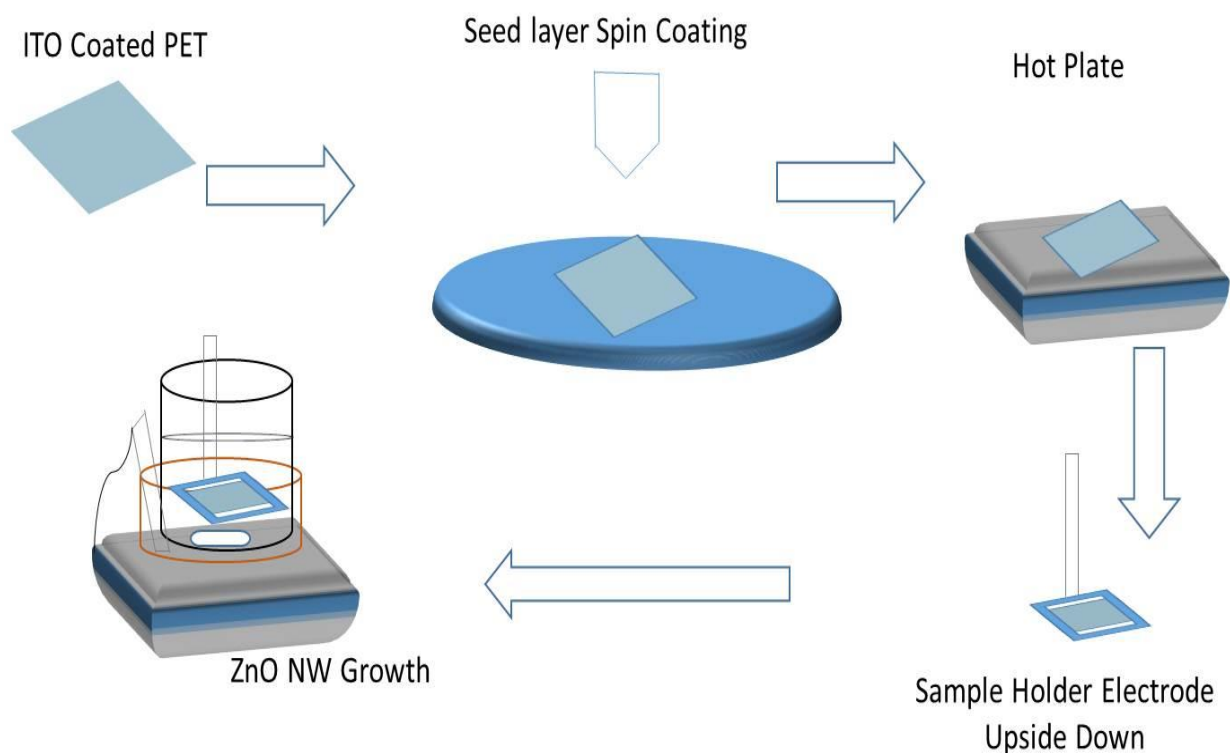


Figure 12. Visual representation of the ZnO NWs fabrication process. Adapted from [15].

2.4 Electrochemical Detection of Piezoelectric Response of ZnO NWs

In this section, a devised electrochemical method for detecting the piezo electric response is explained. The method has been used for various samples that have been fabricated in this project.

The piezo electric effect of the samples is characterized using cyclic voltammetry (CV) in a three-probe electrochemical cell. This specific test is advantageous due to the redox reaction that takes place between the sample and the ferrocene mediator ($Fe(C_5H_5)_2$). The redox state of ferrocene can be changed in an electrochemical process described by:



In an electrochemical cell with a polarizable electrode, the electrochemical potential for the ferrocene redox reaction is about 0.5 V versus a standard calomel electrode (SCE)[35]. The electrochemical potential of the reaction can be detected via the CV method, in which a redox current peak appears near the electrochemical potential when the voltage of the electrode is scanned backed and forth. For a standard polarizable electrochemical electrode (e.g., carbon electrode), the voltage at which the peak is observed is only depends on the concentration of ions in the electrolyte. However, detection of the current and measured voltage is through connections from an external instrument (called potentiostat) to the electrodes of the cell. Therefore, if there is any voltage drop at the interface between the electrode and the electrolyte, that voltage directly affects the voltage of the peak current in the CV measurement.

In cyclic voltammetry there are two types of peak current being measured, one is cathodic peak and other is anodic peak each of the peak are representative of the reduction and oxidation reaction of the analyte. The current being measured is the current at the working electrode with respect to the applied potential. The definition of the current peak is very distinguishable for reversible reaction, whereas for irreversible reaction there is some ambiguity with respect to the exact peak current and its electrochemical potential. In most scenarios the software associated with the potentiostat being used will analyze the CV data to provide the respective key parameters of the experiment, in this case the peak current and electrochemical potential value. Several analytical

techniques can be employed to find the occurrence of the peak current such as residual method, trend reversal, first derivative assessment and many more. A combination of these techniques has been used for accurate peak detection. The first derivative of a peak has a downward trending zero crossing at the peak maximum and potential value where the first derivative is zero. The presence of noise in the measured data can skew the results leading to false peaks; therefore, it is important to smooth the data before processing for peak detection.

Employing this electrochemical feature, the piezoelectric properties of the sample can be accurately studied by monitoring the shift of the peak in the CV results when a mechanical stress is applied to the ZnO NWs. To apply the stress, the sample is placed in an adjustable mount (shown in Figure 13) with a copper contact on one end so that the sample may be used as the working electrode in the cell. A platinum wire is used as the counter electrode, and Ag/AgCl is used as the reference electrode. The electrolyte used for the cell is aqueous based 0.1 M Tris buffer (pH 8.0) with 0.75 mM ferrocene as the redox material. The test is conducted using the VersaSTAT4 Potentiostat and VersaStudio software on a desktop computer. To begin the test, the sample is placed into the adjustable mount and the mount is adjusted to the samples resting curvature. The samples resting curvature is defined as the curvature that the sample was held to during growth and is found by placing the sample into the mount and adjusting the screw until the sample begins to hold tightly in the mount. The length of the sample is measured at this point. A multiple cycle CV scan can be tested on the sample by scanning voltage between -0.8 V to +0.9 V at a scan rate of 50mV/s. After the first CV scan is completed, the mechanical stress can be applied to the NW by simply bending the substrate. The designed structure in Figure 13.b shows that how the sample can be bent by turning the screw at the top of the sample holder. Repeating the experiment for various curvatures, the effect of the generated piezo potential on the CV response can be studied.

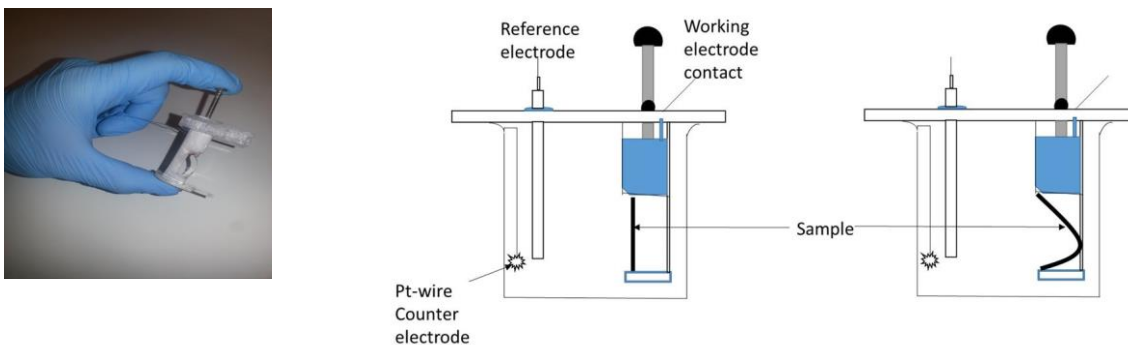


Figure 13. A picture of the sample holder designed for bending the samples (left) and diagram of the electrochemical cell when the sample was tested in the flat and bended mode (right).

The described electrochemical characterization method was previously used in our lab for studying the piezoelectric effect in vertically grown misaligned ZnO NWs [15]. The results of that study is presented here (Figure 14) as the reference to the new study for various ZnO nanostructures. In Figure 14(a), it is observed that there was no peak in the CV scan for ITO in Tris while the CV scan for ITO in ferrocene displayed a pronounced peak around 0.35V. In Figure 14(b) it was observed that bending of the ITO alone did not shift the potential for which the peak took place as for all three scans at different curvatures the peak took place at 0.35V.

As explained in the next chapters, clear shift in the peak is detected in the samples with ZnO nanostructures when the samples are bent.

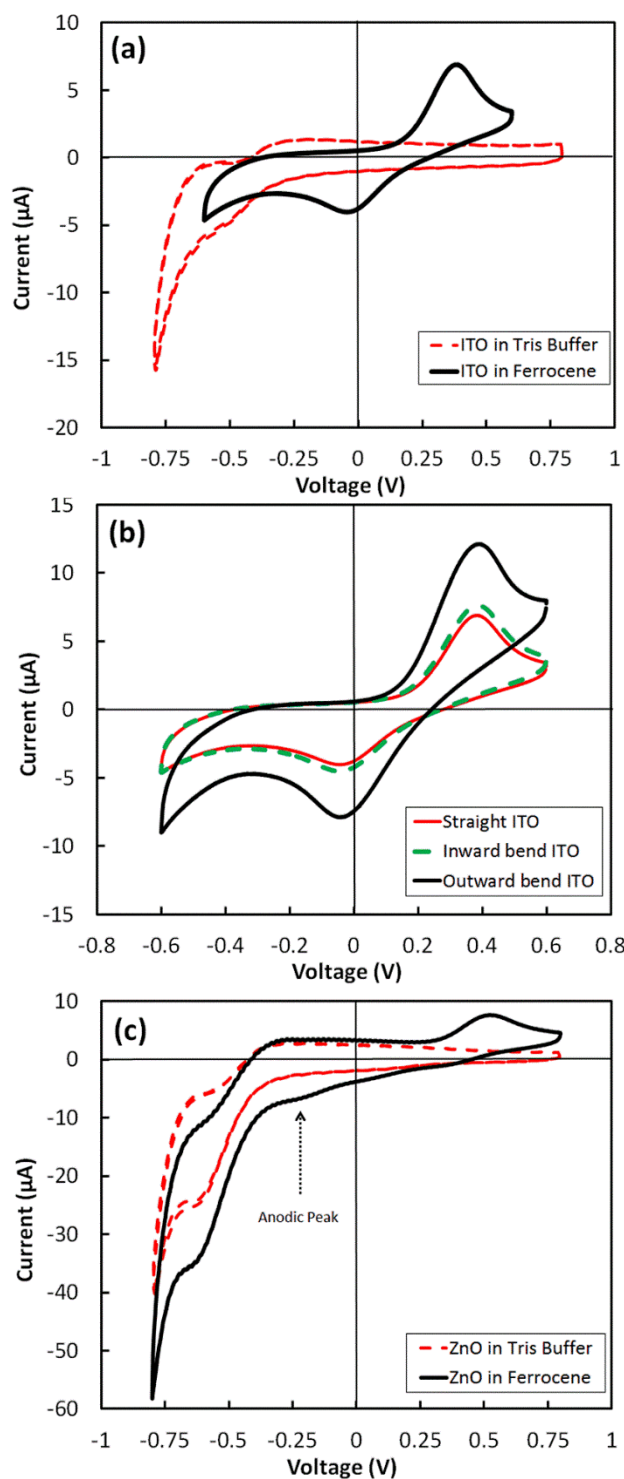


Figure 14. (a) Displays CV scans for both ITO in Tris and ITO in ferrocene which demonstrates that the redox reaction with ferrocene will show a peak in the CV scan. (b) Shows CV scans of straight, inward bent, and outward bent ITO. These results demonstrate that ITO itself does not have a piezoelectric effect that shifts the peak of the redox reaction. (c) Demonstrates that there will still be a peak from the redox reaction when a ZnO sample is present rather than just ITO. Adapted from [15].

CHAPTER 3: ELECTROCHEMICAL MEASUREMENT OF THE PIEZO VOLTAGE IN ZnO NANOWIRES GROWN ON CURVED AND FLAT SUBSTRATES

3.1 Abstract

ZnO NWs have a high electromechanical coefficient and have been widely investigated in electronics, optics and photonics due to their excellent optical and electrical properties. The piezoelectric effect generated by mechanically stressing the substrate with these ZnO NWs have been studied previously using an electrochemical technique and proven to induce a substantial piezoelectric effect potentially suitable for energy harvesting applications. This work focuses on characterizing the differences between ZnO NWs grown on curved and flat substrates incorporating both structural and piezoelectric properties. Piezoelectric properties were tested using an electrochemical cell with an electrochemically active redox material (ferrocene). The difference in piezo voltage between a flat sample and a bent sample that has been intentionally flattened is the main objective of this study. The results show that it is feasible to employ the initial stress on the samples grown on a curved substrate to tune the piezo response of the samples in the flattened mode.

3.2 Introduction

Nanodevices cannot rely on bulky energy sources such as batteries for its functioning. Nanogenerators capable of harvesting energy from ambient vibrational and light are more favorable options for those devices. Nanodevices using nanogenerators as power sources open up a wide range of applications such as implantable bioelectronics, wireless sensors utilized for autonomous structural monitoring, environmental sensing devices and many more [36] Vibrational

energy harvesters come in all sort of sizes such as those embedded within energy scavenger shoes utilizing certain piezoelectric crystal under mechanical strain. Micro generators used in MEMS can be made of two layers of a piezo material in a beam structure (Figure 5). The top piezo layer is under tensile strain and the bottom layer is under compressive strain, which results in positive and negative voltage across the beam. Although the approach is suitable for many micro fabricated systems, such gravity assisted mass loaded vibrational energy harvesters cannot be used for nano devices due to the limitations created by their size. Vibrational energy harvesters are more useful for nano electromechanical systems (NEMS) based devices due to the low requirement of power. Hence piezoelectric power generation at nanoscale using new flexible substrates is the solution to address this issue.

ZnO is one of the promising materials for energy harvesting and sensing applications. Previously many investigations have been performed to study the relation between the size of a piezo nanostructure and piezoelectric coefficients in materials such as ZnO and GaN [37-39]. These studies have revealed that changes in local polarization and reduction of unit cell volume when compared to the bulk values are the main reasons behind the size dependent variation of the piezo effect exhibited[39].

While some works were focused on studying the piezo effect from a single nanowire [27], previously in our group, Ebrahimi et al. investigated the piezo effect of the layer of vertically grown ZnO NWs on a flexible ITO substrate [15]. In that work, the electrochemical method explained in Chapter 2 was used to detect the effect of the generated piezo voltage when the sample was bent. Using Ebrahimi's characterization method, in this chapter, we report on the work that involves ZnO NWs grown on both a flat ITO surface as well as curved ITO surfaces and are tested

comparatively to investigate the effect of initial surface curvature on the piezoelectric properties of the samples.

3.3 Experimentation

3.3.1 ZnO NWs Fabrication Using Hydrothermal Technique

ZnO nanowire synthesis was performed using hydrothermal solution agitation technique adapted from the work of Ebrahimi et.al on ZnO NWs [15]. The details of the process of spin coating the seed layer and the growth bath setup are also explained in Chapter 2. Since this study was focused on investigating if the initial curvature of the sample at the growth time affects their piezo response, two different mounting setups were used for the growth process. As shown in Figure 15(a), one sample holder was designed to keep the ITO substrate in a flat position when it was submerged in the growth solution after being coated with the seeding layer. The other mounting setup (Figure 15b)) was designed to hold the sample in a bending form. Both samples were put in the growth solution for 4 hours.

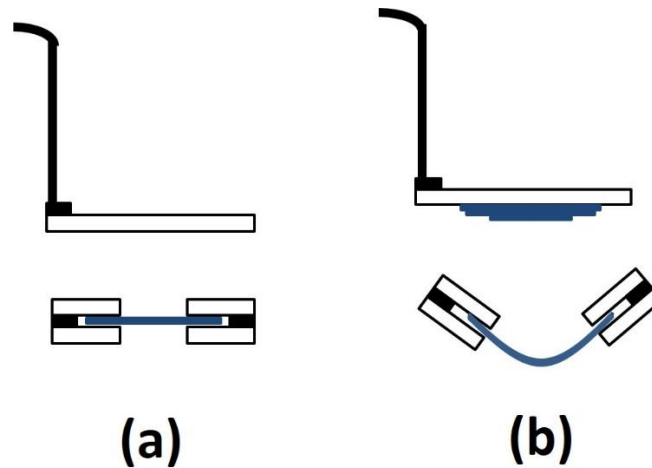


Figure 15. (a) Flat position sample growth holder and (b) bent position sample holder.

3.3.2 Sample Curvature Measurement

After growth, both samples were tested in an electrochemical cell containing ferrocene as the redox mediator (see the details in chapter 2). The redox peak of ferrocene in the electrochemical

CV experiment was used as a probing mechanism to measure the piezo voltage in the samples. To apply mechanical stress, a setup was designed to bend the samples when being submerged in the electrolyte. As shown in Figure 15, the bending setup was made of a stationary and a sliding jaw that the gap between them could be changed via the screw at the top of the sample holder. Samples were loaded in the setup in a flat position by gently adjusting the screw to hold the sample. During the experiment, if different curvatures were desired, the adjustment could be made by turning the screw. Both bending inwards and outwards could be applied to the samples. The previous work by our lab members showed that bending a sample with grown ZnO NWs generates some piezo voltage due to the mechanical stress between adjacent NWs when the substrate was bent [15]. The similar experiment was conducted for this research aiming to find if there is any difference between two samples: one being positioned as a flat substrate and the other in an already curve position during the ZnO NWs growth process. To make the comparison, it was essential to measure the bending curvature at any position when the electrochemical measurement was carried out. The curving measurement was done in a pre-calibrated process by estimating the radius of the curvature. The calibration process is explained here.

To calculate the curvature of the sample precisely, a custom-made setup shown in the figure 16 was used. The setup consisted of a screw mechanism to compress the sample gradually. By increasing the number of turns applied on the screw head, different degrees of curvature was obtained. Table 1 shows the data recorded for the chord length (D) with the increase in the number of turns. The tabulated chord length was measured using a Vernier caliper for three consecutive times and its average was calculated.

Figures 16a and 16b show the curvature inducing set up containing the flat and bent sample respectively. The curvature was calculated by using the chord length and arc length of the sample

as shown in figure 16 c. Arc length (A) denotes the length of the sample. With this increase in the number of turns applied on the screw head, the sample compresses leading to smaller chord length (D) comparatively. If the angle, θ , is expressed in degrees, the equation that relates A to the radius of the curvature, R , would be:

$$A = 2\pi R * \theta / 360. \quad (4)$$

At the same time, D can be defined as:

$$D = 2 * R * (\text{Sin}(\theta / 2)). \quad (5)$$

In these equations, A is a constant (the initial length of the sample in the flat position) and D was measured at different number of screw turns. Solving both equations, one can find R for different length of D . While R is the radius of the curvature, the curvature, κ , is defined as $1/R$ with the unit of cm^{-1} .

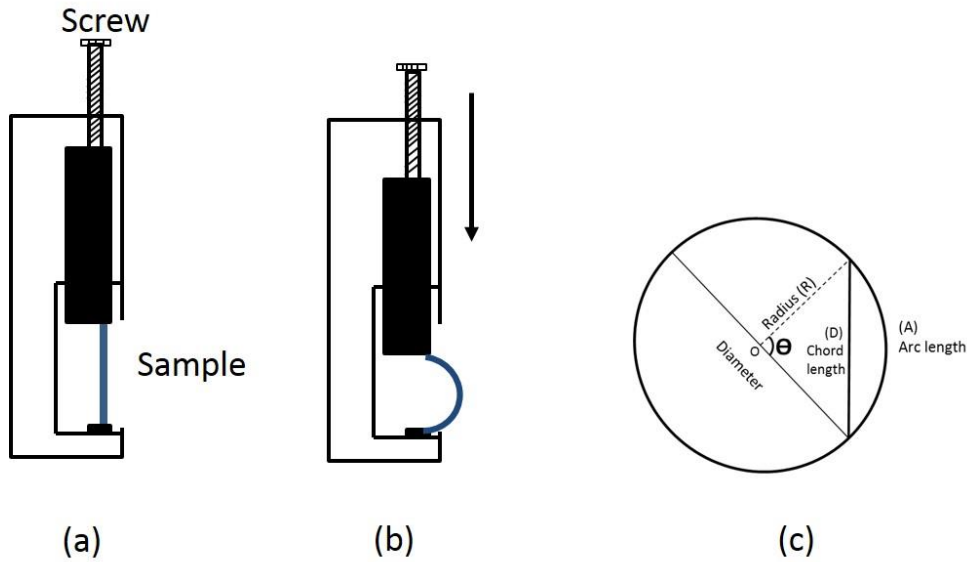


Figure 16. Custom setup used for bending samples during the electrochemical measurements. Two positions are shown: (a) sample under zero compressive strain (b) compressive strain applied on the sample. (c) An illustration of the parameters involved in curvature measurement.

In the calibration process, a piece of PET substrate was cut with the exact length of the samples. The PET substrate was loaded in the setup and D was measured for different number of

turns on the screw. The calculations were done to convert the data to the curvature of the samples and finding the corresponding value of κ at different turnings (results presented in Table 1).

Table 1. Correlation between the number of turns applied in the sample holder to the curvature of the samples with an initial length of $A = 1.94$ cm.

Turns	κ (cm ⁻¹)
0	0.000
1	0.435
4	0.990
6	1.274
8	1.562
10	1.869

3.3 Results and Discussion

Figure 17(a) and 17(b) shows the SEM image of ZnO NW grown through the hydrothermal process on a flat substrate and a curved ITO substrate. In both cases, NWs were grown for a total of 4 hrs and all the growth conditions were preserved to characterize the impact of the growth curvature on the piezoelectric response of the samples. The NWs measured approximately 900 nm – 1100 nm in length and a diameter of 50 nm. Figure 17(a) shows homogeneous coverage of ZnO NWs due to the even coating of the seeding layer on the flat ITO surface. Although majority of the surface on the curved sample was representative of even coverage of ZnO NWs, some clusters were observed, possibly due to the mechanical strain exerted during fabrication and the resulting micro cracks developed on the ITO substrate.

The samples grown on flat and already bent substrates were tested for the electrochemical CV measurements in a three-probe configuration with a Pt wire and Ag/AgCl as the counter and reference electrodes, respectively. The voltage on the working electrode was swept from -0.8 V to +0.8 V. The CV scan rate was set to 0.05 Vs⁻¹. The experiment was performed initially using a flat substrate and measuring the CV response of the sample.

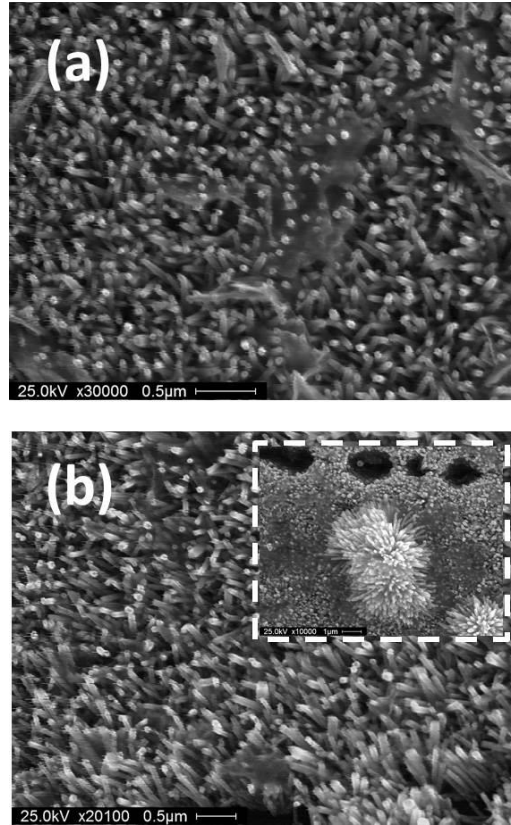


Figure 17. SEM images of 4 hrs grown ZnO NWs on (a) the flat substrate and (b) the curved substrate (Inset: indicative of the ZnO NW clusters).

Figure 18 shows the outward and inward bending CV characterization performed on the flat grown ZnO NWs samples respectively. In Figure 18(a) and (b), it can be seen that the voltage was swept between -0.8 V to + 0.8 V for the flat condition (straight position 0) and subsequent two increasing bending. Due to the shift in the cathodic peak to the right, the sweep was altered to -1 V to +1 V. The flat position yielded the cathodic peak at 0.5 V and further bending pushed the peak to the right, indicating the increase in the piezo potential. Outward bending 1, 2 and 3 represent the curvature of the sample at 0.99 cm^{-1} , 1.274 cm^{-1} and 1.562 cm^{-1} , respectively. The experiment was carried out by bending the sample to the required curvature and performing the CV scan for 5 cycles. The results shown are from the 5th cycle. The sample was bent further from the previous position to evaluate the piezo potential. In the range of bending performed on this

sample, the peak voltage shifted from 0.5 V to 0.575 V in gradual increments. The experiment then was repeated for the same sample being bended inward at those curvatures. The results are presented in Figures 18(c) and (d). As shown in Figure 18 (d), the voltage shift ranged between 0.5 V to 0.54 V. Inward bending 1,2,3, and 4 represent curvature of the sample at 0.99 cm^{-1} , 1.274 cm^{-1} , 1.562 cm^{-1} and 1.8 cm^{-1} respectively.

The curved grown ZnO NWs were also characterized for its piezo response using the same electrochemical setup used for the flat grown sample. The piezo characterization was carried out differently compared to the flat grown sample. The curved grown ZnO NWs has an initial curvature associated with it, due to the way it was fabricated. In this case the curvature was set to 1.0 cm^{-1} inward bending. The curvature value was arbitrarily selected.

The piezo characterization was performed first by flattening the curved grown ZnO sample and measuring the CV response and latter straining the sample in different increasing extends of outward and inward curvature. The sample was flattened after the completion of outward bending and the CV response recorded. The sample was strained outward starting from 1 cm^{-1} to a higher curvature in the range of 1.8 cm^{-1} and the same was true for the inward bending process. This variation in testing the curved grown ZnO sample allowed for the precise behavioral analysis associated with the impact of initial curvature on the overall piezo response. Figures 19 (a) and (b) represent the flattened and outward bending CV response of the sample. The voltage sweep was varied between -0.8 V to 0.9 V. The redox peak for the flattened position represented by straight position 0 in Figure 19 shows that it occurs at 0.45 V. The subsequent outward bending yielded a right shifting cathodic peak with increasing outward curvature. This response is similar to the outward bending response of the flat grown sample. The voltage shifted between 0.44 V to 0.54 V. Figure 19b shows the zoomed view of the CV response.

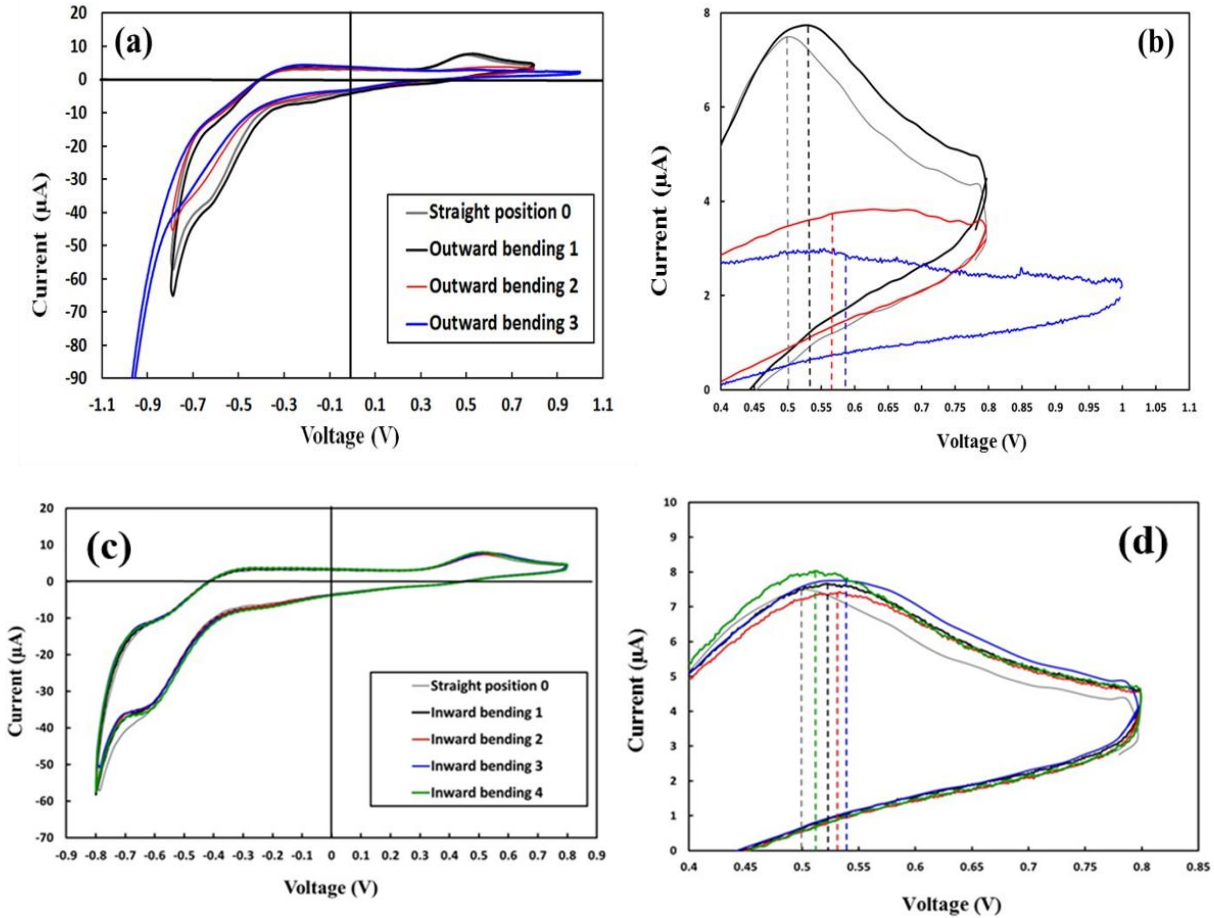


Figure 18. CV results from the 4 hrs grown ZnO NW sample on a flat substrate at (a) different outward and (c) inward curvatures. The zoomed view of (b) outward and (d) inward bending at increasing curvatures.

Figures 19 (c) and (d) show the inward bending CV response of the curved grown ZnO NWs sample. After the completion of CV characterization for the outward bending experimentation, the sample was flattened again using a plastic transparency as a supporting template to retain its flattened shape and recorded its CV response. The initial flattened response and the second flattened response overlapped with one another, this was indicative of an insignificant damage of the sample during the outward bending exercise. The sample was prepped for the inward bending by removing the plastic transparency. The sample regained its initial growth curvature of 1.0 cm^{-1} . Due to the outward curved shape of the sample, performing the inward bending experiment was quite challenging. The sample tried to revert to its original growth

curvature. Care was taken to perform the inward bending process slowly. The inward bending experiment was carried out by bending the sample inwards in increasing extends of curvature. The inward curvature ranged from 1.0 cm^{-1} to 1.8 cm^{-1} . A complete opposite response was observed for the inward bending exercise, the cathodic peak representative of redox potential shifted left with increase of curvature. The decrease of piezo potential could possibly be due to the outward grown ZnO NWs sample failing to attain maximum interaction among ZnO NWs during the inward bending. This response was also observed in the flat grown ZnO sample, where after a certain value of inward curvature the piezo potential dropped.

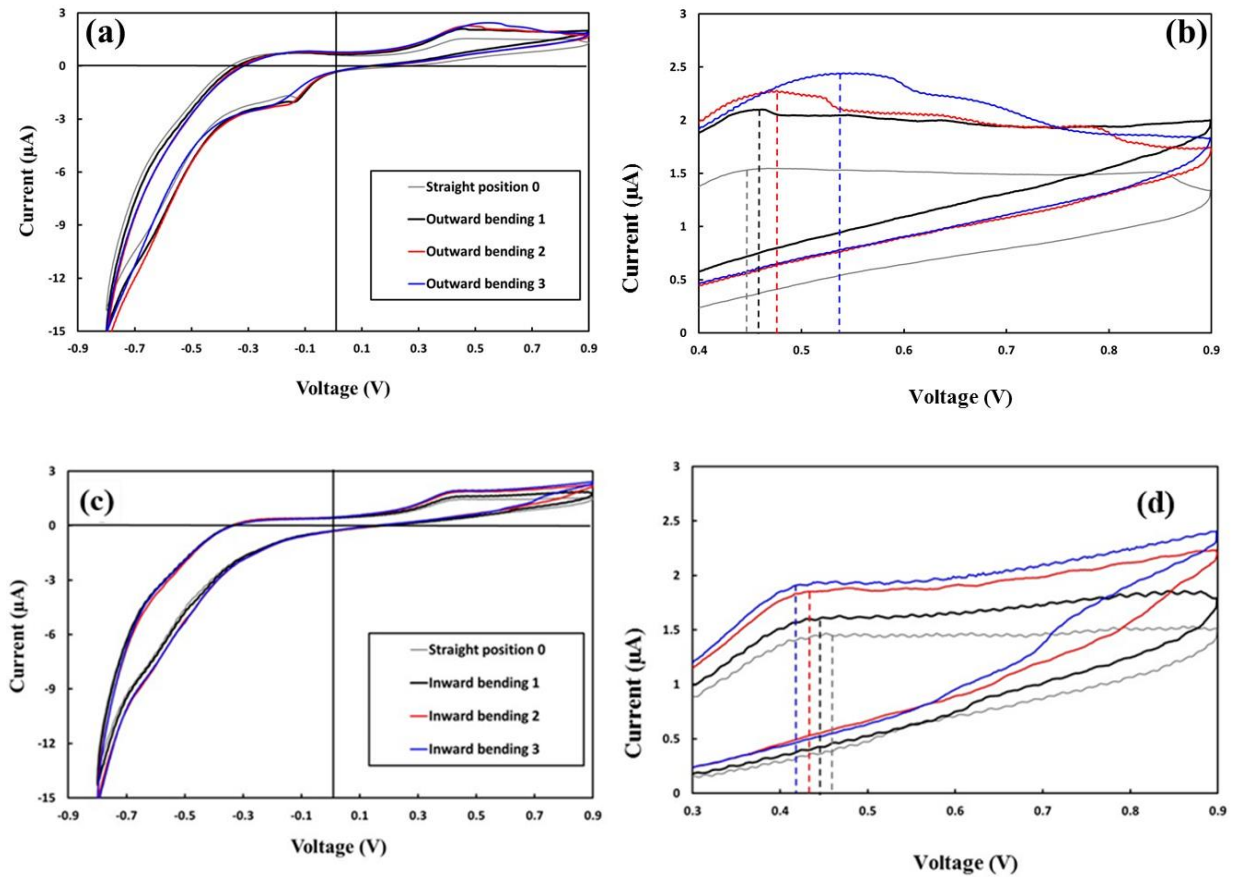


Figure 19. CV results from the 4 hrs grown ZnO NW sample on a curved substrate at (a) different outward and (c) inward curvatures. The zoomed view of (b) outward and (d) inward bending at increasing curvatures.

In order to characterize the piezo response of the two samples, in Figure 20, the potential values at which the peak was observed are plotted versus the curvature of the samples. In this figure, outward bending is presented with negative values of the curvature and inward bending is defined with positive values. The trend in outward bending was similar in both cases in which the voltage value increased as the sample was bended to higher level of curvature. However, inward bending response was different in the two samples. In fact, the sample with the NWs grown on the bending mode showed a consistent trend of reducing voltage as the curvature was changed from outward bending to the flat and further to the inward bending. This indicates that by pre straining the substrate a substantial piezo potential can be held within the ZnO nanowires. By applying an inward strain, the piezo generated charges can be reduced and hence the reduction in piezo potential.

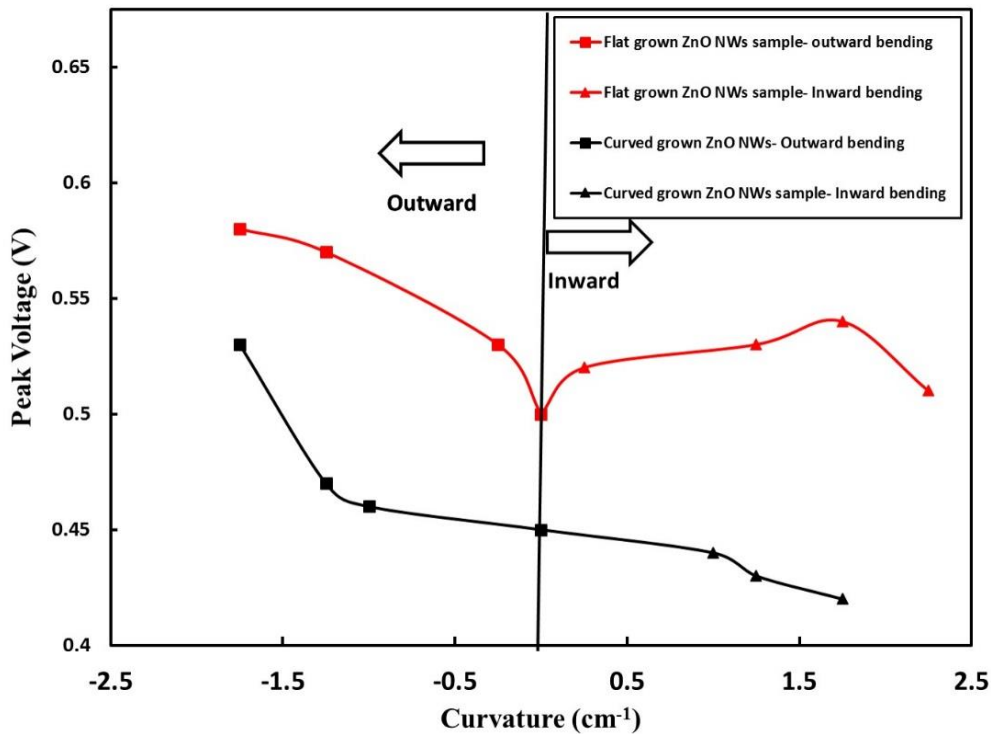


Figure 20. Ferrocene peak potential versus curvature in flat grown and curved grown ZnO NWs samples.

It should be noted that the voltage value in Figure 20 is an indication of the piezo effect but the polarity and magnitude of the voltage drift is not necessarily represent the exact potential or the polarity of the piezo charge on NWs. An obvious reason is that the electrochemical measurement method can show the overall voltage effect by many NWs while the charge distribution and piezo potential across each NW can be very different than other NWs. Nevertheless, the results confirm that the growth conditions can be controlled to generate some initial stress among entangled NWs in order to engineer structures with a more predictable piezo response.

3.4 Conclusion

A densely packed and randomly aligned ZnO NWs was fabricated on an ITO substrate with no strain and pre strained surface. An innovative electrochemical piezo characterization technique was employed to evaluate ZnO NWs on different mechanically strained substrates. The shift in the ferrocene redox reactive was utilized to characterize the piezo potential from the nominal redox reduction potential of 390 mV for ferrocene. It was seen that by using the growing the NWs on a pre strained substrate, the piezo potential of the flattened substrate can be manipulated as per the application requirement. Overall, a desired piezo potential can be developed on the ZnO NWs through pre straining method. This paves ways for usage of ZnO NWs for energy engineering in many devices.

CHAPTER 4: PIEZO CHARACTERIZATION OF ZnO NANOSTRUCTURES USING ELECTROCHEMICAL APPROACH

4.1 Abstract

Piezo response of piezoelectric materials is highly influenced by the morphology of the material. Hence understanding the impact of morphology is a key in being able to utilize the piezoelectric nanostructures to its full potential. In this work, three types of ZnO nanostructures (i.e. ZnO nanowires, ZnO nanoforests, and thin-film sputtered ZnO) are characterized for piezo response using electrochemical cell containing an electrochemically active redox material. It was found that 100 nm thick ZnO nano film can match or even give a higher piezo potential when compared with the 1 μm thick ZnO nanowires in the range of 170 mV to 305 mV. The branched nanoforest yield twice as much piezo potential compared the single step nanowires when strained in a preferential outward curvature.

4.2 Introduction

ZnO has applications in chemical and biological sensors due to its biocompatible, non-toxic, biodegradable and high sensitivity properties [18, 40, 41]. Nano actuators find ZnO useful due to its piezo electric and pyroelectric nature [42]. Water splitting, photovoltaic and charge storage devices utilize ZnO for its photocatalysis property [18, 43-45]. Naturally, due to these properties, ZnO has applicability in a wide range of fields like electronics, optics and photonics to name a few. ZnO is a unique and versatile technology material that exhibits semiconducting and piezoelectric dual properties. It is also transparent to visible light, making it a key material for optoelectronic devices [46]. The strong piezoelectric property in ZnO is a result of large

electromechanical coupling due to the absence of a center of symmetry in Wurtzite crystal. Wurtzite ZnO has a hexagonal structure, the structure can be described as a number of alternative planes composed of tetrahedrally oriented O^{2-} and Zn^{2+} ions [18, 47]. Shrinking ZnO to its nanoscale leads to varied behavior which is heavily dependent on size and shape [48]. By changing the morphological aspect of ZnO through synthesis, it is possible to obtain a wide variety of structures with finely tuned properties. A pervasive phenomenon with these wide range of ZnO nanostructures is quantum confinement [49]. Quantum confinement refers to the phenomenon where de Broglie wavelength associated with the electronics starts to become larger than the nanostructures. As the size of the particle reaches nanoscale range, the decrease in confining dimensions leads to discretization of energy levels and an increase in the band gap [48, 50]. Nano particles of the same material have a larger energy band gap compared to its bulk counter parts as a result of quantum confinement [49].

Several nanostructures of ZnO, such as nanobelts [51, 52], nanorings [53, 54], nanohelices [55, 56], nanotubes [57, 58], nanorods [59, 60], and nanowires [61-63], can be synthesized using different techniques, namely aqueous solution synthesis [15, 64-67], thermal evaporation [68, 69], laser ablation [70, 71], electrodeposition [72], and metal-organic vapor phase epitaxy [73]. The vapor transport technique involves generating zinc and oxygen vapor through carbothermal reduction of ZnO powder at temperatures of 900° C and upwards [74, 75]. Solution-based ZnO synthesis is one of the widely used techniques for applications using flexible substrates due to its low temperature, wide range of substrate compatibility like paper [76], polyethylene terephthalate (PET) [15] and silicon wafer [77].

Among the ZnO nanostructures, nanowires and its derivatives play a key role in several applications such as sensors, actuators, nano generators due to its aspect ratio and ease of

fabrication. 1D structures can range between 1 nm to 100 nm in diameter. Few of the important properties of nanowires are large surface area to volume ratio, carrier mobility comparable to bulk ZnO, low thermal conductivity, quantum confinement resulting in size and shape dependent optical and electrical properties [78]. ZnO crystallization and anisotropic growth properties makes it a very useful functional material for 1D nanostructures [79]. 1D nanostructures of ZnO like nanowires, nano rods, and nano ribbons help to improve electron diffusion creating a direct path when used as an electron transport material in photovoltaic applications [80]. Shortest 1D structure are preferred for the obvious least resistive path, but surface area of the functional material is also sacrificed for this purpose [80]. The solution to this inconvenience is to use branched nanostructure that combines the benefits of providing the least resistive path and also increase the surface area.

Considering these advantages and incorporating the piezo properties of these ZnO nanostructures for use in the optoelectronics field will prove fruitful. Investigating the piezo response of the branched ZnO nanowires will give an idea about the behavior of these nanostructures with shorter length.

In this work, three types of ZnO nanostructures have been characterized for their piezo response. Nanowires, nanoforest and nano film were the test morphologies used in this work. The electrochemical technique has been employed for the piezo characterization [15].

4.3 Experimentation

4.3.1 1D ZnO Nanostructure Fabrication

The fabrication of ZnO NWs requires the following materials: Indium Tin Oxide (ITO) coated polyethylene terephthalate (PET) were used as a substrate. 10 mM solution of zinc acetate dehydrate prepared in ethanol were used as the seeding layer and the growth solution was an equimolar 25 mM zinc nitrate hexahydrate and hexamethylenetetramine (HMTA) in deionized (DI) water.

In order to fabricate the ZnO NWs, the ITO sample was coated with the seeding layer using spin coater at 1500 rpm for 45 secs and annealed on the hotplate at 150° C for 2 minutes and this process was repeated 10 times to get an even coating of seeding layer. The ITO with seeding layer was transferred into a growth solution maintained at 90° C using a water bath. The sample was suspended downwards with the help of a custom setup. The NWs were grown for about 4 hrs.

The ZnO nanoforest synthesis requires a two-step hydrothermal process. ITO substrate grown with ZnO NWs for 2 hrs was washed with DI water to clear any preexisting growth sludge and prepped for second seeding layer deposition. The seeding layer deposition was carried on for 10 times and latter ZnO NWs were grown using the same hydrothermal process as explained before. In the both cases, the solution was agitated to obtain a randomly misaligned NWs mesh. A 100 nm thick ZnO nano film is fabricated through the conventional sputtering technique.

4.3.2 Piezo Characterization of ZnO Morphologies

The electrochemical setup consists of three probes, counter electrode (Pt wire), reference electrode (Ag/AgCl) and the working electrode having ITO covered with ZnO samples. For the cyclic voltammetry (CV) experiment, the voltage on the working electrode was scanned between -0.8 V to +0.8 V (versus the reference) with 0.05 V.s⁻¹ rate. The experiment was performed initially using flat samples and measuring the CV response of the sample in an electrolyte containing ferrocene. Using the custom made setup, the samples were bent at different curvatures and the effect of the piezo voltage was measured by monitoring the shift in the redox peak voltage.

4.4 Results and Discussion

Figure 21 shows the SEM image of the hydrothermally grown ZnO NW on an ITO substrate. The growth was carried out for 4 hrs and the measured cross section thickness of these ZnO NWs ranged between 900 nm – 1100 nm for the 4 hrs growth. Solution agitation has a key role in this process; it allows the nanowires to be intertwined between one another. This

intertwining leads to localized strain induction between the nanowires when the sample is put under mechanical strain, enhancing the piezo response of the sample. There is although an optimum growth time ranging between 3-4 Hrs to obtain reasonable piezo effect [15]. The average diameter of the ZnO NWs was between 30 and 50 nm. The ZnO NW diameter can be tuned to obtain the desired dimension by varying the ZnO seed layer thickness. Most literatures have reported size variations ranging between 30-200 nm [81]. The SEM image shows that the ZnO NWs were densely packed, yet another key component responsible for the best piezo response.

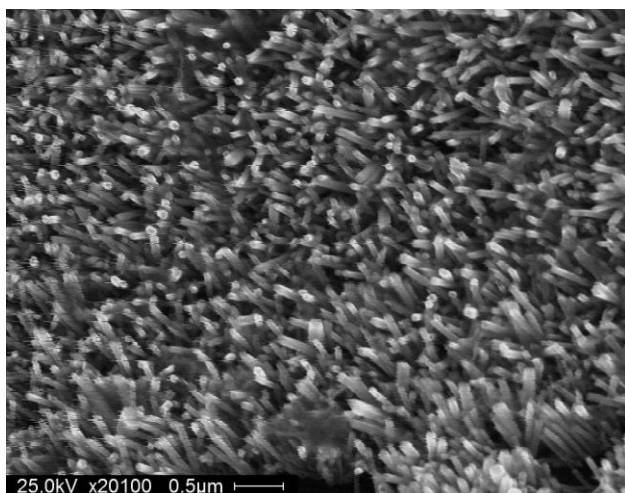


Figure 21. SEM image of the hydrothermally grown ZnO nanowires on an ITO substrate.

Figure 22 shows the SEM image of the sample with two steps of growing nanowires. The flower shape of ZnO nanostructure is due to the fabrication steps. After two hours of growing the first layer of the nanowires, the sample was coated with the seeding layer before the second step of the growth. This resulted in growing NWs on the first layer of NWs, forming branched nanostructures.

Although the results from 4 hours grown NWs are presented in Chapter 3, the results are shown again in Figures 21 and 22 to compare them with the flower-shape and thin-film samples. The process of testing was the same as explained in Chapter 3. Outward bending 1, 2, and 3 represent the curvature of the sample at 0.99 cm^{-1} , 1.274 cm^{-1} and 1.562 cm^{-1} , respectively.

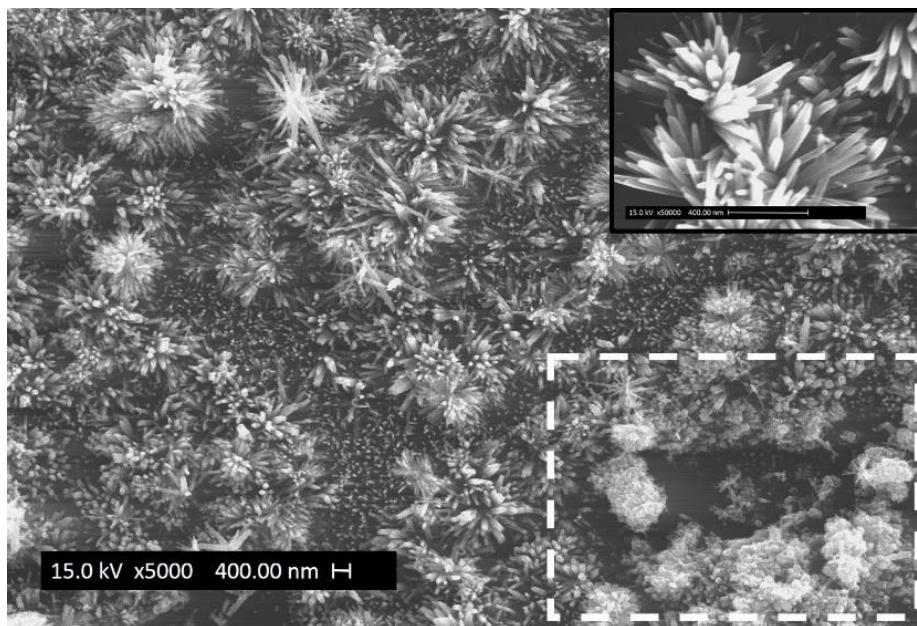


Figure 22. SEM image of the hydrothermally grown ZnO nanoforest on an ITO substrate. (Inset flower shaped ZnO formation with the landscape of ZnO nanoforest). Lower right corner highlights one of the growth synthesis defects that may affect the cumulative piezo response of the sample under investigation.

The results from the similar test for the ZnO nanoforest sample are shown in Figure 23. The data was collected by mechanically straining the substrate under outward and inward curvatures, respectively. The surface area of the WE in the electrolyte was kept constant at 2 cm^2 . The voltage was swept between -0.9 V to 0.9 V . The sample was tested under four different curvatures starting with flat position and followed by three increasing ranges of outward curvature. The piezo potential increased upon the increase of outward curvature. Outward and inward bending 1, 2 and 3 represent the curvature of the sample at 0.5 cm^{-1} , 0.75 cm^{-1} and 1.25 cm^{-1} respectively. The peak voltage shifted from 0.65 V to 0.725 V . Figure 23b shows the zoomed CV response of the outward bent ZnO nanoforest sample.

Inward curvature is known to decrease the piezo potential value due to the possible micro cracks that were developed during the straining process. The inward bending 1 led to an unstable CV measurement due to the sudden inward strain applied on the sample, the sample recovered

with the subsequent inward bendings. The cathodic peak moved to the left indicating the sharp drop in piezo potential. The voltage peak shifted from 0.65 V to 0.475 V.

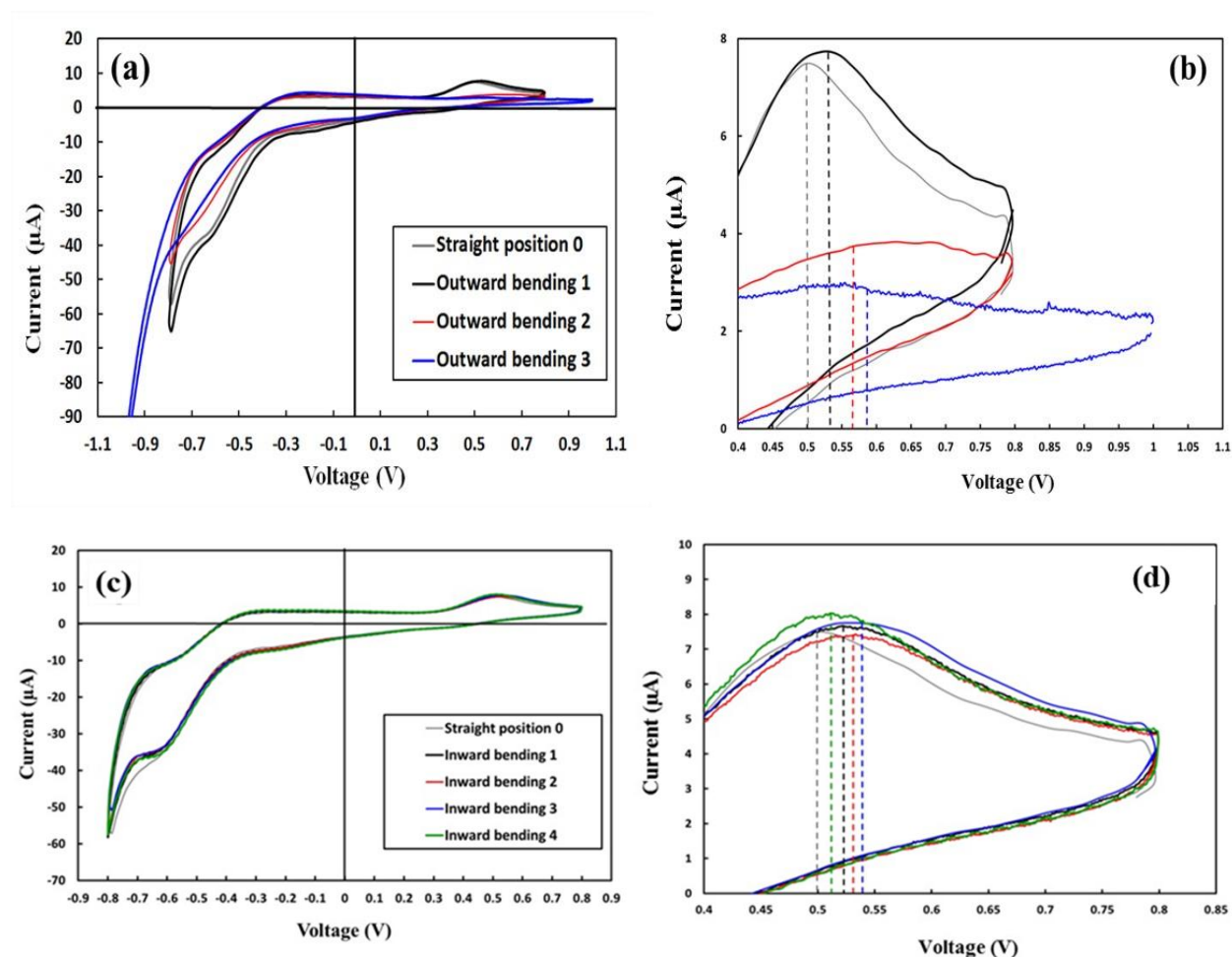


Figure 23. CV results from the 4 hrs grown ZnO NW sample on a flat substrate at different (a) outward and (c) inward curvatures. The zoomed view of (b) outward and (d) inward bending at increasing curvatures.

Finally, the 100 nm thick planar ZnO nanofilm was characterized to evaluate the difference in piezo response between ZnO planar and the nanostructures. Figure 24 shows the CV graphs corresponding to ZnO nanofilm on ITO functioning as the working electrode (WE) under different bending conditions. The results of the outward bending show the shift of the peak voltage from 0.58 V to 0.75 V as the bending curvature was increased.

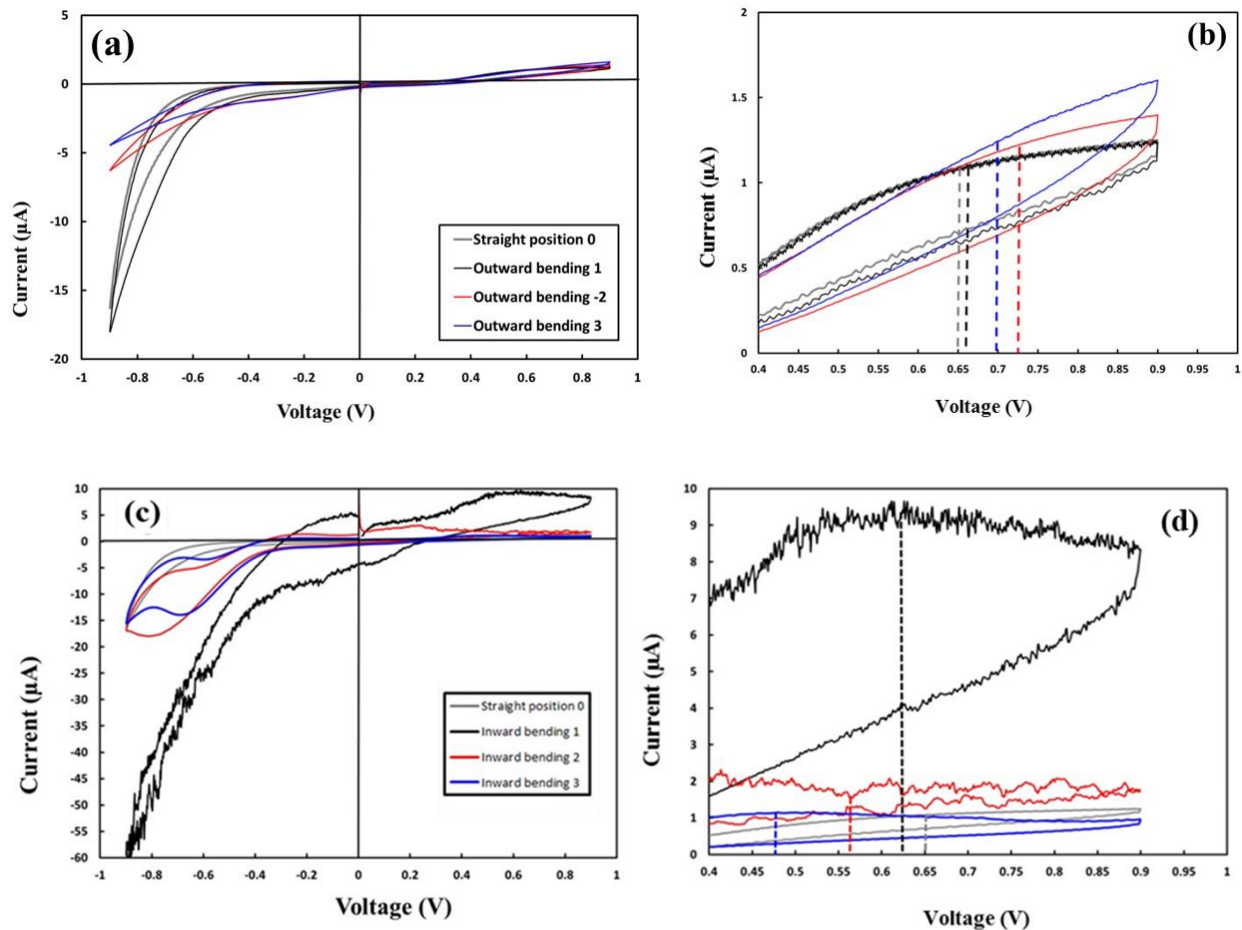


Figure 24. CV results from the two-step hydrothermally grown ZnO nanoforest sample on a flat substrate at different (a) outward and (c) inward curvatures. The zoomed view of the (b) outward and (d) inward bending at increasing curvatures.

When the sample was tested for the inward bending (Figure 25 (c) and (d)), the flat position cathode peak showed a shift from 0.58 V in the previous test to 0.715 V. This upwards shift could point towards the micro and nano cracks that would have developed on the ZnO and ITO surfaces leading to nanostructures of ZnO formed unintentionally. Figure 26 shows the cracks formed during the mechanical straining. It was observed that larger cracks were developed during the inward bending process.

In order to analyze the impact of morphology on the piezo potential, in Figure 27, the voltage of the cathodic peak in the CV experiments are plotted versus the curvature of the substrate for all three samples and for both inward and outward bending. The outward bending is presented

with negative curvature values. It can be seen that the piezo potential for the flat position for nanowires, nanoforest and nanofilm were 110 mV, 260 mV and 170 mV respectively during the initial flat response measurement. An increase piezo potential was noticed from the nanofilm after completion of outward bending, possible due to the formation of micro cracks. Largest piezo potential of 335 mV was noticed for ZnO nanoforest owing to its branched structure leading to greater nanowire interaction. Although the largest piezo potential value was noticed for nanoforest, it also was the most affected by the inward bending experiment, with the piezo potential falling by almost 170 mV with respect to the flat position potential of 260 mV.

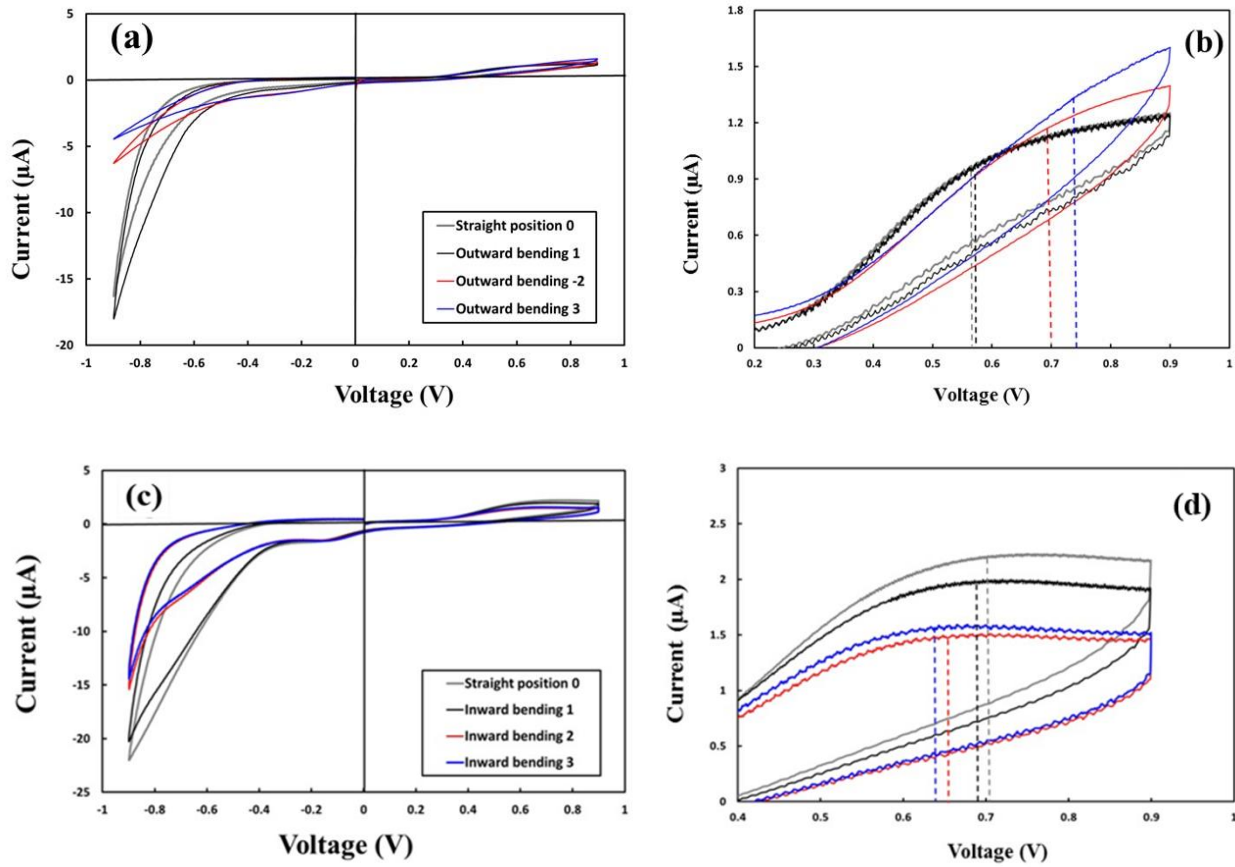


Figure 25. CV results from the 100 nm planar ZnO nano film on a flat substrate at different (a) outward and (c) inward curvatures. The zoomed view of the (b) outward and (d) bending at increasing curvatures.

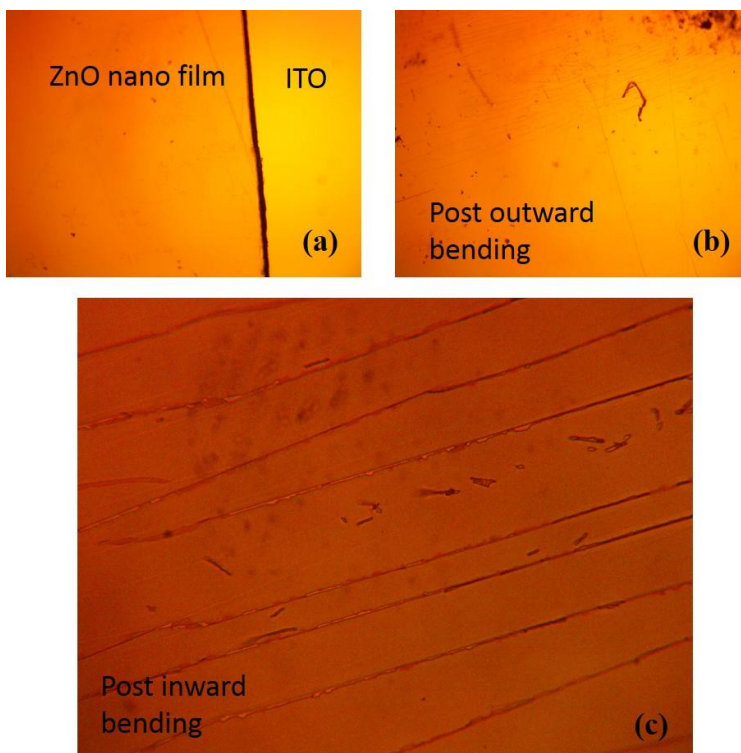


Figure 26. Microscopic image of ZnO nanofilm in different stages of mechanical straining (a) Flat ZnO nano film with no strain (b) small crack formation due to outward bending and (c) slightly bigger cracks due to inward bending.

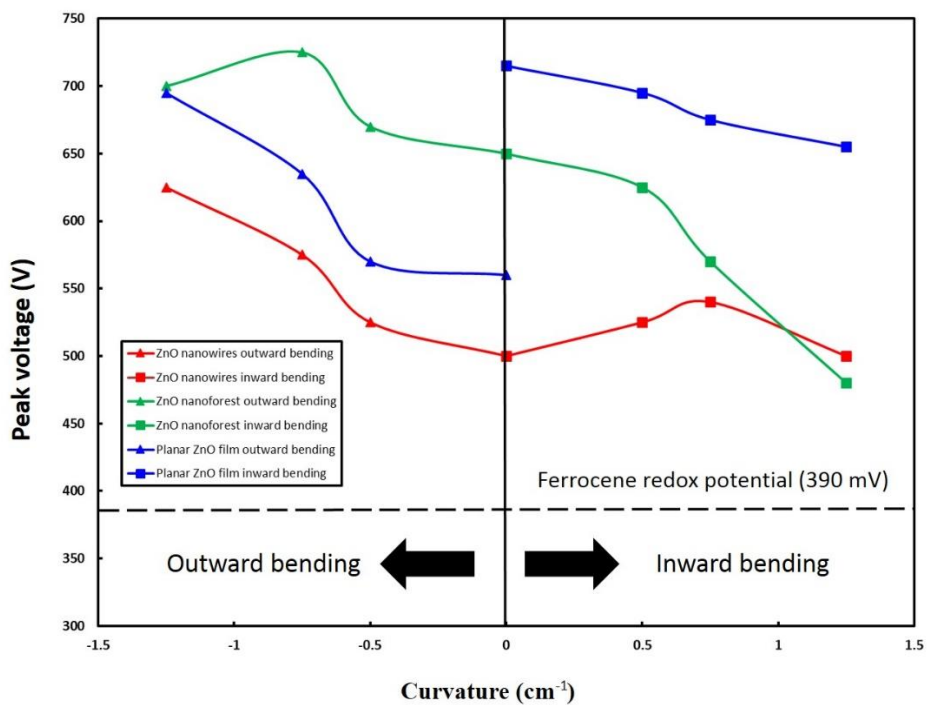


Figure 27. Ferrocene peak potential versus curvature for ZnO nanowires, nanoforest and nanofilm.

Overall, nanowires, nanoforest and nanofilm have their own unique advantages when used as piezo functional material with respect surface area, surface coverage and aspect ratio. The key finding of this work are the ability to use ZnO nanofilm similar to nanowires and nanoforest. A branched nanowire structure was found to yield the largest piezo potential comparatively.

4.5 Conclusion

Three types of ZnO nanostructures namely nanowires, nanoforest and nanofilm on a flexible ITO were characterized for their piezo response. Piezo characterization was performed using a novel electrochemical approach. Using the CV technique, the piezo voltage from the bent samples was measured through the shift in the peak potential of a redox reaction. The feasibility of ZnO nanofilm usage in planar devices requiring piezo functional material was explored and found to have evidence in achieving significant piezo potential. Nanoforest architecture of ZnO yielded the largest piezo potential value due to its morphological advantages of large surface area causing increased interaction among ZnO branches. Overall, these piezo characterizations will help promote the use of ZnO nanostructures for new innovative devices utilizing both semiconductor and piezo dual property.

CHAPTER 5: PHOTO-ELECTRIC MEMORY EFFECT IN AN ORGANIC BULK HETEROJUNCTION DEVICE¹

5.1 Abstract

We report on a memory effect observed in an inverted bulk heterojunction organic photovoltaic device, where the electron-collecting electrode is ZnO nanowires grown on an indium tin oxide (ITO) substrate. The device presented a unique response to light by switching from a rectifying behavior in the dark to a resistive response under illumination. After cessation of light, the device slowly stabilized back to its rectifying nature after ~270 minutes, introducing a volatile photoelectric memory effect. The reversibility of the response is verified through multiple cycles of light exposure and placing the device in the dark. The device is also illuminated with different light intensities to study the photovoltaic response through I-V characterization. It is found that the time constant associated to the transition between the rectifying and resistive characteristics is independent from the light intensity. Further study revealed that there is a hysteresis loop in the I-V curve in the dark, but the loop vanished in the resistive mode under illumination. A mechanism based on oxygen absorption-desorption has been suggested to explain the observed effect. Such a memory effect can be used in various optoelectronic devices to save the optical information for an extended time.

¹ Reprinted with permission from Santhanakrishna, A. K., & Takshi, A. (2015). "Photoelectric Memory Effect in an Organic Bulk Heterojunction Device." *Journal of Physical Chemistry*, 119(30), 17253–17259. doi:10.1021/acs.jpcc.5b05107. Copyright (2015) American Chemical Society. Permission is included in the Appendix A.

5.2 Introduction

Organic electronic devices (OEDs) provide a sustainable solution for renewable energy sources, sensors, display systems, memory devices and various other applications due to its low cost materials, solution processing manufacturing and minimal environmental impact.[82] In particular, the market for organic optoelectronic devices is quite large. [83, 84] The effect of light on organic semiconductors has been studied extensively for the application of converting solar energy to electrical energy in organic photovoltaic devices (OPVs). [85, 86] Although a semiconductor is able to generate electron-hole pairs upon absorption of photons, to separate charges in an OPV, it is required to use two different organic semiconductors as the electron donor and the electron acceptor. [84] To enhance the efficiency of generating charges from photons, a bulk heterojunction structure is recommended in which a blend of the two semiconductors is used as the photoactive layer of the device. [87-89] Among various combinations of the materials, poly 3-hexylthiophene (P3HT) and phenyl-C₆₁-butyric acid methyl ester (PCBM) are the most common electron donor and acceptor materials, respectively. [85, 90, 91] To enhance the efficiency in a device, the electrons and holes are transferred to the device electrodes selectively by using hole-blocking and electron-blocking layers between the photoactive layer and the electrodes. The thickness and energy structure of the blocking layers are critical in designing an efficient OPV. [92] One of the most promising structures for making efficient OPVs is to use PEDOT:PSS (Poly(3,4-ethylenedioxythiophene) Polystyrene sulfonate) as the electron blocking layer and a thin layer of a metal oxide (or metal sulfide) as the hole blocking layer.[93-95] Using a transparent electrode such as indium tin oxide (ITO), an inverted bulk heterojunction device can be built with layers of ITO/Metal oxide/P3HT:PCBM/PEDOT/second electrode. [96] Such a structure has been widely practiced and studied by many groups. [93, 95, 97] It has been found that the thickness and structure of each layer has a large impact on the photo-conversion efficiency of the devices. [96]

Due to the design of the structure with energy barriers for separation of electrons and holes, the current-voltage (I-V) characteristic of an OPV in the dark is a non-linear response showing a rectification behavior. [98] Upon illumination the shape of the I-V curve in a solar cell usually remains the same with a shift along the current axis with an amount equal to the short circuit photocurrent. [99-101] In the lack of any storage mechanism, the I-V characteristic returns to the curve in the dark immediately after secession of the light. [102]

In this work, we report on a photo-electric memory effect observed in an inverted bulk heterojunction structure made of ITO/ZnO nanowires/P3HT:PCBM/PEDOT/Ag paste. The observed effect is like a volatile memory, fading off with a relatively large time constant. This memory effect has potential implications on the way organic photovoltaic devices are fabricated and characterized because of the transient time response factor associated with such devices. Various forms of memory effect have been reported before for organic devices. [103-108] An external electrical stimulus can be used for controlling the resistive state of the organic-based resistive memory devices, which either consist of single or multilayers of organic materials sandwiched between two electrodes. [87, 109] The resistance state of the device can be read by applying a very small voltage and this process is nondestructive, hence making this type of memory to be non-volatile. The widely accepted theory to explain the effect is based on the formation of a filament-based conductive path at the low resistive state. [110] Such a path can be generated only via a large electric field (writing stimulus signal). To switch back to a high resistive state, a large opposite electric field has to be applied to push some of the filaments back. [106, 109, 111]

5.3 Experimental Section

5.3.1 Materials and Equipment

Regioregular P3HT and PCBM were purchased from Luminescence Technology Corp. The silver paste was obtained from SPI Supplies. The rest of the chemicals and the indium tin

oxide (ITO) coated polyethylene terephthalate (PET) electrodes were all purchased from Sigma-Aldrich.

~10 mm × 5 mm inverted bulk heterojunction organic memory devices were fabricated in the ambient environment. First, ZnO NWs were vertically grown on the ITO electrode with a sheet resistivity of 60 Ω/square using a conventional hydrothermal method. [15] A 10 mM solution of zinc acetate dehydrate was prepared in ethanol. Also, a mixture of equimolar 25 mM zinc nitrate hexahydrate and hexamethylenetetramine (HMTA) in deionized (DI) water was prepared for the growth solution. 0.15 mL of zinc acetate in ethanol was spin coated on an ITO substrate at 1500 rpm for 45 s under ambient conditions. Immediately after, the sample was annealed at 150 °C on a hotplate for 2 min. The nucleation layer for the formation of the initial ZnO nanocrystals on the ITO substrate provided a foundation for the nanowire growth. Spin coating and annealing processes were repeated 10 times to guarantee a uniform coating of the ZnO seed particles on the ITO. Following this stage, vertical nanowires were grown by dipping the inverted substrate in the 25 mM growth solution for 4 hrs at 90 °C, resulting in approximately 1.1 μm long NWs. The growth solution was constantly agitated using a stirring magnet rotating at 425 rpm. The quality of the grown NWs was studied using scanning electron microscopy (SEM) and X-ray diffraction (XRD) methods.

The photoactive P3HT:PCBM solution was prepared by mixing 1:0.8 proportion of P3HT (10 mg/ml) and PCBM (8 mg/ml) in 1, 2 dichlorobenzene. The solution was sonicated for 10 min before drop casting 15 μL on the ZnO NW layer. After deposition of the active layer, the samples were heated at 60° C for 5 min. Poly(3,4- ethylenedioxythiophene):polystyrene sulfonate (PEDOT:PSS)^[112] diluted in the ratio of 1:1 with isopropanol were then subsequently drop casted on top of the active layer. Then a layer of the Ag paste was applied by gentle brushing and dried

in air. It should be noted that due to the large thickness and roughness in the ZnO NW layer, the organic layers were drop casted to have a large overall thickness (larger than 1.1 μm) avoiding short circuit between the top and the bottom electrodes. The structure of the fabricated inverted bulk heterojunction device is shown in Figure 28 a. The samples were tested by connecting the ITO and Ag electrodes to the instruments for measuring the I-V characteristics and the impedance of the devices. For the impedance measurement and cyclic I-V characteristics (scanning the voltage up and down while measuring the current), Versastat 4 potentiostat was used in the 2-probe mode. The rest of the voltage and current measurements were carried out using a Keithley 2602A source-meter.

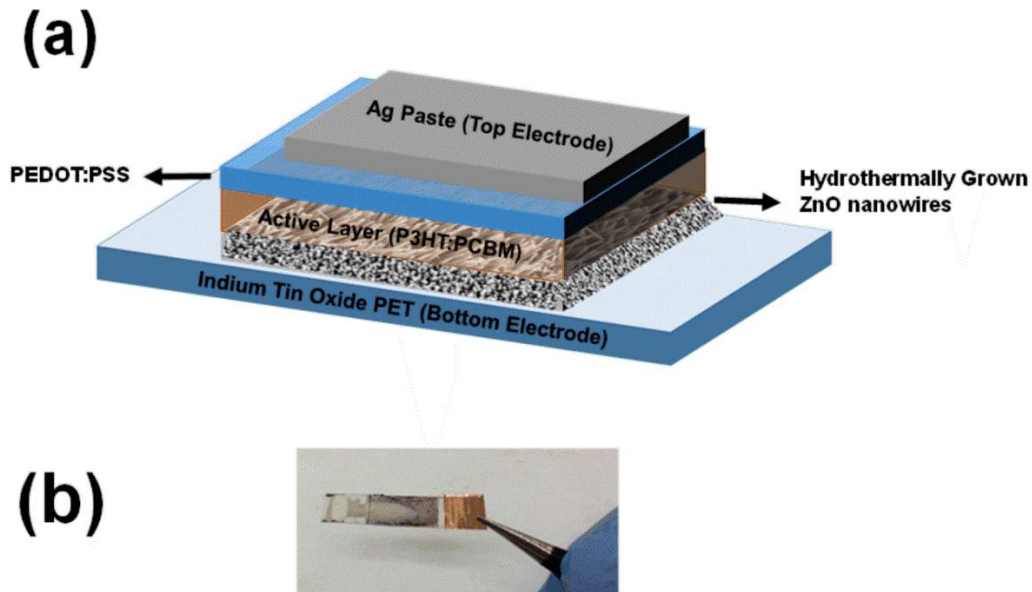


Figure 28. (a) Device structure of an inverted bulk heterojunction ITO/ZnO NWs/P3HT:PCBM/PEDOT/ Ag paste device. (b) Optical image of the organic photoelectric memory device.

To keep the devices in dark, the samples were located in a box. The samples were illuminated by a solar simulator (Radiant Source Technology) with full intensity of $80 \text{ mW}\cdot\text{cm}^{-2}$ (AM1.0) connected to the box through a fiber optic cable (AM1.0 was the available optical filter for the setup). A picture of the fabricated device is shown in Figure 28 b.

5.4 Results and Discussion

With the aim of fabricating an inverted bulk heterojunction OPV, the device in Figure 28 was fabricated. However, unlike the conventional method of using a thin and smooth layer of ZnO, the device was fabricated with a layer of ZnO NWs. As the results in this work shows, the device had a poor photovoltaic effect, but presented a photoelectric memory effect. Several I-V characterization, light illumination study, and impedance characterization were carried out to study the electrical and optical characteristics of the ITO/ZnO NWs/P3HT:PCBM/PEDOT:PSS/Ag paste device.

Figure 29 a shows the SEM image of the grown ZnO NWs. A good surface coverage with NWs diameter of ~50 nm was observed in the sample prepared for the device. The XRD pattern from the sample (Figure 29 b) also shows the crystal orientation in the NWs with dominate orientation for (002) at $2\theta=34.9^\circ$ which is an indication for the c-axis being vertical to the substrate. [113]

First, the device was tested in the dark by scanning the voltage of the bottom electrode from -3 V to $+2\text{ V}$ while the top electrode was grounded. As shown in Figure 30, the I-V curve demonstrated a rectifying characteristic. The knee voltage is in the range of 0.4-0.5 V. The reverse bias current was around $300\ \mu\text{A}$ at -3 V , while the forward current reached to 3.5 mA at 2 V bias.

Analyzing the switching phenomenon of the device, it can be seen that even though the device did not exhibit ideal rectifying performance of exponential increase in current, the current did increase steadily to high value achieving the ON/OFF ratio of 350 at 2 V. The I-V measurement was repeated again by illuminating the sample using the solar simulator ($80\ \text{mW}\cdot\text{cm}^{-2}$) with the ZnO modified ITO electrode facing the light source. The I-V curve, in Figure 30, was measured in less than 60 s after starting the illumination (Keithley instrument time for scanning the voltage and recording the current).

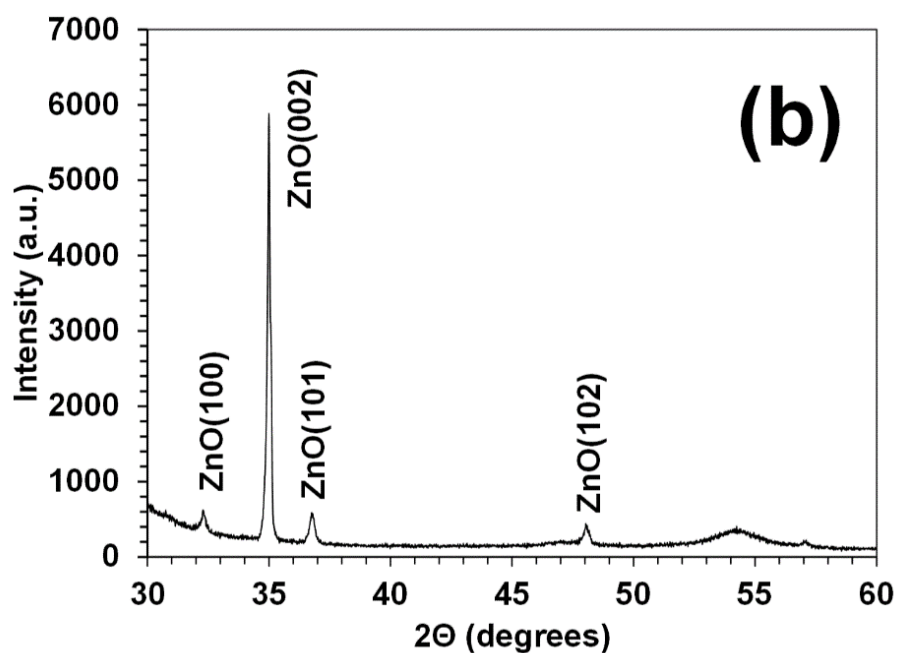
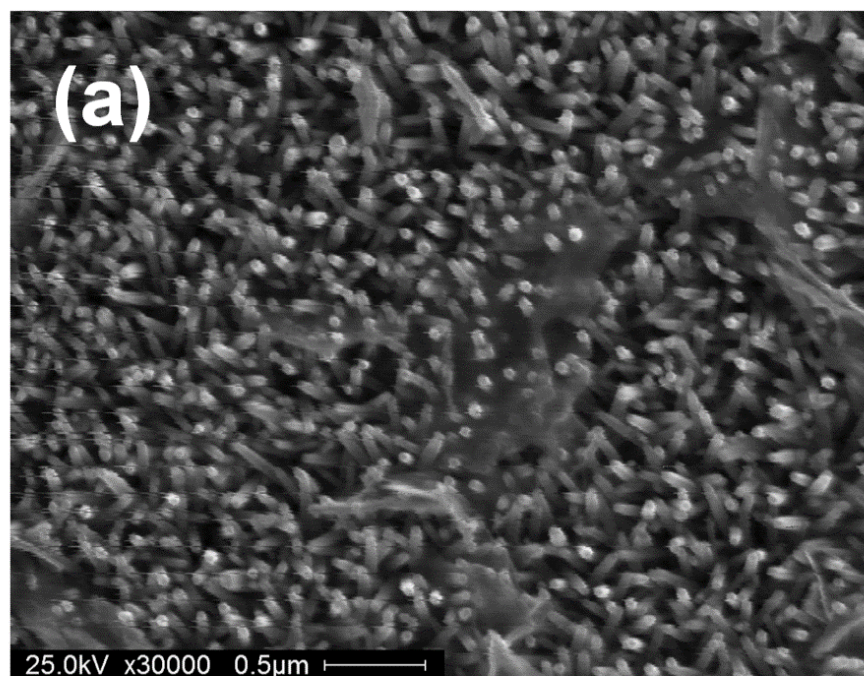


Figure 29. (a) SEM image of hydrothermally growth ZnO nanowires on ITO substrate. (b) XRD pattern of grown ZnO crystalline nanowires (b) XRD pattern from the ITO substrate. The broad peak near $2\theta = 54^\circ$ in the ZnO sample is due to the ITO substrate effect.

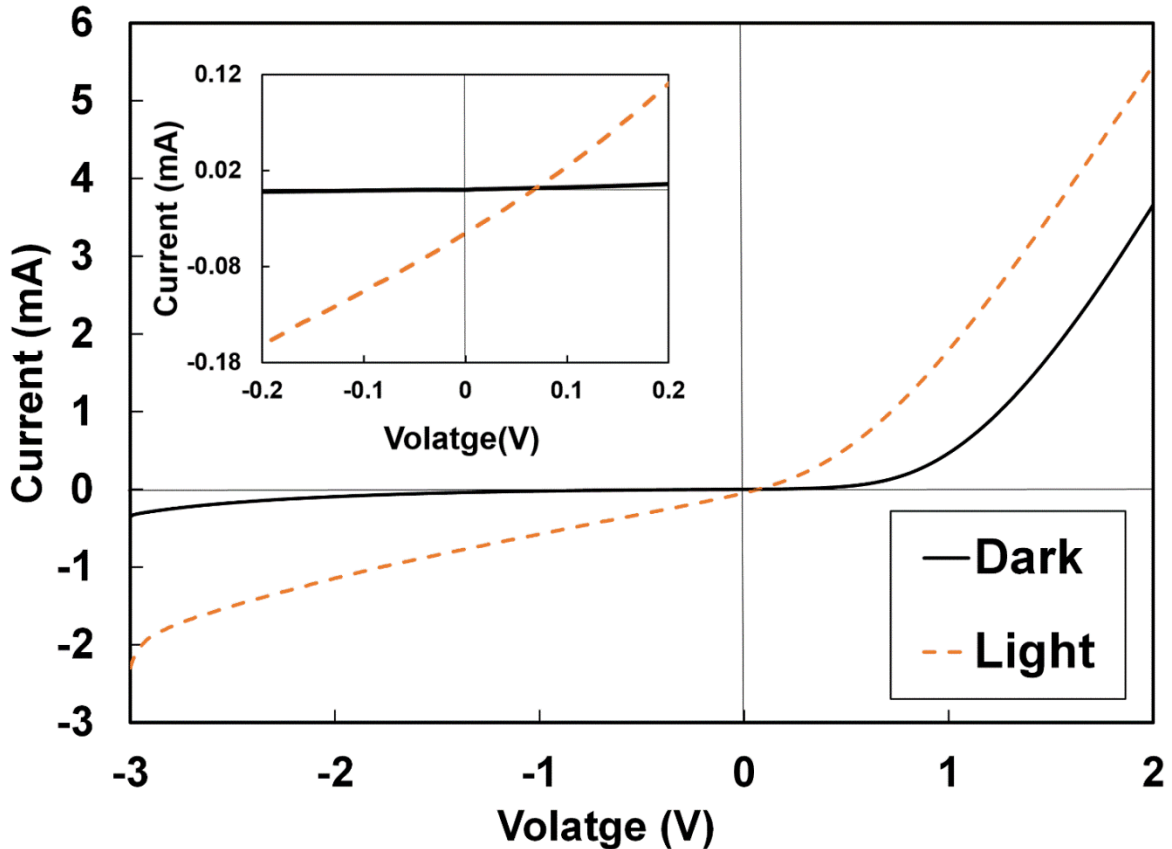


Figure 30. I-V characteristics of the bulk heterojunction device (ITO/ZnO NWs/P3HT:PCBM/PEDOT/Ag paste) in the dark and under illumination (80 mW.cm^{-2}). Inset: Zoomed in view of the same I-V characteristics showing the photocurrent.

Energy conversion efficiency as high as 9.2% has been reported for an inverted bulk heterojunction device. [114] However, a similar OPV device with the same architecture (ITO/ZnO/P3HT:PCBM/PEDOT/Ag) has shown 2.12% efficiency.[96] The efficiency in our device was even much lower showing only $5 \mu\text{A}$ photocurrent at 0 V and open circuit voltage of $\sim 0.1 \text{ V}$ under 80 mW.cm^{-2} solar simulated irradiation (inset Figure 30). Yet, a significant change in the I-V characteristic of the device was observed under illumination (Figure 30), where the rectifying behavior in the dark was transformed to more a resistive response in the light. Under illumination, the current reached the negative and positive peaks of -2.2 mA and 5.2 mA at -3 V and $+2 \text{ V}$ biases, respectively. The positive current of 5.2 mA was almost twice the forward current

observed during the same I-V characterization under the dark condition. Similarly, a large reverse current of 2.5 mA was observed during the illumination, which was 10 times higher than the dark current at -3 V bias.

The change of the device behavior from a good rectifying performance to a resistive-like response upon illumination encouraged us to investigate the device behavior under dark and light conditions at different times, which revealed a photoelectric memory effect on the device. Long after keeping the device in the dark, the same dark I-V characteristic shown in Figure 30 was obtained again. Also, the repeatability and stability of the characteristic were verified by doing several measurements over a course of 3 days of the experiments. It should be noted that all the fabrication and measuring steps were carried out under ambient air conditions.

For the memory effect, the cell was again illuminated for 60 seconds with the same light intensity of 80 mW.cm^{-2} . As expected, the device showed its resistive response again. With the knowledge that the cell recovers from this state, I-V characterization was done for every 15 minutes period after cessation of light, and this was carried out until the cell response was completely recovered to the dark response. Figure 31 shows the I-V responses after 0, 15, 30 and 270 minutes of light cessation (illumination time= 60 s). As expected, the photocurrent disappeared right after turning off the light source. However, it took around 270 minutes for the device to return to its original rectifying characteristics. Looking at the response of the device after 15 minutes of turning off the light source, it can be seen that the recovery was already started with a drop in the reverse current from almost 2.2 mA to 1.2 mA at -3 V. The trend followed throughout this experiment. In the forward bias region, the significant change was the gradual drift from the resistive like behavior in light to more non-linear response and shift in the knee voltage to higher values at longer times after the cessation of light.

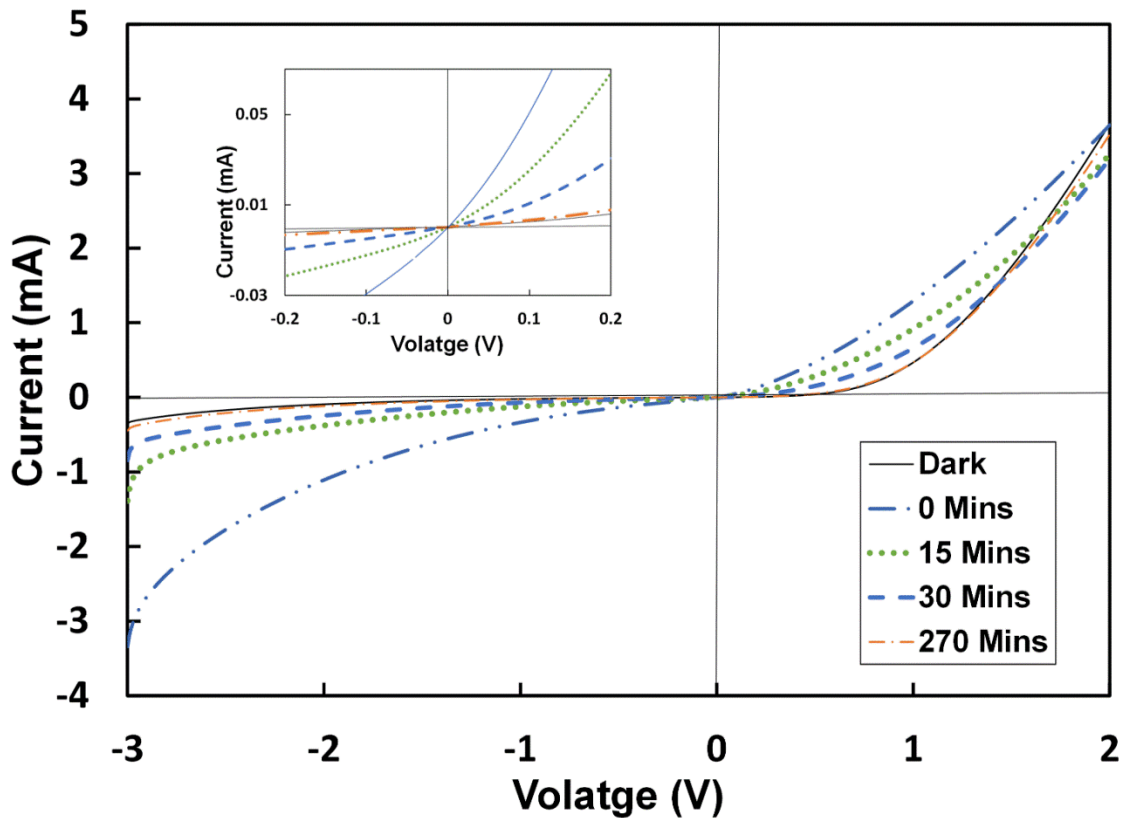


Figure 31. Device recovery process through I-V characterization of an inverted bulk heterojunction photoelectric memory device from illuminated behavior to dark response. Inset: Zoomed in view of the same I-V characteristics showing no photocurrent.

To understand the effect of the light intensity on the device response, after keeping the device in the dark for more than 5 hours before each illumination, the device was illuminated with 80%, 60%, and 40% of the full power ($80 \text{ mW}\cdot\text{cm}^{-2}$) for 5 minutes (longer exposure time than the experiment presented in Figure 28) and the current-voltage characteristics were recorded in less than 60 s being exposed to the light (Figure 32). The results indicate that the light intensity has an effect on the observed resistive-like response. All the bright experiment responses showed small photocurrents, measuring less than $5 \mu\text{A}$. It can be seen that, with the decrease in the light intensity; the device resistance was increased, and the current was dropped. Between the 80% and 40% light

intensities, the current reduction was 1.3 mA and 0.4 mA for the max reverse and forward currents, respectively.

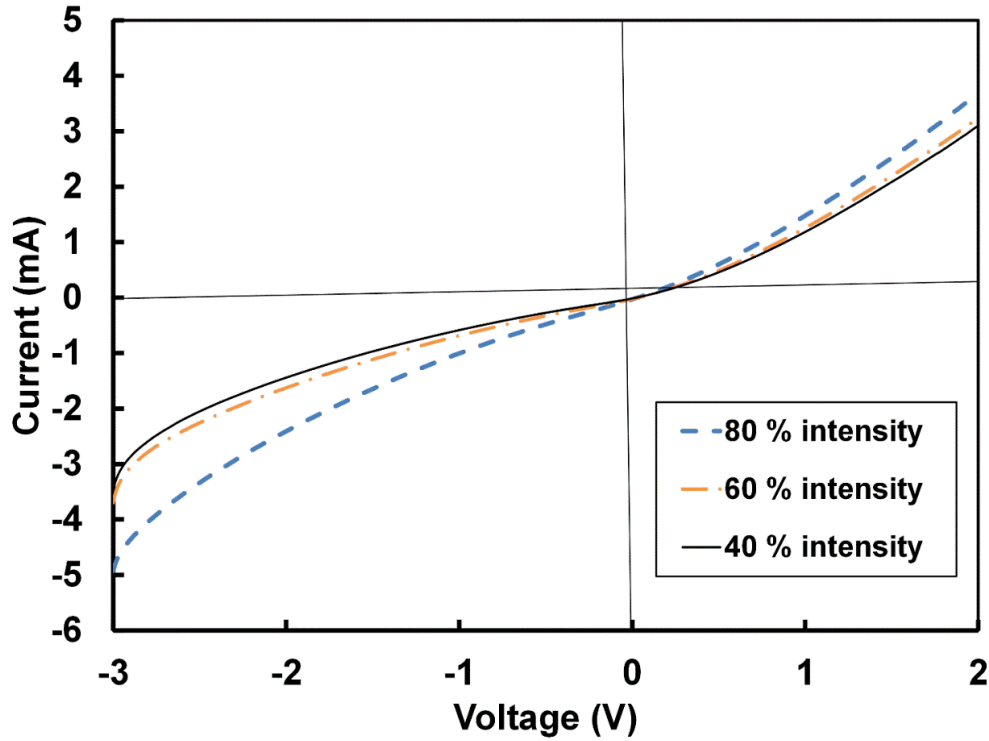


Figure 32. Light intensity study on the bulk heterojunction photoelectric memory device under 80%, 60%, and 40% light intensity.

All the previous experiments in light were carried out for a short illumination time spanning just 60 seconds. To understand further the dynamics of the recovery and the correlation between the steady independent transition and the response to different light intensities, light intensity study was performed by biasing the device at -0.5 V and recording the current while the sample was illuminated at different light intensities for 1000 sec. As shown in Figure 33, the magnitude of the current increased with time when the sample was exposed to light. Moreover, as expected, the current magnitude was larger for higher intensities. Although the currents did not become saturated at the end of 1000 s illumination, the results show clearly that the variation in the current (and the device resistance) is a function of the light intensity even for long illuminations. The sharp reduction of the current magnitude right at the end of the illumination cycle was due to the

photocurrent, which vanished as soon as the light was turned off. However, the transition in the response showed a large time constant to reach back to the stable current in the dark. Using a single time constant model, exponential functions were fitted to the curves for both current transitions in light and dark for all curves shown in Figure 33.

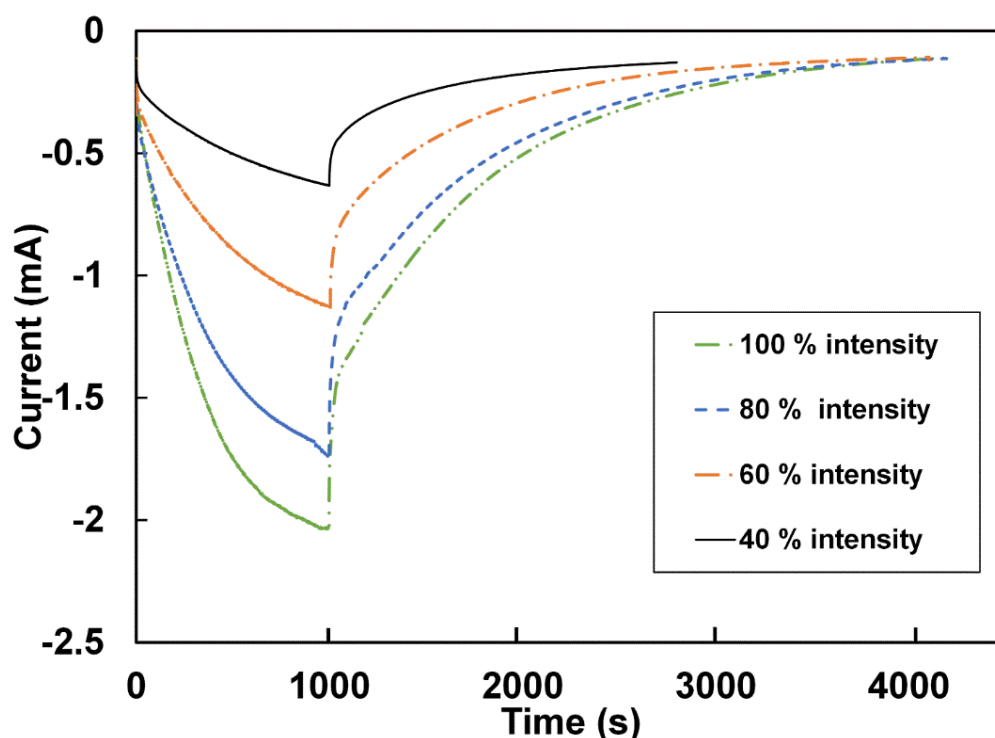


Figure 33. Light exposure study on ITO/ZnO NWs/P3HT:PCBM/PEDOT:PSS/ Ag paste photoelectric memory device under 1000 seconds illumination and four different light intensities ranging from 100% to 40% in 20% decrements. The sample was kept in dark after light cessation until the current was sufficiently low.

The results of the analysis revealed that all the transitions from light to dark had a time constant of 750 s regardless of the light intensity. The time constant for the dark to light transition was also constant for all the curves (time constant = 320 s). This implies that the memory effect is likely due to a device/material structure effect and the time constant is independent from the biasing or the illumination conditions. The detail of the curve fitting is explained in the Supporting Information section.

The device's dark and light responses were further investigated by scanning the voltage from -3 V to +2 V and scanning back to -3 V with a constant scanning rate of $50 \text{ mV}\cdot\text{s}^{-1}$ and repeating the cycle. The results, shown in Figure 34, indicate the repeatability of the response in several cycles of the experiment. Also, the response in the dark showed a hysteresis effect. The semi-log scale in Figure 34 b shows that the hysteresis effect in the I-V curves in the dark appeared in both the forward and reverse biasing. However, due to the larger current in the forward bias, the hysteresis loop is larger at positive voltages (Figure 34 a). The direction of the loop in the hysteresis loop suggests an inductive behavior of the device at very low frequencies. [115] In contrast, the same device was behaving totally resistive with no indication of any hysteresis or inductive behavior when it was illuminated for 1000 s at 100% intensity. It is clear from the results that long enough illumination completely changes the rectifying behavior to a resistive characteristic.

The inductive behavior in an organic Schottky contact has been reported before by Takshi et al. [115] The impedance study of the device in light also showed the inductive behavior at low frequencies (Figure 35). The response was more capacitive at higher frequencies for both cases (dark and light), which is likely due to the junction capacitances and the parallel plate structure of the device. [116] Additionally, the results from the impedance study support the reduction of the impedance under illumination as observed in the I-V curve around 0 V.

To achieve high efficiency in OPVs with a structure similar to the device studied in this work, the thickness and roughness of the ZnO layer has to be very low. [93, 95, 97] Using NWs instead of a planar ZnO layer, not only the nature of the interface between ZnO and the organic layer can be different, but also the thickness and roughness of the ZnO layer are much higher than those in OPVs. [96] Therefore, the observed memory effect in our device can be due to the nature of the interface and both thickness and roughness of the ZnO layer.

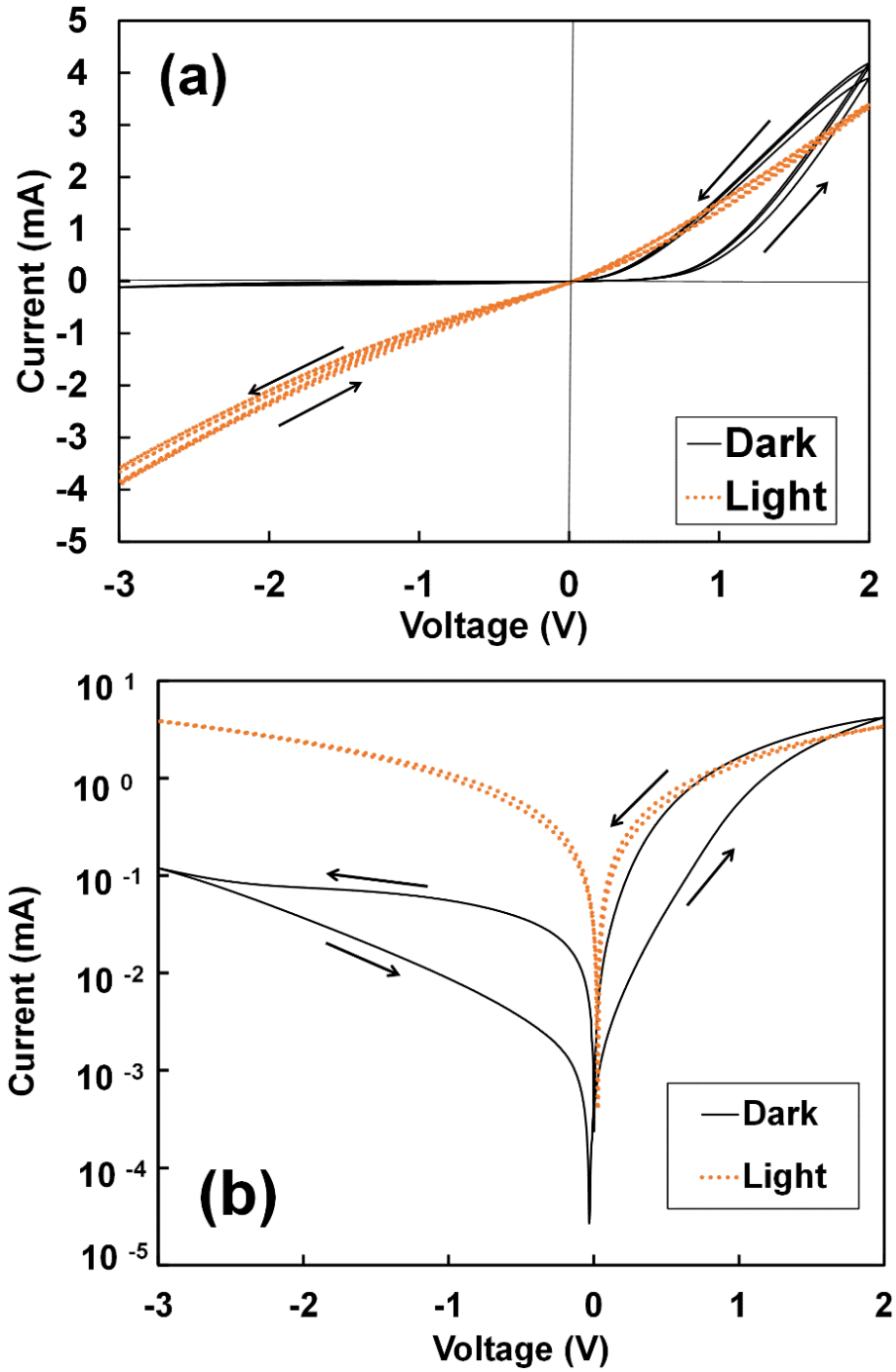


Figure 34. (a) Linear and (b) semi-log scale I-V curves for the device tested under the dark and light conditions. The voltage was scanned back and forth with a rate of $50 \text{ mV}\cdot\text{s}^{-1}$

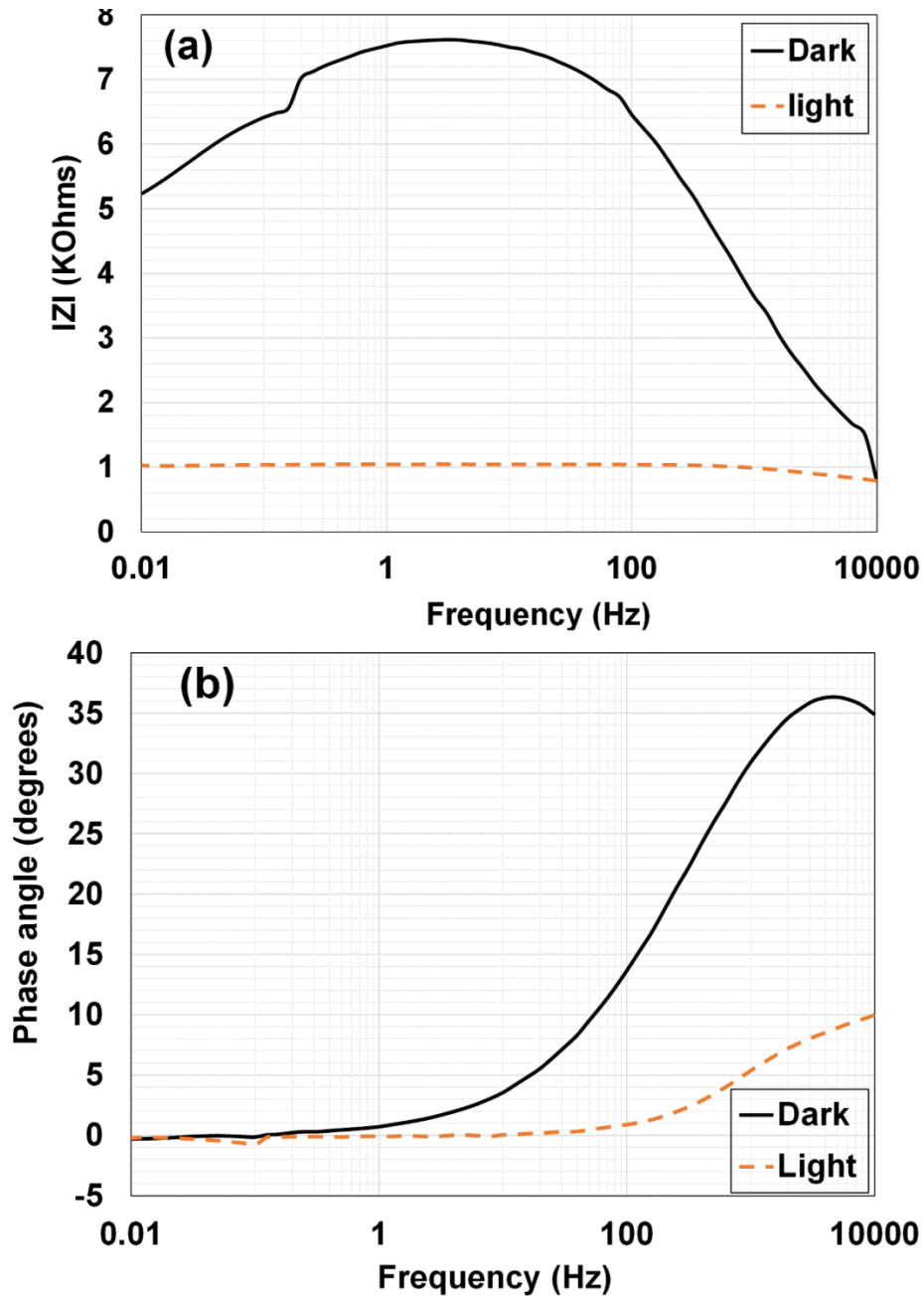


Figure 35. (a) Magnitude and (b) phase impedance of the ITO/ZnO NWs/P3HT:PCBM/PEDOT/Ag paste photoelectric memory device at 0 V bias. The drop in the magnitude at lower frequencies indicate the inductive behavior of the sample with a large time constant.

The large time constant associated to the transition from dark to light and from light to dark suggests that a slow and reversible mechanism should be involved. Possible reasons can be the diffusion of ions/molecules or trapping/releasing charges in/from the deep localized states at the

interfaces or in the amorphous organic semiconductors. In addition, the transition from the rectifying property to the linear response and vanishing the hysteresis effect indicate that, at one of the interfaces, there was an energy barrier in dark and the energy barrier was gradually reduced upon illumination. Although, to the best of our knowledge, the optical effect of switching between the rectifying and linear characteristics has not been reported yet, the change in the I-V curve with large time constants have been experienced before in several OPV devices. [116-118] Recently, Wilken et al. [116] observed a gradual reduction of the forward current with a time constant in the order of 30 min in an ITO/ZnO nanoparticles/P3HT:PCBM/PEDOT device after exposing to ambient air. The change in the response was explained through adsorption and desorption of oxygen at the ZnO surface adjacent to the organic layer, which resulted in change of the band bending in the ZnO layer (surface state charging). The theory was supported by the observation of the transition current in the device upon UV illumination, which can be only absorbed by ZnO in the device. It should be noted that although the UV was not completely filtered in our light source (AM1.0), the observed effect in our device cannot be only because of the UV illumination. A weak memory effect was also observed (the results are not reported here) in the device when the sample was exposed to ambient light in the lab with no UV emission.

In another inverted heterojunction OPV, reported by Lafalce et al., [118] a slow drift in the dark I-V curve of the device was observed when the device was exposed to air. In the absence of the ZnO layer in their device, the change was related to the photo-doping effect of the P3HT by reacting with oxygen and affecting the charge in the space charge region.

The exact mechanism behind the observed photoelectric memory effect in our device is not known. However, the existing theories developed by Wilken [116] and Lafalce [118] can be used for explaining the effect. The energy diagram of the device is presented in Figure 36. The ZnO

band bending introduces an energy barrier for electrons injected from the heterojunction organic layer (Figure 36 a). This barrier can rectify the charge transfer through the device. As explained by Wilken et al., the amount of the barrier and the width of the depletion layer are functions of the trapped electrons at the surface states and controlled by the amount of adsorbed oxygen on the surface of the ZnO layer. [116]

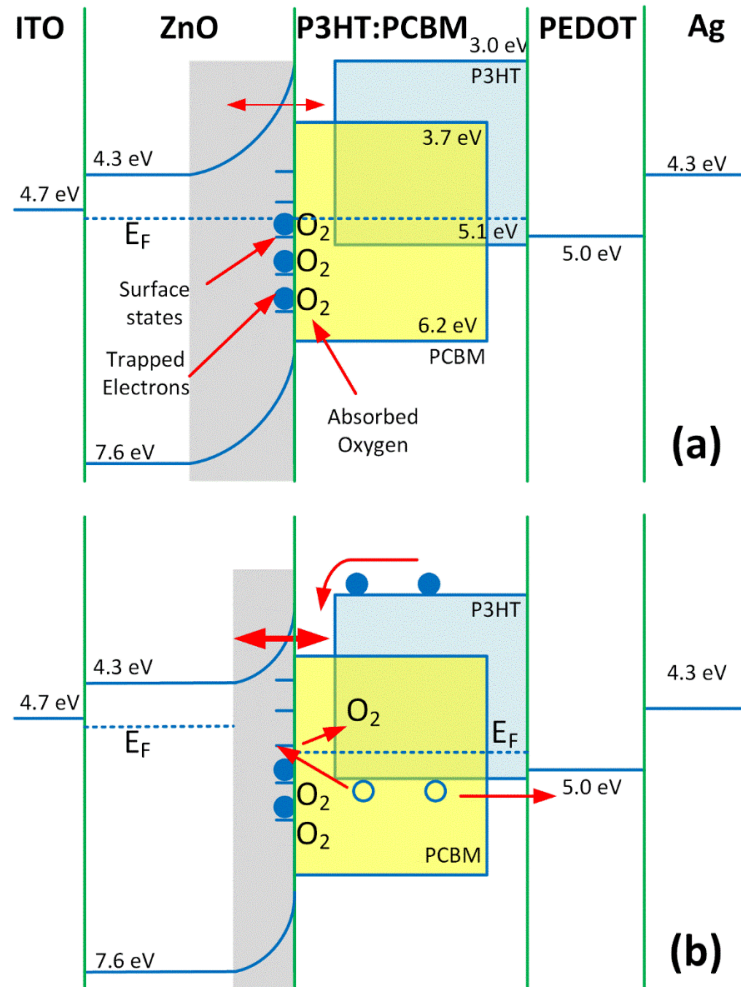


Figure 36. Energy diagram of the device at 0 V bias in (a) the dark and (b) under illumination (or in the transition mode after cessation of the light). (a) The energy barrier for electrons is high and wide in dark resulting in the rectifying behavior. (b) Exposure to light generates holes in the organic materials, which recombine with the trapped electrons in the deep localized surface states. Consequently, O_2 molecules would be desorbed. The barrier is lower and shorter transforming the junction to an Ohmic with electrons tunneling through the barrier. The process is reversible in dark due to the difference of the Fermi level (E_F), but O_2 absorption and electron trapping are slow process introducing the memory effect.

Exposing the device to light generates electron-hole pairs in the organic layer (Figure 36 b). In an efficient OPV, the electrons are supposed to be collected by ZnO and holes are transferred through the PEDOT:PSS layer. However, due to the bulk heterojunction structure of P3HT:PCBM both P3HT and PCBM have interfaces with the ZnO NWs. Therefore, the photo-generated holes in the P3HT molecules can be transferred to the deep localized surface states on the ZnO layer. Consequently, oxygen would be desorbed from the ZnO surface. Simultaneously, oxygen can dope P3HT through the photodoping effect explained by Lafalce et al. [118] The change in the doping level (and the Fermi level in the polymer) can reduce the rectifying barrier. The combination of the both effects after long enough exposure to light can result in a narrow space charge region in ZnO with a low energy barrier between the organic layer and ZnO. Hence, the contact between the NWs and the blend of organics behave as an Ohmic contact, dominated by tunneling charges through the barrier instead of the thermionic emission for passing electrons over the barrier. [115] In the lack of the energy barrier (Ohmic contact), trapping/detrapping the carriers would not lag the current when the voltage was scanned up and down. Hence, there would be no hysteresis effect. [115] In this case, the time constant depends on the relaxation time of the deep localized states and the diffusion of oxygen through the organic layer. Since under illumination, the Fermi level can be different in the ZnO and the organic layers, after cessation of light, there would be a driving force to reverse the process to reach the thermal equilibrium. Therefore, electrons can be trapped at the surface states again, and oxygen would be adsorbed to the ZnO surface while the polymer would be dedoped. Considering the long time constant associated to the deep localized states and the slow diffusion of oxygen to be adsorbed, the recovery time could be very slow as observed in our experiment. In presence of the localized state and the energy barrier, the device shows a rectifying behavior with a hysteresis in the I-V curve as explained before. [115]

It should be emphasized that the above discussion is only a possible explanation, focusing on the interface between ZnO NWs and the organic layer, because this memory effect has never been reported when a thin and smooth layer of ZnO was used. Such complicated hetero structure is not easy to be analyzed. Further experiments are required to gain a better understanding of the mechanism governing the memory effect and controlling the time constant. Based on the effect, various optoelectronic memory devices can be designed to store optical information. As an example, such a device can be used as pixel sensors in all organic high mega-pixel cameras. Reading information from all pixels needs fast electronics. Due to the limited bandwidth in organic transistors, the optical information can be saved in each pixel through the photoelectric memory effect, until the circuit can scan the data from all pixels.

5.5 Conclusion

In this work, we reported a photo electric memory effect observed in a bulk heterojunction structure made of ITO/ZnO nanowires/P3HT:PCBM/PEDOTS/Ag paste. The effect was studied by investigating the reversible change in the electrical response of the device under dark and illuminated conditions changing from rectifying response to resistive behavior. It was found that the device response changed from a linear resistive behavior to a rectifying behavior slowly and gradually after cessation of light, taking about approximately 270 minutes for the complete recovery to the dark response. The slow transition after illumination indicated a light sensitive information retention capability of the structure. The exact mechanism behind the photoelectric memory effect has to be investigated further to get a proper understanding of the process behind it, but oxygen adsorption and desorption at the ZnO layer causing band bending may be the reason behind the drift in the I-V response. Another reason that could explain this phenomenon is related to the photo-doping effect of the P3HT by reacting with oxygen and affecting the charge in the space charge region. Overall, photoelectric memory effect will open doors for many more

multifunctional devices utilizing the bistable memory effect under dark condition and resistive manipulation through illumination.

CHAPTER 6: OPTICAL MEMORY EFFECT IN ZnO NANOWIRE-BASED ORGANIC BULK HETEROJUNCTION DEVICES²

6.1 Abstract

Due to the required established field to separate photogenerated electrons and holes, the current- voltage (I-V) characteristic in almost all photovoltaic devices in dark is an exponential curve. Upon illumination, the shape of the curve remains almost the same, but the current shifts due to the photocurrent. In addition, because of the lack of any storage mechanism, the I-V curve returns to the dark characteristic immediately after light cessation. Here, we are reporting a case study performed on a photoelectric memory effect in an organic bulk heterojunction device made of ZnO nanowires as the electron transport layer under ambient conditions and within a sealed transfer box filled with nitrogen. The I-V characteristic in dark and light showed a unique change from a rectifying response in dark to a resistive behavior in light. Additionally, after light cessation, a memory effect was observed with a slow transition from the resistive to rectifying response same as the original dark characteristic. The memory effect and its I-V characteristics were tested for the two cases. For practical applications as a photo memory device, further experiments are required to gain a better understanding of the mechanism behind the observed memory effect for the two different cases.

² Reprinted with permission from Santhanakrishna, A. K., & Takshi, A. (2015). "Optical Memory Effect in ZnO Nanowire Based Organic Bulk Heterojunction Devices." *Proceedings of the International Society for Optics and Photonics*, 95690O(2015). doi:10.1117/12.2187689. Copyright (2015) International Society for Optics and Photonics. Permission is included in the Appendix A.

6.2 Introduction

Organic electronic devices can be classified as an unique branch of electronics which offers a sustainable, low cost alternative to conventional electronics for some applications such as sensors, photovoltaic cells, light emitting diodes and also open up a completely new field of devices due to its properties of mechanical flexibility and light weight in case of flexible solar cells. Organic electronics have been used for various applications, such as organic memory devices, light emitting diodes (OLEDs), flexible photovoltaic devices, sensors, functional electronics[119]. The environmental impact in manufacturing organic electronic devices has a much lower carbon footprint and also inexpensive[120]. Among all the categories of organic devices available, OLEDs have been a true success story with a wide commercial use[119]. Although it may be impractical to replace conventional silicon based photovoltaic systems with equivalent organic electronic devices due to the present limitation of device stability and efficiency, great progress has been made in the past few decades with the efficiency reaching as high as 9.2 %[121]. The charge generation mechanism in organic photovoltaics (OPVs) or organic materials in general is different compared to the inorganic materials due to the presence of highest occupied molecular orbital (HOMO) and lowest unoccupied molecular orbital LUMO with respect to the valence and conduction bands in inorganic materials. For efficient charge exchange and separation, organic materials require a combination of donor and acceptor species[85]. Among the various combinations of organic semiconductor materials Poly 3 hexylthiophene (P3HT) and Phenyl – C₆₁ Butyric acid Methyl ester (PCBM) are the most commonly used electron donor and acceptor materials, respectively[90, 122]. An intimately mixed combination of acceptor and donor materials, constitute the bulk heterojunction devices with an increased surface area for charge generation, was first studied by Yu et al[123].

In order to increase the charge extraction efficiency, appropriate materials are to be used as electron and hole transfer materials. Various metal oxide materials such as TiO₂, ZnO are used as electron transfer materials and likewise poly(3,4-ethylenedioxythiophene):polystyrene sulfonate (PEDOT:PSS) is the most promising hole transfer material[124]. A typical structure of an OPV is bottom transparent electrode/metal oxide (Electron transfer layer)/ heterojunction semiconductor/ hole transfer layer/ top electrode. As a result of the structure with energy barrier for the separation of hole and electron, the I-V response of a photovoltaic device under dark condition exhibits a rectifying behavior. The illuminated response is similar to the dark response with an exception of the response being shifted downwards (toward negative currents) due to the short circuit current.

A memory effect was observed in an inverted bulk heterojunction organic photovoltaic devices (ITO/ZnO nanowires/ P3HT:PCBM/PEDOT:PSS/Ag paste), where the electron collecting electrode is ZnO nanowires grown hydrothermally on an Indium tin oxide (ITO) substrate (bottom electrode)[125]. The device exhibited a unique response to illumination by switching from rectifying behavior under dark conditions to a resistive response after illumination. The response of the device slowly recovered to the original dark rectifying response with a transition time associated with the change. The observed photoelectric memory effect can be described as the ability of the device to slowly transition from the resistive illuminated response to the dark rectifying response gradually. The photo electric memory effect was studied in detail which included the effect of light intensity and varied duration of exposure. The result of that study has been published recently [125]. Various forms of memory effect have been reported before for organic devices [126-128]. A type of resistive organic memory that changes the resistance state of the devices with external stimulus has been studied before [126-128]. The memories consist of

either single or multiple organic materials sandwiched between two electrodes. A theory based on conductive filament due to the applied external stimulus between the electrodes is a widely accepted theory to explain the memory effect observed in these resistive organic memories. However, the observed memory effect in our device is completely different.

To further understand the exact nature of the memory effect observed in bulk heterojunction devices, the device was tested under ambient conditions and then transferred into a glove box for a period of 3 days. The sample was tested using a sealed transfer box to maintain the sample under glove box condition and its memory effect was studied. The study of device performance in ambient condition and under glove box condition is the focus of this work.

6.3 Methodology

6.3.1 Materials and Equipment

Indium Tin Oxide (ITO) Polyethylene terephthalate (PET) electrodes, materials required for ZnO nanowires fabrication such as zinc acetate dehydrate, zinc nitrate dehydrate, hexamethylene tetra amine (HMTA) and PEDOT:PSS were purchased from Sigma Aldrich. Organic semiconductors regioregular P3HT and PCBM were purchased from Luminescence technology corp and Silver paste required for the top electrode was obtained from SPI supplies.

The organic memory devices were illuminated using a solar simulator from Radiant Source Technology (RST) with full intensity of 80 mW.cm^{-2} (AM 1.0) connected to the testing box through a fiber optic cable. I-V and cyclic voltammetry (CV) characterization was performed using Keithley 2602A source meter and Versastat 4 potentiostat, respectively.

6.3.2 Device Fabrication

An inverted organic bulk heterojunction memory device measuring $10 \text{ mm} \times 5 \text{ mm}$ in dimensions was fabricated under ambient conditions. Firstly, ZnO NWs were grown on ITO PET electrode using a hydrothermal process. The ITO electrode was spin coated with 10 mM solution

of zinc acetate dehydrate prepared in ethanol at 1500 rpm for 45 seconds. The spin-coated sample was then transferred on to a hotplate at 150° C and annealed for 2 minutes. This process was repeated for 10 times to ensure uniform coverage of seeding layer on the ITO electrode. The ITO substrate with the seeding layer was mounted on a custom-made sample holder, such that the surface with the seeding layer faced down. This sample holder was then immersed into a zinc nitrate dehydrate (25 mM) and HMTA (25 mM) in deionized water growth solution maintained at 90° C with the help of a water bath. The solution was constantly stirred at 425 RPM for 4 h. Finally, the sample was removed and dried. The ZnO NWs grown using the hydrothermal process yielding 1.1 μm long NWs. The quality of the grown NWs was characterized using scanning electron microscope (SEM) (Figure 37).



Figure 37. SEM image of the hydrothermally grown ZnO nanowires on an ITO substrate.

The photoactive P3HT: PCBM solution was prepared by mixing 1:0.8 proportion of P3HT (10 mg/ml) and PCBM (8 mg/ml) in 1, 2 dichlorobenzene. The solution was sonicated for 10 min before drop casting 15 μL on the ZnO NW layer. After deposition of the active layer, the samples were heated at 60° C for 5 min. Poly (3, 4- ethylenedioxythiophene):polystyrene sulfonate (PEDOT: PSS) [15] diluted in the ratio of 1:1 with isopropanol were then subsequently drop casted on top of the active layer. Then a layer of the Ag paste was applied by gentle brushing and dried in air. The structure of the fabricated inverted bulk heterojunction device is shown in Figure 38 a.

6.3.3 Glove Box Setup

The sample was transferred from the glove box to the solar simulator using a custom made sealed transfer box to retain the sample under similar environment compared to the glove box. The transfer box is shown in figure 38 b

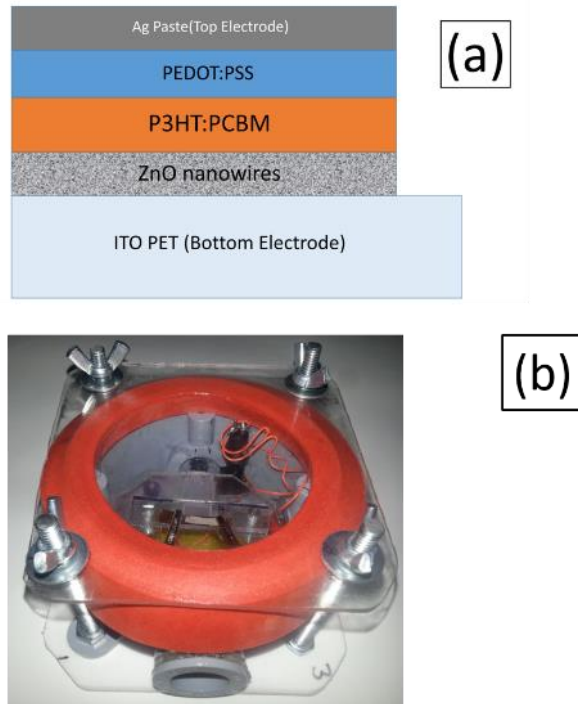


Figure 38. (a) Pictorial illustration showing the structure of the bulk heterojunction organic memory device and (b) the transfer box used to isolate the sample to maintain conditions similar to glove box for IV characterization and memory effect study.

6.4 Results and Discussion

An organic inverted bulk heterojunction device (ITO/ZnO NWs/P3HT:PCBM/PEDOT/Ag paste) was tested for its memory effect under two different test conditions .The sample was fabricated under ambient conditions and I-V characterization was performed to understand its electrical performance and memory effect of the device. Later the device was transferred into the glove box and isolated for three days under controlled environment. The sample from the glove box was transferred for testing, using a sealed transfer box and tested for both I-V characterization in dark and under illuminated conditions.

Figure 39 shows the I-V characteristics of the device performed by scanning the voltage of the bottom electrode from -2.0 V to 2.0 V while the top electrode was grounded. The dark response of the device, as shown in Figure 39, represents that of a rectifying behavior. The current while forward biased is approximately 2.3 mA at 2.0 V bias, whereas the reverse current is -0.75 mA at -2.0 V bias. The knee voltage was around (0.6-0.7 V). Although the reverse current was not very low, the rectifying response exhibited by the device was decent, with the forward current at 2.0 V being 3 times greater than the reverse current at -2.0 V. The I-V characterization in light was performed after constant illumination for 5 minutes using the solar simulator (80 mW.cm⁻²). The illuminated response was resistive with the forward and reverse current for 2.0 V and -2.0 V bias being 4.3 mA and -2.0 mA respectively. The device showed a weak photocurrent in the range of 100-150 μA.

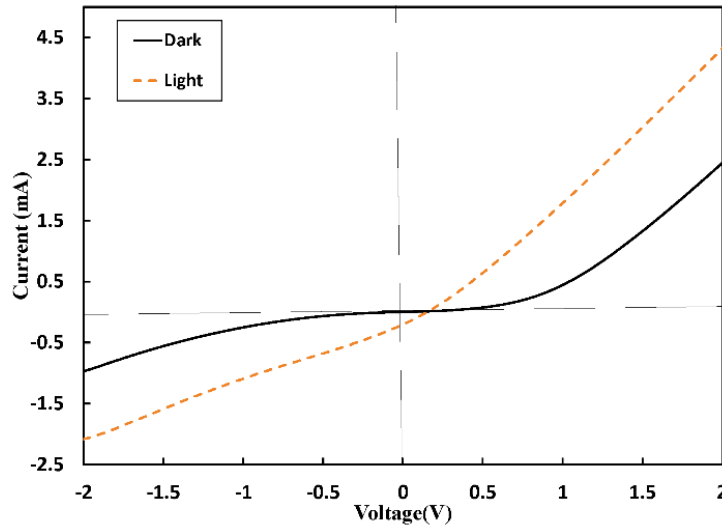


Figure 39. I-V characterization of the device in the dark and under illumination performed in ambient conditions.

Figure 40 illustrates the transformation of the ambient condition test sample from the illuminated resistive response to the dark rectifying response. The device was illuminated for 5 minutes with a light intensity of 80 mW.cm⁻². The gradual recovery from the resistive response is evident with the change in the reverse current at -2.0 V bias from -1.7 mA to -0.8 mA and 4.2 mA

to 2.2 mA for forward bias at 2.0 V. The original dark response prior to illumination had a knee voltage of 0.7 V. The transition indicates that the knee voltage was significantly decreased for the response recorded immediately after the cessation of light to almost 0.2-0.3 V and increased as the device recovered and reached a knee voltage of 0.65 V during the due course of 195 minutes.

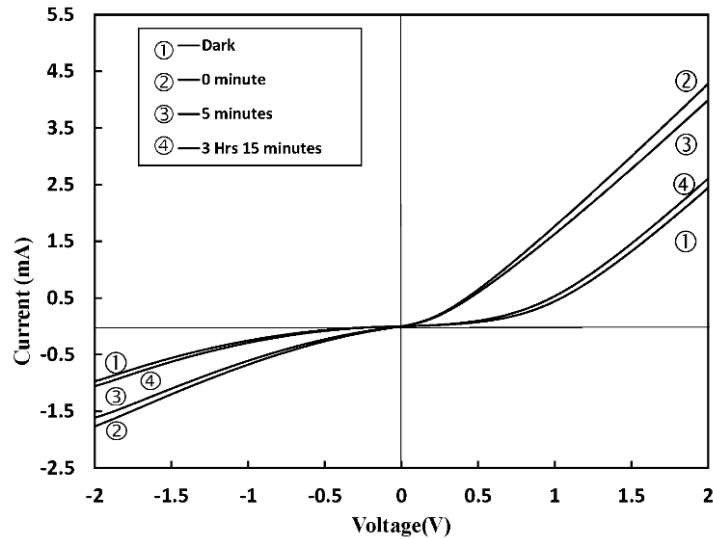


Figure 40. Memory effect experimentation of the sample tested under ambient conditions through I-V characterization showing gradual return to the dark response.

Since the memory effect has not been reported before in inverted OPVs, a hypothesis is that our device was behaving differently due to the effect of oxygen [125, 129]. Because oxygen can act as a dopant in organic semiconductors, it is recommended to fabricate organic devices in an inert environment, such as a glove box filled with N_2/Ar , and test them in the same environment or seal them before transferring from the glove box to the ambient condition[130].

To study the effect of oxygen on the memory-effect, the fabricated device in the ambient condition was transferred into a glove box (N_2 environment) and stored for 3 days. Then the device was transferred out while it was in a sealed container. Although this method cannot remove all oxygen molecules trapped in the device, it is expected that some oxygen would be diffused out during loading the sample (vacuum in the load lock process) and 3 days of stay in an oxygen free

environment. Figure 41 shows the I-V characterization performed on the transfer box sample after the device was isolated in an oxygen controlled environment for consecutive three days. The device was monitored under dark conditions for approximately 21 h to obtain a stable dark response. Furthermore, the sample was illuminated for 5 minutes and the light was turned off. The dark response of the sample in the transfer box still exhibited a rectifying response. The forward and reverse current at 2.0 V and -2.0 V bias were 3.2 mA and -2.9 mA, respectively. The overall voltage span shows that the current at extreme bias of the experiment did not vary by much. The illuminated response represents a resistive behavior with a reduced photocurrent of 45 μ A. The currents at +2.0 V and -2.0 V bias were 4.8 mA and -3.5 mA, respectively.

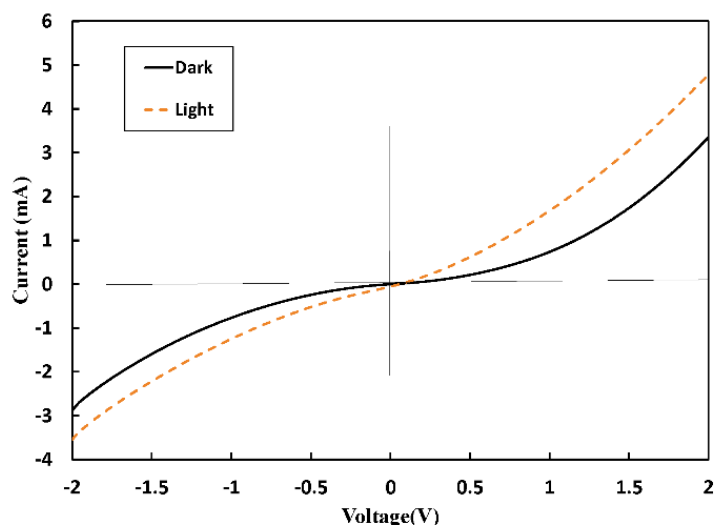


Figure 41. I-V characterization of the bulk heterojunction device in the dark and under illumination performed using a sealed transfer glove box with conditions similar to glove box.

Keeping with the trend to test for the memory effect exhibited by the sample at each test condition, the sample was monitored for the change in the I-V characteristics after cessation of light at 0, 5 and 480 minutes (Figure 42). Comparing the I-V characterization results between the two test conditions, it is evident that the response exhibited for the sample tested under ambient conditions that the device response clearly transitions from a rectifying response under dark to a

resistive behavior under illumination. Whereas for the sample tested using a sealed transfer box, the response for dark and illumination conditions have different dark performance with the current increasing almost exponentially for the forward bias and current decreasing exponentially for the reverse bias. The illuminated response remained the same for both the test cases with the device exhibiting a resistive behavior. The reverse current changed through a short range compared to the ambient test phase from -3.1 mA to -2.8 mA over a period of 8 h. A similar trend was observed in the forward bias at 2.0 V changing from 4.5 mA to 3.1 mA. The knee voltage changed from (0.2 – 0.3 V) for 0 minute to 0.4 V after 8 h.

In order to study the exact change in memory effect in these two experimental conditions, percentage change in current with respect to the current reading obtained immediately after light cessation were recorded using the difference between the current for the response recorded immediately after the cessation of light and the response after 5 minutes during the transition period were tabulated for both the forward and reverse bias at +2.0 V and -2.0 V, respectively. The results are tabulated in Table 1.

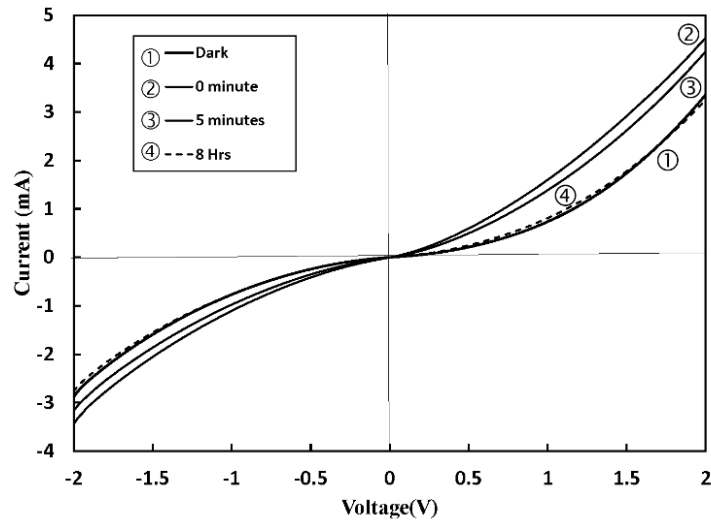


Figure 42. Device recovery process of the sample in a sealed transfer box through I-V characterization of an inverted bulk heterojunction photoelectric memory device from illuminated behavior to dark response.

Table 2. Open circuit voltage study of the cells under various conditions.

Test phase	ΔI % (Forward bias at 2 V)	ΔI % (Reverse bias at -2 V)
Ambient condition	5.13	8.98
Transfer box condition	11.24	7.84

The percentage change of current for ambient experiment was the smaller compared to the transfer box experiment, indicating a long transition time. Whereas the percentage change in the current for the reverse bias condition indicates that the transition was almost similar for both the cases. It is evident from the change in the transition time associated with these two experimental test conditions that the change in oxygen exposure had a significant impact on the memory effect. The exact reason behind the changes observed needs to be investigated further to fully understand the role of oxygen on the electrical performance of the device.

6.5 Conclusion

The IV characterization was performed on the inverted bulk heterojunction junction (ITO/ZnO NWs/ P3HT:PCBM/PEDOT:PSS/Ag paste) device to study the dark and illuminated response of the sample under two different test conditions of ambient testing and isolation in glove box for three consecutive days and later testing using a sealed transfer box. The memory effect exhibited by the device was also investigated to study the impact of isolation in a glove on the performance of the device. The device showed a decent rectifying response for dark condition and the illuminated response was resistive. The memory effect study performed on the under ambient condition showed that the device recovered from the resistive response to the rectifying response with a long transition time. This was indicated by the memory study that the sample tested under ambient condition had a slower percentage change in current (5.13%) with respect to the recordings obtained immediately after light cessation and 5 minutes during this process. In contrast, the device tested using a transfer box exhibited a different type of response as indicated

by a faster fall in current values for the measurement performed at 0 minutes and 5 minutes, respectively, with a percentage fall of 11.24%. The impact of oxygen on the device performance is profound and further study is required to understand the exact impact on the device and the response behind the change.

CHAPTER 7: CONCLUSION AND SUGGESTED FUTURE WORK

7.1 Conclusion

In this work, synthesis and characterization of crystalline ZnO nanowires, nanoforest and planar ZnO nanofilm was reported along with the application of these ZnO nanostructures in optoelectronic devices. Low temperature, flexible substrate compatible and facile hydrothermal technique was utilized for the fabrication of 1D nanostructures. Scanning electron microscopy analyses have shown that the geometric dimension, length and other critical physical properties of these nanostructures depend on the fabrication method and process. Specifically the length of the nanowires in this work was primarily controlled by the duration of growth. Noncentro symmetry of crystalline ZnO nanostructures makes it an excellent candidate to be used as piezo functional material and these nanostructures are characterized using electrochemical cell containing ZnO electrode as the working electrode.

For studying the effect of an initial stress, flexible ITO substrates were used to grow ZnO nanowires at different growth curvature to study the impact of pre-straining the growth substrate during the nanowire synthesis process. The piezo characterization of flat grown ZnO and curve grown ZnO nanowires showed that it was possible to obtain densely packed bed of misaligned ZnO nanowires with an inherent piezopotential by manipulating the growth curvature; this allowed the use of ZnO nanowires to perform energy interface engineering during its application in optoelectronic devices.

ZnO nanostructures like nanowires, nanoforest and planar nanofilm were similarly characterized for piezo property using electrochemical technique. Different devices require

distinguishing physical and electrical properties of ZnO nanostructures; hence, morphology, surface area, surface coverage and thickness of these nanostructures were evaluated for their piezoresponse. It was shown that it was possible to obtain similar piezoresponse among different ZnO nanostructures in addition to taking advantage of the structural benefits among various categories of nanostructures as per requirement.

Employing hydrothermally grown ZnO NWs as the electron transfer layer in an inverted bulk heterojunction organic photovoltaic device, a memory effect was observed in the device. The I-V characteristic of the device was significantly changed from a non-linear form to a linear one after being exposed to the light. The device response returned to the original form after a long (~270 min) and gradual transition.

The slow transition after illumination indicated a light sensitive information retention capability of the structure. The exact mechanism behind the photoelectric memory effect has to be investigated further to get a proper understanding of the process behind it, but oxygen adsorption and desorption at the ZnO layer causing band bending may be the reason behind the drift in the I-V response. Another reason that could explain this phenomenon is related to the photo-doping effect of the P3HT by reacting with oxygen and affecting the charge in the space charge region. Overall, photoelectric memory effect will open doors for many more multifunctional devices utilizing the bistable memory effect under dark condition and resistive manipulation through illumination.

We can summarize the contribution of this research toward synthesis, piezo characterization of ZnO nanostructures and its application for optoelectronic devices as:

- Electrochemical piezo characterization extended to test several novel ZnO nanostructures.

- Tunable piezo potential techniques using pre straining method suitable for flexible substrate having ZnO nanostructures
- Variable piezo response characteristics of nanostructures through morphology study.
- Illustration of photo electric memory in a bulk heterojunction structure made of ITO/ZnO nanowires/P3HT:PCBM/PEDOTS/Ag paste.
- Analyzed the impact of oxygen exposure in a bulk heterojunction device on its photo electric memory effect.

7.2 Suggestions for Future Work

The presented research can be used as the proof-of-the-concept that ZnO nanostructures can be designed and fabricated with a prestrain to adjust the piezo response of the material under external forces. Therefore, the structure with the prestrain can be employed in various electronic and optical devices where the piezo voltage can be used for adjusting the energy band bending at an interface. The primary application of this structure can be in organic and thin-film solar cells. ZnO is a commonly used electron transfer layer in those devices. However, efficient collection of electrons from the active layer of a solar cell requires a small or no energy barrier at the ZnO surface. While controlling the energy structure of a material at its surface is difficult due to the pinning effect, the proposed method can be used to modify the energy structure at the interface by tuning the piezo voltage of the ZnO layer with a prestrain design. This concept has been filed as a patent under the author and the project supervisor (US Patent 9,911,540). Designing a solar cell with the prestrained ZnO nanostructures is strongly encouraged as a future project to address the need of designing and fabricating efficient solar cells.

Also, the devised electrochemical method provides an opportunity to study the piezo electric effect in other ZnO nanostructures and even other piezo materials. Controlling the growth process to fabricate structures with a more predictable mechanical structure is suggested, as well.

The results from this project have opened new venues to our lab and it is expected to provide more opportunity for other graduate and undergraduate students to explore other aspects of the piezo nanostructures and fabricate efficient piezotronic devices.

REFERENCES

1. Fan, F.R., W. Tang, and Z.L. Wang, *Flexible Nanogenerators for Energy Harvesting and Self-Powered Electronics*. *Advanced Materials*, 2016. **28**(22): p. 4283-4305.
2. Tan, Y.K. and S.K. Panda, *Energy Harvesting From Hybrid Indoor Ambient Light and Thermal Energy Sources for Enhanced Performance of Wireless Sensor Nodes*. *IEEE Transactions on Industrial Electronics*, 2011. **58**(9): p. 4424-4435.
3. Wang, Z.L., *Towards Self-Powered Nanosystems: From Nanogenerators to Nanopiezotronics*. *Advanced Functional Materials*, 2008. **18**(22): p. 3553-3567.
4. Markets, M.a., *Piezoelectric Devices Market by Material (Piezoceramics, Piezopolymers, Piezocomposites, Piezocrystals), Product (Actuators, Transducers, Motors, Sensors, Generators), Application (Industrial, Automotive, Healthcare, Consumer) - Global Forecast to 2022*.
5. Sahoo, B., *PZT to Lead Free Piezo Ceramics: A Review AU - Panda, P. K. Ferroelectrics*, 2015. **474**(1): p. 128-143.
6. Haertling, G.H., *Ferroelectric Ceramics: History and Technology*. *Journal of the American Ceramic Society*, 1999. **82**(4): p. 797-818.
7. Wang, Z.L., *Piezopotential gated nanowire devices: Piezotronics and piezo-phototronics*. *Nano Today*, 2010. **5**(6): p. 540-552.
8. Kasap, S., *Principles of Electronic Materials and Devices*. 2006: McGraw-Hill, Inc. 768.
9. Heywang, W., K. Lubitz, and W. Wersing, *Piezoelectricity: Evolution and Future of a Technology*. 2008: Springer Publishing Company, Incorporated. 582.
10. Anton, S.R. and H.A. Sodano, *A review of power harvesting using piezoelectric materials (2003–2006)*. *Smart Materials and Structures*, 2007. **16**(3): p. R1-R21.
11. Wang, Z.L. and J. Song, *Piezoelectric Nanogenerators Based on Zinc Oxide Nanowire Arrays*. *Science*, 2006. **312**(5771): p. 242.
12. Fu, Y.Q., et al., *Recent developments on ZnO films for acoustic wave based bio-sensing and microfluidic applications: a review*. *Sensors and Actuators B: Chemical*, 2010. **143**(2): p. 606-619.

13. Majdoub, M.S., P. Sharma, and T. Çağın, *Dramatic enhancement in energy harvesting for a narrow range of dimensions in piezoelectric nanostructures*. Physical Review B, 2008. **78**(12): p. 121407.
14. Schmidt-Mende, L. and J.L. MacManus-Driscoll, *ZnO – nanostructures, defects, and devices*. Materials Today, 2007. **10**(5): p. 40-48.
15. Ebrahimi, H., et al., *Electrochemical Detection of Piezoelectric Effect from Misaligned Zinc Oxide Nanowires Grown on a Flexible Electrode*. Electrochimica Acta, 2014. **134**: p. 435-441.
16. *Handbook of Advanced Dielectric, Piezoelectric and Ferroelectric Materials*. 2008, CRC Press.
17. Broitman, E., et al., *Nanoscale piezoelectric response of ZnO nanowires measured using a nanoindentation technique*. Physical Chemistry Chemical Physics, 2013. **26**: p. 11113-11118.
18. Özgür, Ü., et al., *A comprehensive review of ZnO materials and devices*. Journal of applied physics, 2005. **98**(4): p. 041301.
19. Ludi, B. and M. Niederberger, *Zinc oxide nanoparticles: chemical mechanisms and classical and non-classical crystallization*. Dalton Transactions, 2013. **42**(35): p. 12554-12568.
20. Kołodziejczak-Radzimska, A. and T. Jesionowski, *Zinc Oxide—From Synthesis to Application: A Review*. Materials, 2014. **7**(4).
21. Wang, Z.L., *ZnO nanowire and nanobelt platform for nanotechnology*. Materials Science and Engineering: R: Reports, 2009. **64**(3): p. 33-71.
22. Wang, Z.L., et al., *Lateral nanowire/nanobelt based nanogenerators, piezotronics and piezo-phototronics*. Materials Science and Engineering: R: Reports, 2010. **70**(3): p. 320-329.
23. Wen, B., J.E. Sader, and J.J. Boland, *Mechanical properties of ZnO nanowires*. Physical review letters, 2008. **101**(17): p. 175502.
24. Xiang, H., et al., *Piezoelectricity in ZnO nanowires: a first-principles study*. Applied physics letters, 2006. **89**(22): p. 223111-223111-3.
25. Özgür, Ü., et al., *A comprehensive review of ZnO materials and devices*. Journal of Applied Physics, 2005. **98**(4): p. 041301.
26. Wang, X., et al., *Piezoelectric Field Effect Transistor and Nanoforce Sensor Based on a Single ZnO Nanowire*. Nano Letters, 2006. **6**(12): p. 2768-2772.

27. He, J.H., et al., *Piezoelectric gated diode of a single ZnO nanowire*. *Advanced Materials*, 2007. **19**(6): p. 781-784.
28. Wang, Z.L., *Progress in Piezotronics and Piezo-Phototronics*. *Advanced Materials*, 2012. **24**(34): p. 4632-4646.
29. Shi, J., M.B. Starr, and X. Wang, *Band Structure Engineering at Heterojunction Interfaces via the Piezotronic Effect*. *Advanced Materials*, 2012. **24**(34): p. 4683-4691.
30. Wang, Z.L., *Piezotronic and piezophototronic effects*. *The Journal of Physical Chemistry Letters*, 2010. **1**(9): p. 1388-1393.
31. Trolier-McKinstry, S. and P. Muralt, *Thin film piezoelectrics for MEMS*. *Journal of Electroceramics*, 2004. **12**(1-2): p. 7-17.
32. Carcia, P., et al., *Transparent ZnO thin-film transistor fabricated by rf magnetron sputtering*. *Applied Physics Letters*, 2003. **82**(7): p. 1117-1119.
33. Baruah, S. and J. Dutta, *Hydrothermal growth of ZnO nanostructures*. *Science and Technology of Advanced Materials*, 2009. **10**(1): p. 013001.
34. Zhu, G., et al., *Flexible high-output nanogenerator based on lateral ZnO nanowire array*. *Nano letters*, 2010. **10**(8): p. 3151-3155.
35. Connelly, N.G. and W.E. Geiger, *Chemical Redox Agents for Organometallic Chemistry*. *Chemical Reviews*, 1996. **96**(2): p. 877-910.
36. Gao, P.X., et al., *Nanowire Piezoelectric Nanogenerators on Plastic Substrates as Flexible Power Sources for Nanodevices*. *Advanced Materials*, 2007. **19**(1): p. 67-72.
37. Araneo, R., et al., *Effect of the scaling of the mechanical properties on the performances of ZnO piezo-semiconductive nanowires*. *AIP Conference Proceedings*, 2014. **1603**(1): p. 14-22.
38. Minary-Jolandan, M., R.A. Bernal, and H.D. Espinosa, *Strong piezoelectricity in individual GaN nanowires*. *MRS Communications*, 2011. **1**(1): p. 45-48.
39. Agrawal, R. and H.D. Espinosa, *Giant Piezoelectric Size Effects in Zinc Oxide and Gallium Nitride Nanowires. A First Principles Investigation*. *Nano Letters*, 2011. **11**(2): p. 786-790.
40. Liang, W. and A. Yoffe, *Transmission spectra of ZnO single crystals*. *Physical Review Letters*, 1968. **20**(2): p. 59.
41. Jin, B., S. Im, and S.Y. Lee, *Violet and UV luminescence emitted from ZnO thin films grown on sapphire by pulsed laser deposition*. *Thin Solid Films*, 2000. **366**(1): p. 107-110.

42. Zhao, M.-H., Z.-L. Wang, and S.X. Mao, *Piezoelectric characterization of individual zinc oxide nanobelt probed by piezoresponse force microscope*. Nano Letters, 2004. **4**(4): p. 587-590.
43. Maeda, K., et al., *GaN: ZnO solid solution as a photocatalyst for visible-light-driven overall water splitting*. Journal of the American Chemical Society, 2005. **127**(23): p. 8286-8287.
44. Ravirajan, P., et al., *Hybrid polymer/zinc oxide photovoltaic devices with vertically oriented ZnO nanorods and an amphiphilic molecular interface layer*. The Journal of Physical Chemistry B, 2006. **110**(15): p. 7635-7639.
45. Liao, Z.-M., et al., *Photovoltaic effect and charge storage in single ZnO nanowires*. Applied physics letters, 2008. **93**(2): p. 023111.
46. Guo, X.-L., et al., *Fabrication and optoelectronic properties of a transparent ZnO homostructural light-emitting diode*. Japanese Journal of Applied Physics, 2001. **40**(3A): p. L177.
47. Wang, Z.L., *Zinc oxide nanostructures: growth, properties and applications*. Journal of Physics: Condensed Matter, 2004. **16**(25): p. R829.
48. Xiang, H., et al., *Piezoelectricity in ZnO nanowires: a first-principles study*. Applied physics letters, 2006. **89**(22): p. 223111-223111.
49. Gu, Y., et al., *Quantum confinement in ZnO nanorods*. mh, 2004. **2**(2): p. 2r2.
50. Wei, B., et al., *Size-dependent bandgap modulation of ZnO nanowires by tensile strain*. Nano letters, 2012. **12**(9): p. 4595-4599.
51. Wei, Y., et al., *Growth of vertically aligned ZnO nanobelt arrays on GaN substrate*. The Journal of Physical Chemistry C, 2008. **112**(48): p. 18935-18937.
52. Lao, C.S., et al., *ZnO nanobelt/nanowire Schottky diodes formed by dielectrophoresis alignment across Au electrodes*. Nano Letters, 2006. **6**(2): p. 263-266.
53. Hughes, W.L. and Z.L. Wang, *Controlled synthesis and manipulation of ZnO nanorings and nanobows*. Applied Physics Letters, 2005. **86**(4): p. 043106.
54. Kong, X.Y., et al., *Single-crystal nanorings formed by epitaxial self-coiling of polar nanobelts*. Science, 2004. **303**(5662): p. 1348-1351.
55. Gao, P.-X., Y. Ding, and Z.L. Wang, *Electronic transport in superlattice-structured ZnO nanohelix*. Nano letters, 2008. **9**(1): p. 137-143.
56. Gao, H., et al., *Super-uniform ZnO nanohelices synthesized via thermal evaporation*. Solid state communications, 2006. **140**(9): p. 455-458.

57. Liu, B. and H.C. Zeng, *Direct growth of enclosed ZnO nanotubes*. Nano Research, 2009. **2**(3): p. 201-209.
58. Han, J., et al., *ZnO nanotube-based dye-sensitized solar cell and its application in self-powered devices*. Nanotechnology, 2010. **21**(40): p. 405203.
59. Yi, G.-C., C. Wang, and W.I. Park, *ZnO nanorods: synthesis, characterization and applications*. Semiconductor Science and Technology, 2005. **20**(4): p. S22.
60. Wang, X., C.J. Summers, and Z.L. Wang, *Large-scale hexagonal-patterned growth of aligned ZnO nanorods for nano-optoelectronics and nanosensor arrays*. Nano Letters, 2004. **4**(3): p. 423-426.
61. Hsueh, T.-J., et al., *ZnO nanowire-based CO sensors prepared at various temperatures*. Journal of The Electrochemical Society, 2007. **154**(12): p. J393-J396.
62. Ra, H.-W., et al., *Formation and Characterization of ZnO/aC Core– Shell Nanowires*. The Journal of Physical Chemistry C, 2009. **113**(9): p. 3512-3516.
63. Kang, D.-S., et al., *ZnO nanowires prepared by hydrothermal growth followed by chemical vapor deposition for gas sensors*. Journal of Vacuum Science & Technology B, 2009. **27**(3): p. 1667-1672.
64. Zhao, Y. and Y.-U. Kwon, *Templateless hydrothermal synthesis of aligned ZnO nanorods*. Chemistry letters, 2004. **33**(12): p. 1578-1579.
65. Liu, B. and H.C. Zeng, *Hydrothermal synthesis of ZnO nanorods in the diameter regime of 50 nm*. Journal of the American Chemical Society, 2003. **125**(15): p. 4430-4431.
66. Akhavan, O., et al., *Hydrothermal synthesis of ZnO nanorod arrays for photocatalytic inactivation of bacteria*. Journal of Physics D: Applied Physics, 2009. **42**(22): p. 225305.
67. Vayssieres, L., *Growth of arrayed nanorods and nanowires of ZnO from aqueous solutions*. Advanced Materials, 2003. **15**(5): p. 464-466.
68. Xing, Y., et al., *Thermal evaporation synthesis of zinc oxide nanowires*. Applied Physics A, 2005. **80**(7): p. 1527-1530.
69. Zhang, Y., et al., *Synthesis of nano/micro zinc oxide rods and arrays by thermal evaporation approach on cylindrical shape substrate*. The Journal of Physical Chemistry B, 2005. **109**(27): p. 13091-13093.
70. Ishikawa, Y., et al., *Preparation of zinc oxide nanorods using pulsed laser ablation in water media at high temperature*. Journal of colloid and interface science, 2006. **300**(2): p. 612-615.

71. He, H., et al., *Surface decoration of ZnO nanorod arrays by electrophoresis in the Au colloidal solution prepared by laser ablation in water*. Langmuir, 2010. **26**(11): p. 8925-8932.
72. Park, S.K., et al., *Hydrothermal– Electrochemical Synthesis of ZnO Nanorods*. Crystal Growth and Design, 2009. **9**(8): p. 3615-3620.
73. Park, W.I., et al., *Metalorganic vapor-phase epitaxial growth of vertically well-aligned ZnO nanorods*. Applied Physics Letters, 2002. **80**(22): p. 4232-4234.
74. Rojo, J.C., et al. *Physical vapor transport crystal growth of ZnO*. in *Integrated Optoelectronic Devices 2006*. 2006. International Society for Optics and Photonics.
75. Kuo, T.-J., et al., *Growth of ultralong ZnO nanowires on silicon substrates by vapor transport and their use as recyclable photocatalysts*. Chemistry of Materials, 2007. **19**(21): p. 5143-5147.
76. Manekkathodi, A., et al., *Direct Growth of Aligned Zinc Oxide Nanorods on Paper Substrates for Low-Cost Flexible Electronics*. Advanced materials, 2010. **22**(36): p. 4059-4063.
77. Sun, Y., et al., *Synthesis and photoluminescence of ultra-thin ZnO nanowire/nanotube arrays formed by hydrothermal growth*. Chemical Physics Letters, 2006. **431**(4): p. 352-357.
78. Djurišić, A.B. and Y.H. Leung, *Optical properties of ZnO nanostructures*. small, 2006. **2**(8-9): p. 944-961.
79. Xu, S. and Z.L. Wang, *One-dimensional ZnO nanostructures: solution growth and functional properties*. Nano Research, 2011. **4**(11): p. 1013-1098.
80. Ko, S.H., et al., *Nanoforest of hydrothermally grown hierarchical ZnO nanowires for a high efficiency dye-sensitized solar cell*. Nano letters, 2011. **11**(2): p. 666-671.
81. Yang, P., et al., *Controlled growth of ZnO nanowires and their optical properties*. Advanced Functional Materials, 2002. **12**(5): p. 323.
82. Li, G., R. Zhu, and Y. Yang, *Polymer solar cells*. Nature Photonics, 2012. **6**(3): p. 153-161.
83. Forrest, S.R., *The path to ubiquitous and low-cost organic electronic appliances on plastic*. Nature, 2004. **428**(6986): p. 911-918.
84. Clarke, T.M. and J.R. Durrant, *Charge photogeneration in organic solar cells*. Chemical reviews, 2010. **110**(11): p. 6736-6767.
85. Günes, S., H. Neugebauer, and N.S. Sariciftci, *Conjugated Polymer-Based Organic Solar Cells*. Chemical Reviews, 2007. **107**(4): p. 1324-1338.

86. Shaheen, S.E., et al., *2.5% efficient organic plastic solar cells*. Applied Physics Letters, 2001. **78**(6): p. 841-843.
87. Lee, T. and Y. Chen, *Organic resistive nonvolatile memory materials*. MRS bulletin, 2012. **37**(02): p. 144-149.
88. Ameri, T., et al., *Organic tandem solar cells: a review*. Energy & Environmental Science, 2009. **2**(4): p. 347-363.
89. Yu, G., et al., *Polymer photovoltaic cells: enhanced efficiencies via a network of internal donor-acceptor heterojunctions*. Science-AAAS-Weekly Paper Edition, 1995. **270**(5243): p. 1789-1790.
90. Hummelen, J.C., et al., *Preparation and Characterization of Fulleroid and Methanofullerene Derivatives*. The Journal of Organic Chemistry, 1995. **60**(3): p. 532-538.
91. Dang, M.T., et al., *Polymeric solar cells based on P3HT: PCBM: Role of the casting solvent*. Solar Energy Materials and Solar Cells, 2011. **95**(12): p. 3408-3418.
92. Scharber, M.C., et al., *Design rules for donors in bulk-heterojunction solar cells—Towards 10% energy-conversion efficiency*. Advanced Materials, 2006. **18**(6): p. 789-794.
93. Hau, S.K., et al., *Air-stable inverted flexible polymer solar cells using zinc oxide nanoparticles as an electron selective layer*. Applied Physics Letters, 2008. **92**(25): p. 253301.
94. Na, S.I., et al., *Efficient and Flexible ITO-Free Organic Solar Cells Using Highly Conductive Polymer Anodes*. Advanced Materials, 2008. **20**(21): p. 4061-4067.
95. Sun, Y., et al., *Inverted Polymer Solar Cells Integrated with a Low-Temperature-Annealed Sol-Gel-Derived ZnO Film as an Electron Transport Layer*. Advanced Materials, 2011. **23**(14): p. 1679-1683.
96. Cheun, H., et al., *Electrical and optical properties of ZnO processed by atomic layer deposition in inverted polymer solar cells†*. The Journal of Physical Chemistry C, 2010. **114**(48): p. 20713-20718.
97. Wang, J.-C., et al., *Highly efficient flexible inverted organic solar cells using atomic layer deposited ZnO as electron selective layer*. Journal of Materials Chemistry, 2010. **20**(5): p. 862-866.
98. Wöhrle, D. and D. Meissner, *Organic solar cells*. Advanced Materials, 1991. **3**(3): p. 129-138.
99. Koster, L., et al., *Origin of the light intensity dependence of the short-circuit current of polymer/fullerene solar cells*. Applied Physics Letters, 2005. **87**(20): p. 203502.




100. Koster, L.J.A., et al., *Light intensity dependence of open-circuit voltage of polymer: fullerene solar cells*. Applied Physics Letters, 2005. **86**(12): p. 123509-123509-3.
101. Schilinsky, P., et al., *Simulation of light intensity dependent current characteristics of polymer solar cells*. Journal of Applied Physics, 2004. **95**(5): p. 2816-2819.
102. Hoppe, H. and N.S. Sariciftci, *Organic solar cells: An overview*. Journal of Materials Research, 2004. **19**(07): p. 1924-1945.
103. Donhauser, Z., et al., *Conductance switching in single molecules through conformational changes*. Science, 2001. **292**(5525): p. 2303-2307.
104. Guo, P., et al., *Nonvolatile multilevel conductance and memory effect in molecule-based devices*. Electron Device Letters, IEEE, 2007. **28**(7): p. 572-574.
105. Yang, Y., et al., *Electrical switching and bistability in organic/polymeric thin films and memory devices*. Advanced Functional Materials, 2006. **16**(8): p. 1001-1014.
106. Hensch, H. and W. Smith, *Switching in organic polymer films*. Applied Physics Letters, 1974. **24**(12): p. 589-591.
107. Lai, P.Y. and J.-S. Chen, *Electrical bistability and charge transport behavior in Au nanoparticle/poly (N-vinylcarbazole) hybrid memory devices*. Applied Physics Letters, 2008. **93**(15): p. 153305-153305-3.
108. Sawa, A., *Resistive switching in transition metal oxides*. Materials today, 2008. **11**(6): p. 28-36.
109. Kim, T.-W., et al., *Resistive switching characteristics of polymer non-volatile memory devices in a scalable via-hole structure*. Nanotechnology, 2009. **20**(2): p. 025201.
110. Gao, S., et al., *Dynamic processes of resistive switching in metallic filament-based organic memory devices*. The Journal of Physical Chemistry C, 2012. **116**(33): p. 17955-17959.
111. Carchano, H., R. Lacoste, and Y. Segui, *Bistable electrical switching in polymer thin films*. Applied Physics Letters, 1971. **19**(10): p. 414-415.
112. Hau, S.K., et al., *Interfacial modification to improve inverted polymer solar cells*. Journal of Materials Chemistry, 2008. **18**(42): p. 5113-5119.
113. Ladanov, M., et al., *Structure and opto-electrochemical properties of ZnO nanowires grown on n-Si substrate*. Langmuir, 2011. **27**(14): p. 9012-9017.
114. He, Z., et al., *Enhanced power-conversion efficiency in polymer solar cells using an inverted device structure*. Nature Photonics, 2012. **6**(9): p. 591-595.
115. Takshi, A. and J.D. Madden, *Large apparent inductance in organic Schottky diodes at low frequency*. Journal of applied physics, 2006. **99**(8): p. 084503.


116. Wilken, S., J.r. Parisi, and H. Borchert, *Role of Oxygen Adsorption in Nanocrystalline ZnO Interfacial Layers for Polymer–Fullerene Bulk Heterojunction Solar Cells*. The Journal of Physical Chemistry C, 2014. **118**(34): p. 19672-19682.
117. Pivrikas, A., et al., *A review of charge transport and recombination in polymer/fullerene organic solar cells*. Progress in Photovoltaics: Research and Applications, 2007. **15**(8): p. 677-696.
118. Lafalce, E., et al., *Photo annealing effect on p-doped inverted organic solar cell*. Journal of Applied Physics, 2014. **115**(24): p. 244511.
119. Li, G., R. Zhu, and Y. Yang, *Polymer solar cells*. Nature Photonics, 2012. **6**: p. 153.
120. Forrest, S.R., *The path to ubiquitous and low-cost organic electronic appliances on plastic*. Nature, 2004. **428**: p. 911.
121. He, Z., et al., *Enhanced power-conversion efficiency in polymer solar cells using an inverted device structure*. Nature Photonics, 2012. **6**: p. 591.
122. Dang, M.T., et al., *Polymeric solar cells based on P3HT:PCBM: Role of the casting solvent*. Solar Energy Materials and Solar Cells, 2011. **95**(12): p. 3408-3418.
123. Yu, G., et al., *Polymer Photovoltaic Cells: Enhanced Efficiencies via a Network of Internal Donor-Acceptor Heterojunctions*. Science, 1995. **270**(5243): p. 1789.
124. Hau, S.K., et al., *Air-stable inverted flexible polymer solar cells using zinc oxide nanoparticles as an electron selective layer*. Applied Physics Letters, 2008. **92**(25): p. 253301.
125. Santhanakrishna, A.K. and A. Takshi, *Photoelectric Memory Effect in an Organic Bulk Heterojunction Device*. The Journal of Physical Chemistry C, 2015. **119**(30): p. 17253-17259.
126. Donhauser, Z.J., et al., *Conductance Switching in Single Molecules Through Conformational Changes*. Science, 2001. **292**(5525): p. 2303.
127. Guo, P., et al., *Nonvolatile Multilevel Conductance and Memory Effect in Molecule-Based Devices*. IEEE Electron Device Letters, 2007. **28**(7): p. 572-574.
128. Henisch, H.K. and W.R. Smith, *Switching in organic polymer films*. Applied Physics Letters, 1974. **24**(12): p. 589-591.
129. Wilken, S., J. Parisi, and H. Borchert, *Role of Oxygen Adsorption in Nanocrystalline ZnO Interfacial Layers for Polymer–Fullerene Bulk Heterojunction Solar Cells*. The Journal of Physical Chemistry C, 2014. **118**(34): p. 19672-19682.
130. Liang, Y., et al., *For the Bright Future—Bulk Heterojunction Polymer Solar Cells with Power Conversion Efficiency of 7.4%*. Advanced Materials, 2010. **22**(20): p. E135-E138.

APPENDIX A: COPYRIGHT PERMISSIONS

Below is permission for the use of material in Chapter 5.

5/2/2016 Rightslink® by Copyright Clearance Center

 **Copyright Clearance Center**  [Home](#) [Account Info](#) [Help](#)  Live Chat

 **ACS Publications** Most Trusted. Most Cited. Most Read. **Title:** Photoelectric Memory Effect in an Organic Bulk Heterojunction Device Logged in as: Anand kumar Santhanakrishna [LOGOUT](#)

Author: Anand Kumar Santhanakrishna, Arash Takshi

Publication: The Journal of Physical Chemistry C

Publisher: American Chemical Society

Date: Jul 1, 2015
Copyright © 2015, American Chemical Society

PERMISSION/LICENSE IS GRANTED FOR YOUR ORDER AT NO CHARGE

This type of permission/license, instead of the standard Terms & Conditions, is sent to you because no fee is being charged for your order. Please note the following:

- Permission is granted for your request in both print and electronic formats, and translations.
- If figures and/or tables were requested, they may be adapted or used in part.
- Please print this page for your records and send a copy of it to your publisher/graduate school.
- Appropriate credit for the requested material should be given as follows: "Reprinted (adapted) with permission from (COMPLETE REFERENCE CITATION). Copyright (YEAR) American Chemical Society." Insert appropriate information in place of the capitalized words.
- One-time permission is granted only for the use specified in your request. No additional uses are granted (such as derivative works or other editions). For any other uses, please submit a new request.

[BACK](#) [CLOSE WINDOW](#)

Copyright © 2016 Copyright Clearance Center, Inc. All Rights Reserved. [Privacy statement](#). [Terms and Conditions](#). Comments? We would like to hear from you. E-mail us at customercare@copyright.com

https://s100.copyright.com/AppDispatchServlet 1/1

Below is permission for the use of material in Chapter 6.

Dear Mr. Santhanakrishna,

28 January 2019

Thank you for seeking permission from SPIE to reprint material from our publications. As author of *Optical memory effect in ZnO nanowire based organic bulk heterojunction devices*, SPIE shares the copyright with you, so you retain the right to reproduce your paper in part or in whole.

Publisher's permission is hereby granted under the following conditions:

- (1) the material to be used has appeared in our publication without credit or acknowledgment to another source; and
- (2) you credit the original SPIE publication. Include the authors' names, title of paper, volume title, SPIE volume number, and year of publication in your credit statement.

Sincerely,
Katie Sinclair
Editorial Assistant, Publications
SPIE
1000 20th St.
Bellingham, WA 98225
+1 360 685 5436 (office)
katies@spie.org

SPIE is the international society for optics and photonics. <http://SPIE.org>

SPIE.